Department of AERONAUTICS and ASTRONAUTICS
STANFORD UNIVERSITY

RONALD K. HANSON

AN EXPERIMENTAL AND ANALYTICAL INVESTIGATION OF SHOCK-WAVE REFLECTION IN A CHEMICALLY RELAXING GAS

This research was sponsored by the
National Aeronautics and Space Administration
under Research Grant NASA NGR 05-020-245

MAY
1968

SUDAAR
NO. 345

Department of Aeronautics and Astronautics
Stanford University
Stanford, California

AN EXPERIMENTAL AND ANALYTICAL INVESTIGATION OF SHOCK-WAVE REFLECTION IN A CHEMICALLY RELAXING GAS

by

Ronald K. Hanson

SUDAAR No. 345
May 1968

This research was sponsored by the
National Aeronautics and Space Administration
under Research Grant NASA NGR 05-020-245

ABSTRACT

The normal reflection of a shock wave from a shock-tube end wall is studied analytically and experimentally for a chemically relaxing diatomic gas. The pressure exerted on the end wall during the reflection process is obtained analytically by means of inner and outer asymptotic solutions. Knowledge of the pressure solution enables computation of the time evolution of all thermodynamic properties adjacent to the end wall; these calculations typically consume less than one minute of computing time. The results agree closely with those obtained from more exact calculations which require several hours of computing time.

A fast-response pressure gauge with a risetime of .2 μsec and a useful recording time of up to 14 μsec is used to measure end-wall pressure histories in pure N_2 for incident shock speeds ranging from 4 to 7 km/sec. The chemical reaction rates of the shock-heated N_2 are inferred by using the theoretical solution for pressure. These new rates are compared with existing data, and justifications for applying this technique in future chemical-kinetics studies are given.

An interesting result of the unsteady reflection process is the formation of a non-uniform entropy layer adjacent to the end wall. Numerical results are presented to describe the character and extent of this entropy layer in chemically or vibrationally relaxing O_2, N_2 and CO_2.

ACKNOWLEDGMENTS

The author wishes to express his sincere appreciation to Professor Donald Baganoff for his guidance and encouragement during the course of this investigation and for his instruction in the use of the pressure guage.

Personal gratitude is extended to Mr. Leroy Presley for making it possible to perform experiments at NASA-Ames Research Center and for his continued willingness to discuss technical aspects of this research. It is a pleasure to acknowledge Mrs. Elsie Williams, also of Ames Research Center, for her friendly and efficient cooperation in writing and modifying the computer programs used in this work.

Thanks also go to Mrs. Jerri Rudnick for her expeditious typing of the manuscript.

The author is indebted to NASA for the financial assistance provided through a NASA Traineeship. The initial phases of this research were supported by a contract with NASA-Ames (NAS2-3647); the remainder of the research was supported by NASA Grant NGR-05-020-245.

TABLE OF CONTENTS

TABLE OF CONTENTS (Cont'd)

LIST OF FIGURES

LIST OF FIGURES (Cont'd)

LIST OF FIGURES (Cont'd)

LIST OF FIGURES (Cont'd)

NOMENCLATURE

a	speed of sound
b	reaction rate parameter
e	internal energy per unit mass
h	enthalpy per unit mass
k_d	dissociation reaction rate
k_r	recombination reaction rate
p	gas pressure
r	distance behind reflected shock wave
s	distance behind incident shock wave
t	time after reflection
u	gas velocity
v	gas specific volume
x	distance from shock-tube end wall
A	atom
A_2	diatomic molecule
B	reaction rate parameter
K	equilibrium concentration constant
L	characteristic length
M	Mach number; collision partner in chemical reaction
R	gas constant per unit mass of molecules; relative collision efficiency
T	gas temperature
V	shock wave velocity
W	molecular weight of molecular species

NOMENCLATURE (Cont'd)

GREEK SYMBOLS

α	atomic-species mass fraction
γ	isentropic exponent
δ	small change or correction
η	ratio of incident-shock density to initial density
λ	density ratio across reflected shock wave
ξ	ratio of reflected-shock density to initial density
ρ	gas density
τ	characteristic time
ψ	function of temperature
θ	characteristic temperature

SUBSCRIPTS

1	initial shock-tube conditions
2	conditions behind incident shock wave
5	conditions behind reflected shock wave
d	dissociation
r	reflected shock wave
s	incident shock wave
v	vibration
E	equilibrium
F	frozen
L	laboratory

SUPERSCRIPTS

*	reference equilibrium state
'	final end-wall thermodynamic state

1. INTRODUCTION

Although numerous studies of relaxation phenomena behind incident shock waves have been discussed in the literature, only a few reported studies have considered the effects relaxation has on the state of the gas in the reflected region of a shock tube. Calculations of the thermodynamic state in the reflected region have typically been based on the assumption that the reflected shock wave moves with a constant equilibrium speed. Until recently, no solutions have been presented which apply near a shock-tube end wall where the gas is processed by an unsteady reflected shock wave. The unsteady reflection process causes an entropy layer to be formed, wherein the state of the gas differs from that given by calculations using a constant shock speed.

Knowledge of the correct gas state near the end wall is important to those experiments which utilize shock-wave reflection as a method for obtaining a well-defined sample of high-temperature gas. Typically in such experiments (e.g., shock-tunnel investigations, radiation experiments, and relaxation studies) one assumes that the state of the gas is homogeneous and ignores possible non-uniformities. The effort here has been directed toward developing a technique for calculating the flow near the end wall for cases in which chemical relaxation is important. The ability to calculate the time-varying state of the gas in the reflected region, for a given set of reaction rates, is then used to infer the dissociation rate of shock-heated N_2 from end-wall pressure measurements.

Previous work involving shock reflection with chemical relaxation has recently been completed by L. Presley and this author at the Physics

Branch of NASA-Ames Research Center.[1] The method of characteristics was used to calculate the time-varying state of the gas in the reflected region for cases involving relaxation behind both the incident and reflected shock waves. Unfortunately the lengthy computing time required for each case prohibits extensive use of this program.

The Ames work was begun with the hope of using the characteristics technique to infer chemical reaction rates from density measurements obtained near a shock-tube end wall. The impractical time requirements of the "exact" computer solution became a strong motivation to seek an approximate model for use with data reduction; this in essence was the beginning of the investigation presented here. Five different cases in pure O_2 have been solved with the NASA program and the results for these cases will soon be published.[1] Some of the results also appear in later chapters of this work to provide a standard of comparison for the approximate results presented.

Two studies of interest have been published concerning shock-wave reflection in vibrationally relaxing CO_2. Baganoff used a fast-response pressure gauge[2] mounted on the end wall of a shock tube to infer vibrational relaxation times in the incident-shocked flow.[3] Johannesen et al.,[4] presented numerical solutions for the reflected-shock flow field based on the same relaxation rates which apply behind incident shock waves. His group also obtained interferometer records to confirm their calculations of the flow field density, and one of Baganoff's pressure records was utilized to confirm their predictions of the end-wall pressure history. The remarkable agreement between experiment and theory indicates that the vibrational relaxation rates which properly describe the

incident-shock flow also provide an adequate description of the reflected shock-wave problem. Johannesen's results thus provide some justification for using the reflected shock-wave region for relaxation rate measurements.

In another pertinent study, Smith[5] presented a simple model for interpreting the shock-reflection process in an ionized monatomic gas. His model accounts for the series of shock and rarefaction waves which occur because of the interaction between the incident-shock ionization front and the reflected shock wave. Utilizing the pressure-gauge concept developed by Baganoff, end-wall pressure histories were obtained for a range of strong shock waves in xenon, and ionization relaxation times were inferred from the measurements.

The investigation to be presented here involves shock-wave reflection with chemical relaxation rather than vibrational or ionization relaxation. Using inner and outer asymptotic solutions, a simple theory is developed for predicting the end-wall pressure behavior in a dissociating gas. Results obtained with the simple theory agree closely with those obtained at Ames Research Center.[1] Calculated pressure histories are presented for a number of different shock conditions in O_2 and N_2.

To complement the analytical results, experimental observations of the pressure on a shock-tube end wall are presented. An improved version of the fast-response pressure gauge described in Ref. 6 is used to obtain a number of pressure histories in chemically relaxing N_2. The reaction rates of the shock-heated N_2 are then inferred from the pressure measurements by using the theoretical solution for pressure. The measurements were performed in two different shock tubes in order to

provide a check on the results. These rates are compared with those obtained by other investigators from measurements behind incident shock-waves.

The ability to predict the end-wall pressure for a given set of reaction rates also allows one to calculate the time-dependent values of other thermodynamic properties near the end wall. Results are presented for chemically relaxing O_2 and N_2. The final end-wall properties represent an upper bound on the thermodynamic variations in the non-uniform entropy layer caused by the unsteady shock-reflection process. Numerical results are presented to describe the thermodynamic variations and the spatial extent of the entropy layer for O_2 and N_2.

If only the final end-wall properties are desired, a simple model for shock reflection can be employed which does not depend on the rate of the nonequilibrium processes involved. The model applies to both chemical and vibrational relaxation processes and is suitable for either hand or machine computations. The calculations make use of an approximate relation for the compressional work done on the gas during the relaxation processes. Final end-wall properties are presented for vibrationally relaxing O_2, N_2 and CO_2 as well as for chemically relaxing O_2 and N_2.

2. CHARACTERISTIC TIMES FOR CHEMICAL RELAXATION DURING SHOCK REFLECTION

The solution for the reflection of a shock wave in an ideal gas is reviewed in Appendix A for the purpose of defining the symbols and the coordinate system to be used here. An analysis of shock reflection in a chemically relaxing gas is more complicated since the time dependence of the nonequilibrium processes must be considered. Because of the scope of this investigation, sophisticated concepts of rate chemistry will not be employed. The vibrational temperature will be assumed everywhere in equilibrium with the translational temperature, and the reaction rates utilized will be of the simple form given by classical collision theory when vibration-dissociation coupling is neglected.

This chapter describes the approximate time scales of the pressure history on a shock-tube end wall during shock reflection in a chemically relaxing diatomic gas. In the case of an ideal gas (see Appendix A) the pressure history is merely a step with a jump in pressure level equal to the Rankine-Hugoniot value. The aim here is to study the difference in wall-pressure history between the ideal pressure step and the actual case for a chemically relaxing gas.

It is well known that the pressure is an insensitive variable for studying the flow in the relaxing region behind an incident shock wave, and that the density or temperature of the flow is a far more useful quantity to record for analysis. When an incident shock wave is reflected, however, the pressure on the end wall also becomes a sensitive quantity for exhibiting relaxation effects.

In addition to relaxation phenomena, there are other non-ideal mechanisms which can affect the end-wall pressure. Baganoff[3] has discussed a pressure perturbation which arises from heat conduction to the shock-tube end wall. For the experimental conditions to be considered here, the time scale of the perturbation caused by a cold end wall is usually less than the risetime of the instrumentation used ($\approx .2$ μsec). The effects of a heat-conducting end wall can therefore be ignored in the present analysis.

Other factors which might affect the behavior of the flow behind a reflected shock wave are the boundary layer on the side wall of the shock tube and the curvature of the incident shock wave. Because of the size of the shock tubes employed in the experiments (one tube was 2-inches square while the other was 3-inches in diameter), and the extremely short duration of the measurements (less than 14 μsec), disturbances caused by the side-wall boundary layer can be ignored. Shock curvature effects are similarly ignored on the grounds that the pressure levels employed in this study allow little deviation from the assumed one-dimensional flow.

2.1 Shock Reflection in a Relaxing Gas

An inspection of a schematic x-t diagram for shock reflection in a relaxing gas (see diagram below) shows that in general the gas undergoes relaxation in two regions; i.e., behind the incident shock wave and behind the reflected shock wave. Therefore the reflected shock wave propagates into a region of non-uniform conditions. The resulting flow field can be conceptually simplified by approximating the flow with a

combination of two separate processes: (1) a relaxation in region 5 alone, with region 2 remaining at uniform frozen conditions; and (2) the propagation of a reflected shock wave into a flow which is in the process of relaxing in region 2, but which does not undergo further relaxation in region 5.

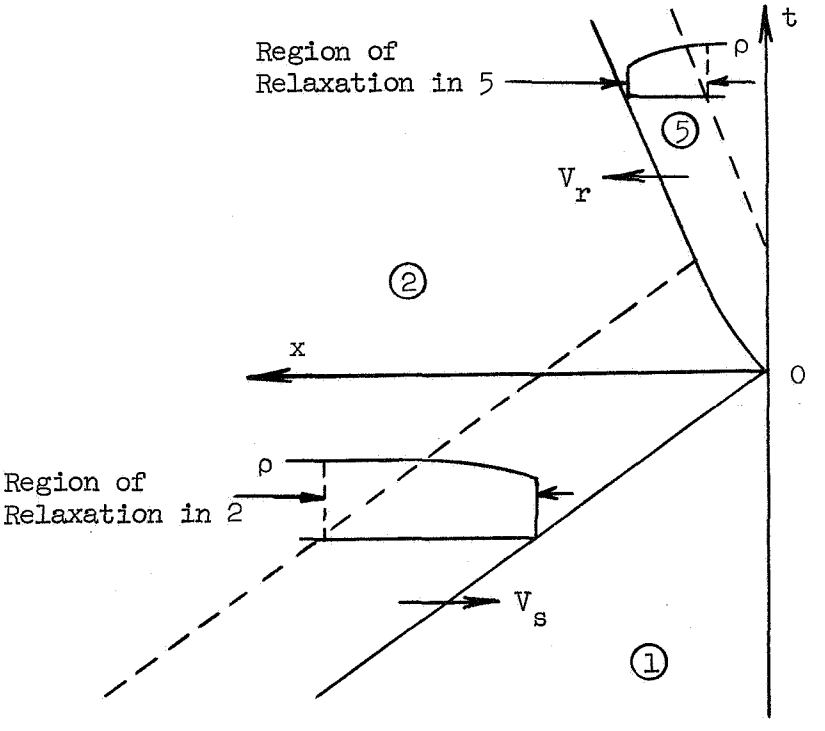

Case (1) can be realized by suddenly setting a piston into uniform motion in a quiescent gas and viewing the piston as being the shock-tube end wall. The piston motion causes the formation of a shock wave followed by a relaxation region. An analysis of this case for chemical relaxation shows that the wall pressure should decrease slightly ($\approx 9\%$ for O_2,

M_s = 11 and P_1 = 1 torr) from the initial frozen value to the final equilibrium value, in somewhat the manner shown in Fig. 1a. The decay time, τ_5, is approximately that of the relaxation time for the gas in region 5. For details of an analysis of this type the reader is directed to a paper by Spence.[7] The important conclusion is that the relaxation in region 5 decreases the wall pressure from the initial frozen value.

Case (2) can be visualized as the situation which would occur if the gas is allowed to relax in region 2 but not in region 5. An analysis of this case, again for chemical relaxation, shows that the wall pressure should increase significantly ($\approx$ 53% for O_2, M_s = 11 and P_1 = 1 torr) from the frozen to the equilibrium value. This effect is depicted in Fig. 1b where the time scale of the pressure increase is essentially the incident-shock relaxation time in laboratory coordinates, τ_{2L}.

The actual process of shock reflection is a combination of the two cases presented above and is schematically represented in Fig. 1c, assuming $\tau_5 \ll \tau_{2L}$, and in Fig. 1d, assuming $\tau_5 \lesssim \tau_{2L}$. The individual pressure levels identified in Fig. 1 can be calculated for any form of relaxation once the shock speed and initial conditions are specified. Some results for these pressure levels in chemically reacting O_2 and N_2 are presented in Chapter 6.

The sensitivity of the end-wall pressure to the gasdynamic processes in regions 2 and 5 can be further emphasized with the following relations.[3] Solving the continuity and momentum equations for the exact jump relations across the incident and reflected shocks (the velocities, referred to laboratory coordinates, are all positive) one obtains

$$p_5 - p_2 = \rho_2 u_p V_s \qquad (2.1.1)$$

$$u_p/V_s = (\eta-1)/\eta \qquad (2.1.2)$$

and

$$V_r/V_s = (\eta-1)/(\xi-\eta) \qquad (2.1.3)$$

where

$$\eta = \rho_2/\rho_1 \quad \text{and} \quad \xi = \rho_5/\rho_1 \ .$$

These symbols are the same as those used in Appendix A for an ideal gas. Substituting equations (2.1.2) and (2.1.3) into (2.1.1) results in

$$(p_5-p_2)/\rho_1 V_s^2 = \frac{\xi}{\xi-\eta}\,\frac{\eta-1}{\eta}\,(\eta-1) \ . \qquad (2.1.4)$$

Since the mass density increases along a particle path during the relaxation process, it is apparent from the last equation that relaxation in region 5 (case (1)) causes the pressure in 5 to decrease (note ξ is always larger than η). Relaxation in region 2 (case (2)) causes the pressure in 5 to increase.

Further insight can be gained by approximating equation (2.1.4) with a simpler expression; for $\xi \gg \eta \gg 1$, and $p_5 \gg p_2$, the result is

$$p_5/\rho_1 V_s^2 \approx \eta \ .$$

This relation involves little error for the strength shock waves of interest in most relaxation studies. Dividing the equilibrium value by the frozen value, one obtains

$$p_{5E}/p_{5F} \approx \eta_E/\eta_F \ . \qquad (2.1.5)$$

The fractional variation in the wall pressure during shock reflection is therefore nearly the same as the fractional variation in the density behind the incident shock wave. This is a reasonable conclusion since the pressure in the reflected region should be a manifestation of the dynamic pressure of the incident-shocked gas (as seen by the reflected shock wave). Note that this result is independent of the type of non-equilibrium flow involved, e.g., vibrational, chemical, or ionization relaxation. The end-wall pressure is thus a sensitive quantity for studying relaxation effects behind incident shock waves. The fact that ξ does not appear in the last expression indicates that the wall pressure is not very sensitive to relaxation in region 5.

2.2 Characteristic Times for Chemical Relaxation

In this section expressions are obtained for characteristic relaxation times in regions 2 and 5. The results show that τ_5 is much less than τ_{2L} for most shock conditions in O_2 and N_2. For these cases composite end-wall pressure histories can be obtained by combining two separate pressure solutions, one valid for short end-wall times $(t < \tau_5)$ and the other valid for long end-wall times $(t > \tau_5)$.

Although chemical relaxation is not an exponential process, characteristic times for relaxation can still be defined from the values of the reaction rate immediately behind the incident and reflected shock waves. For the dissociation-recombination reaction of a homonuclear diatomic molecule,

$$A_2 + M \underset{k_{r,M}}{\overset{k_{d,M}}{\rightleftarrows}} 2A + M \quad , \tag{2.2.1}$$

the rate equation is[8,9]

$$\frac{D\alpha}{Dt} = \frac{W}{\rho} \{k_{d,M}[A_2][M] - k_{r,M}[A]^2[M]\} \qquad (2.2.2)$$

where W is the molecular weight of the molecule A_2, α is the mass fraction of the atomic species, $k_{d,M}$ is the dissociation rate applicable for collisions with species M, $k_{r,M}$ is the recombination rate, and the square brackets denote species concentrations (in units of moles/vol). The symbol M denotes a general collision partner which, for a pure gas, may be either A or A_2. The reaction rates are different for each possible collision partner.

Immediately behind a shock wave with no upstream dissociation, the atomic mass fraction is zero. Therefore the rate equation simplifies to

$$\frac{D\alpha}{Dt} = \frac{\rho}{W} k_{d,A_2} \quad , \qquad (2.2.3)$$

and the characteristic relaxation time along a particle path is approximately[10]

$$\tau \approx \frac{W}{\rho k_{d,A_2}} \quad .$$

In region 5, laboratory time is essentially the same as particle time, so the end-wall time characterizing relaxation in 5 is given by

$$\tau_5 \approx \left.\frac{W}{\rho k_{d,A_2}}\right|_{5F} \quad . \qquad (2.2.4)$$

The end-wall time which exhibits the effects of relaxation in region 2 is approximately the characteristic time for a particle in 2 divided by the incident shock-wave density ratio, i.e.,

$$\tau_{2L} \approx \frac{\tau_2}{\eta_F} \approx \left.\frac{W}{\eta \rho k_{d,A_2}}\right|_{2F} \quad . \tag{2.2.5}$$

The subscript F is used in both cases to denote frozen chemistry conditions.

The dissociation rate is taken to be of the classical collision theory form,[8,11]

$$k_{d,A_2} = BT^{-b} e^{-\theta_d/T} \quad , \tag{2.2.6}$$

where B and b are constant coefficients and θ_d is the characteristic dissociation temperature for the reaction. With the use of the approximate values (typical for the present work) $b = 2$, $T_{5F} = 2T_{2F}$, $\rho_{5F} = 4\rho_{2F}$ and $\eta_{2F} = 7$, the ratio of the characteristic times is found to be

$$\tau_{2L}/\tau_5 \approx \frac{1}{7} e^{\theta_d/T_{5F}} \quad . \tag{2.2.7}$$

This analysis is concerned only with shock waves strong enough to cause dissociation in region 2, but too weak to cause ionization in region 5. For these shock conditions in either O_2 or N_2, the frozen temperature in region 5 (computed with all internal energy modes equilibrated with the translational energy mode) is bounded approximately by

$$3.5 \lesssim \theta_d/T_{5F} \lesssim 12$$

where $\theta_d = 59400°K$ in O_2 and $113000°K$ in N_2. Except for the strongest shock waves to be considered, it is clear from equation (2.2.7) that the characteristic time in region 2 is much larger than that in region 5 (e.g., in N_2, a relatively weak shock wave, $M_s = 10$, provides $\tau_{2L}/\tau_5 \approx 6000$; a strong shock wave, $M_s = 19$, provides $\tau_{2L}/\tau_5 \approx 8$).

It should be noted that the above analysis considered relaxation of the variable α. The characteristic times for pressure relaxation will be somewhat different, but to a first approximation one may assume that the ratio of the characteristic times for pressure remains the same as that obtained for α. Solutions for the end-wall pressure history in a chemically relaxing diatomic gas are thus expected to be of the form shown in Fig. 1c for most shocks and of the form shown in Fig. 1d for strong shock waves causing nearly complete dissociation of the gas in region 5.

An exact end-wall pressure solution considering simultaneous relaxation in regions 2 and 5 would be very difficult, but the extent of the separation in the characteristic times suggests that individual solutions are possible for each time regime. Such solutions are the subject of the next chapter.

The existence of two time scales for the pressure history on a shock-tube end wall was first noted by Baganoff[3] and subsequently confirmed by Johannesen's calculations in vibrationally relaxing CO_2.[4] There are subtle differences, however, between shock reflection in vibrationally and chemically relaxing gases. Johannesen showed that the initial end-wall pressure gradient in vibrationally relaxing CO_2 is negative only for $M_s > 2$, and that τ_5 becomes a smaller fraction of

τ_{2L} as shock strength increases. For chemical relaxation, as shown here, the opposite is true. The initial pressure gradient is negative only for shock strengths less than some critical value of M_s, and the characteristic times for relaxation become more widely separated as shock strength decreases. Furthermore, because of the large characteristic temperature for dissociation compared with that for vibration, the extent of the time scale separation is much greater for chemical relaxation. It is this fact which allows one to formulate separate pressure history solutions for chemical relaxation but not for vibrational relaxation.

3. SOLUTION FOR THE WALL-PRESSURE HISTORY

The previous chapter established that shock reflection in a chemically relaxing diatomic gas is characterized by two different time scales. One can thus form separate inner and outer solutions for the end-wall pressure which will be valid for short and long times respectively.

3.1 Inner Solution for Wall Pressure

The inner solution presented here is based on an initial slope approximation. Results for a case similar to that presented in Fig. 1c are shown schematically below. The bounding values for the pressure level are computed by first assuming the gas is frozen chemically in regions 2 and 5 (P_{F2F5}) and then frozen in 2 but in equilibrium in 5 (P_{F2E5}).

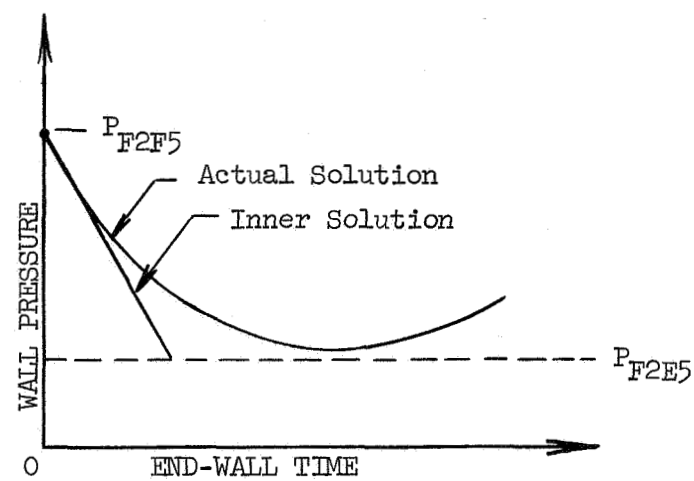

By accounting for the initial rate of relaxation in both regions, 2 and 5, the inner solution also provides results for the initial pressure slope in cases similar to that shown in Fig. 1d. These cases occur for strong shocks where the time scales of relaxation in 2 and 5 cannot be considered separate. In fact, for very strong shocks the initial pressure gradient actually turns out to be highly positive rather than negative.

At the end of this section the accuracy of the inner solution is checked by comparing results with the more exact computer program at Ames Research Center.[1]

3.1.1 Description of the Inner Solution

The rate of change of end-wall pressure is first written in terms of the rates at which density changes occur in 2 and 5, since these can be related to the reaction rates. With the assumption of independent but simultaneous relaxation in both regions, the initial end-wall pressure slope is given by

$$\left(\frac{dp_5}{dt}\right)_{x,t=0} = \left(\frac{\partial p_5}{\partial \eta}\right)_{\xi} \left(\frac{d\eta}{dt}\right)_{x,t=0} + \left(\frac{\partial p_5}{\partial \xi}\right)_{\eta} \left(\frac{d\xi}{dt}\right)_{x,t=0}, \qquad (3.1.1)$$

or in shorter form

$$\left(\frac{dp}{dt}\right)_{x,t=0} = \left(\frac{dp_5}{dt}\right)_{\substack{x,t=0 \\ \xi}} + \left(\frac{dp_5}{dt}\right)_{\substack{x,t=0 \\ \eta}} . \qquad (3.1.2)$$

This equation relates the initial rate of pressure change to the sum of non-coupled contributions from 2 and 5. One contribution is given

by the sensitivity of p_5 to η times the initial rate at which changes in η are "felt" on the end wall; the other term is given by the sensitivity of p_5 to ξ times the initial rate at which changes in ξ are "felt" on the end wall. Since the relation for p_5 as a function of η and ξ is[12]

$$\frac{p_5}{p_1} = 1 + \gamma_1 M_s^2 \frac{(\eta-1)(\xi-1)}{\xi-\eta} \quad , \tag{3.1.3}$$

then

$$\left.\frac{\partial p_5}{\partial \eta}\right)_{\xi} = p_1 \gamma_1 M_s^2 \left(\frac{\xi-1}{\xi-\eta}\right)^2 \tag{3.1.4}$$

and

$$\left.\frac{\partial p_5}{\partial \xi}\right)_{\eta} = -p_1 \gamma_1 M_s^2 \left(\frac{\eta-1}{\xi-\eta}\right)^2 \quad . \tag{3.1.5}$$

The variations in η, which occur in region 2, are first sensed along the reflected shock-wave trajectory and then transmitted as pressure waves in the reflected region. The pressure is assumed to remain constant along a straight characteristic of slope a_{5F} (a_{5F} denotes the frozen speed of sound in region 5). The initial slope of the end-wall pressure due to variations in η is therefore approximately

$$\left.\frac{dp_5}{dt}\right)_{\substack{x,t=0 \\ \xi}} \approx \left.\frac{\partial p_5}{\partial \eta}\right)_{\xi} \left.\frac{\partial \eta}{\partial t}\right)_{r,t=0} (1+V_r/a_{5F})^{-1} \tag{3.1.6}$$

where r is used to indicate coordinates fixed to the reflected shock wave.

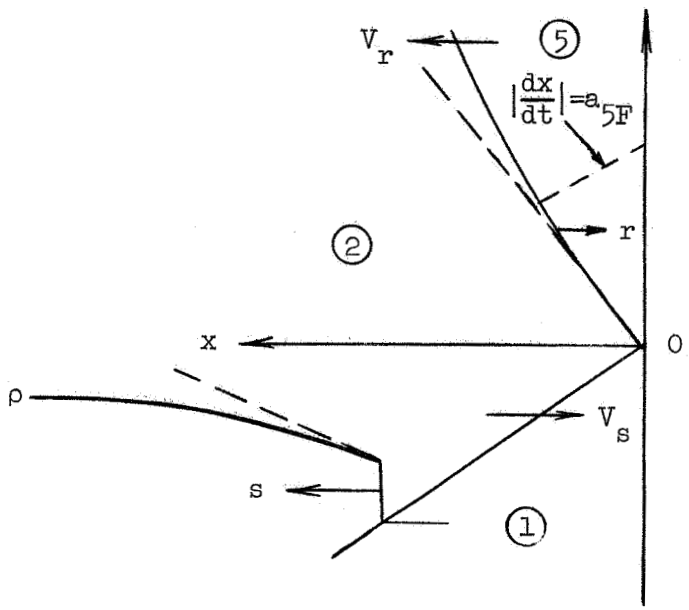

Changing from reflected-shock to incident-shock coordinates, and recalling that relaxation profiles are stationary in incident-shock coordinates, one then finds

$$\left.\frac{dp_5}{dt}\right)_{\substack{x,t=0\\ \xi}} \approx p_1\gamma_1 M_s^2 \left[\left(\frac{\xi-1}{\xi-\eta}\right)^2 \frac{1+V_r/V_s}{1+V_r/a_{5F}}\right]_{x,t=0} \left(\eta \frac{D\eta}{Dt}\right)_{s=0} . \qquad (3.1.7)$$

Although this appears to be a complicated relation, the physical meaning can still be seen because

$$\left(\frac{\xi-1}{\xi-\eta}\right)^2\left(\frac{1+V_r/V_s}{1+V_r/a_{5F}}\right) \approx 1 \quad .$$

With this simplification the initial pressure gradient is given by

$$\left.\frac{dp_5}{dt}\right)_{\substack{x,t=0\\ \xi}} \approx p_1\gamma_1 M_s^2 \left(\eta \frac{D\eta}{Dt}\right)_{s=0} = V_s \frac{\partial}{\partial s}\left(\rho_2 V_s^2\right) \quad .$$

Since $\rho_2 V_s^2$ is approximately the dynamic pressure in region 2, then $V_s \frac{\partial}{\partial s}(\rho_2 V_s^2)$ is nearly the rate of change of the dynamic pressure at a fixed laboratory position such as the end wall. This is the expected result because the reflected shock effectively transforms dynamic pressure to static pressure as the gas is brought to rest.

At this point equation (B.8) from Appendix B is employed to relate the rate equation in η to the more familiar rate equation in terms of α, i.e.,

$$\left.\eta \frac{D\eta}{Dt}\right)_{s=0} \approx \frac{2}{9}\left\{\eta^2\psi(T)\left[1 - \frac{7}{9}\frac{1}{\eta-1}\right]^{-1} \frac{D\alpha}{Dt}\right\}_{2F} \qquad (3.1.8)$$

where

$$\psi(T_{2F}) = \theta_d/T_{2F} - 3 - e_v/RT_{2F} \quad , \qquad (3.1.9)$$

e_v is the vibrational energy of the molecules,[8] and R is the gas constant per unit mass of the molecular species. The subscript $2F$ denotes chemically frozen conditions in region 2 (the internal energy modes are assumed equilibrated with the translational temperature). The final expression for the end-wall pressure gradient resulting from

relaxation in region 2 is given by substitution of equation (3.1.8) into equation (3.1.7).

The last term in the pressure-slope equation, (3.1.2), is concerned with relaxation in region 5 only. To a first approximation it is assumed that the value of the reflected-shock velocity adjusts instantly to changes of ξ on the end wall so that p_5 is still related to ξ through the relation (3.1.3). In this case one can write

$$\left.\frac{dp_5}{dt}\right)_{\substack{x,t=0\\ \eta}} \approx \left.\frac{\partial p_5}{\partial \xi}\right)_{\eta} \left.\frac{D\xi}{Dt}\right)_{x,t=0}$$

where the substantial derivative is utilized to emphasize the fact that the end wall is a particle path.

Because the gas particles on the end wall undergo an adiabatic process, the rate of change of density along this path can be directly related to the rate of change of p_5 and α, as shown in equation (C.4) of Appendix C. Using that relation and recalling equation (3.1.5) yields

$$\left.\frac{dp_5}{dt}\right)_{\substack{x,t=0\\ \eta}} \approx -p_1\gamma_1 M_s^2 \frac{2}{9}\left\{\xi\left(\frac{\eta-1}{\xi-\eta}\right)^2 \left.\frac{D\alpha}{Dt}\right|_{5F} \psi(T_{5F})\left[1+\frac{(\eta-1)(\xi)}{(\xi-\eta)(\xi-1)}\frac{7}{9}\right]^{-1}\right\}_{x,t=0} \tag{3.1.10}$$

The solution for the initial end-wall pressure gradient is given by the sum of equations (3.1.7) and (3.1.10). In the case of weak shocks the contribution of equation (3.1.10) is dominant while for very strong shocks the contribution of equation (3.1.7) dominates.

If further simplification in the pressure solution is desired, at

the expense of some loss in accuracy, several of the small terms in equations (3.1.7) and (3.1.10) can be omitted while others are approximated. Such an abbreviated form is

$$\left(\frac{dp_5}{dt}\right)_{x,t=0} \approx p_1\gamma_1 M_s^2 \eta^2 \frac{2}{9}\left[\frac{D\alpha}{Dt}\Big|_{2F}(\theta_d/T_{2F}-4) - \frac{1}{\xi}\frac{D\alpha}{Dt}\Big|_{5F}(\theta_d/T_{5F}-4)\right] . \tag{3.1.11}$$

Substitution of reasonable values for η, ξ, T_{2F} and T_{5F} into equation (2.2.3) and then into the equation above provides a simple answer for the initial pressure slope owing to chemical relaxation.

3.1.2 Results of the Inner Solution

Results for the initial slope based on equations (3.1.7) and (3.1.10) can be presented if a dissociation rate is specified. On the basis of the assumption that the nonequilibrium dissociation and recombination rates are related through the equilibrium constant, it is sufficient to specify the recombination rate which includes no exponential term. With the use of the recombination rates

$$k_{r,O_2} = 2.04 \times 10^{16}\, T^{-.5}\ \text{cm}^6/(\text{mole}^2\text{-sec})$$

and

$$k_{r,N_2} = 3.0 \times 10^{32}\, T^{-4.5} ,$$

Figs. 2 and 3 provide the initial pressure slope over a range of shock conditions in O_2 and N_2. The oxygen rate was suggested by Wray[13] on the basis of experiments performed by Camac. The nitrogen rate is

the one established in Chapter 5 of this thesis. The initial slope is seen to change from negative to positive values at a Mach number of about 11.4 in O_2 and 13.4 in N_2.

Since the analysis presented here is not mathematically exact, it is worthwhile to compare results with the solutions obtained at Ames Research Center.[1] Comparisons are presented in Figs. 4 and 5 for two shock conditions in O_2. The rates used in these cases for both the Ames work and the inner solution were

$$k_{r,O} = k_{r,O_2} = 7.29 \times 10^{21}\ T^{-2}\ cm^6/(mole^2\text{-}sec) \quad .$$

For these cases only, electronic excitation was not considered in the inner solution in order to be consistent with the NASA calculations.

Fig. 4 presents a comparison for a moderately strong shock wave. The initial part of the outer solution, to be presented in the next section of this chapter, is also shown to indicate the range of time within which the inner solution is employed. The outer solution is utilized as soon as the inner and outer solutions cross.

Fig. 5 represents the case of a very strong shock wave which causes extensive dissociation in region 5. In this case the effects of relaxation in 2 are strong enough to cause a positive initial slope. The unusual structure of the NASA solution, which begins with a steep initial slope followed by a decrease in slope and then another increase, can be understood from equation (3.1.10). For very strong shock waves the term $\psi(T)$ changes from a positive to a negative value so that the initial effect of relaxation in region 5 is to help increase the pressure from

the frozen value rather than to decrease it. The first decrease in the slope of the NASA solution is a result of decreasing temperature in region 5 which reverts the sign of ψ back to its usual positive condition. As the temperature in region 5 decreases further, the relaxation in 5 becomes less important and the relaxation in 2 becomes dominant, thus causing a new increase in slope.

The composite pressure solution is taken to be the inner solution for short time and the outer solution for long time. The composite solution transfers directly from the inner to the outer solution when the results match in magnitude, as in Fig. 4. For those cases where the initial pressure slope is positive, as in Fig. 5, the inner and outer solutions never intersect; a composite solution is then formed by assuming a constant frozen pressure until the outer solution is crossed.

3.2 Outer Solution for Wall Pressure

The outer solution is concerned with end-wall pressure changes which occur on the same time scale as that of the relaxation in region 2. Since $\tau_5 \ll \tau_{2L}$ for the dissociation cases studied here, one may neglect the nonequilibrium effects in region 5 and absorb the relaxation zone into the structure of the reflected shock wave. Furthermore, because effects with a time scale of τ_5 are not noticeable on the time scale of τ_{2L}, the shock will appear to reflect with an initial speed corresponding to conditions of chemically frozen gas in 2 and equilibrium gas in 5, i.e., $V_{r\ F2E5}$. On the assumption that the value of the reflected shock velocity does not change significantly from $V_{r\ F2E5}$ to $V_{r\ E2E5}$ (denoted here simply as V_r^*) a simplified x-t diagram can be drawn

using a constant speed trajectory for the reflected shock wave.

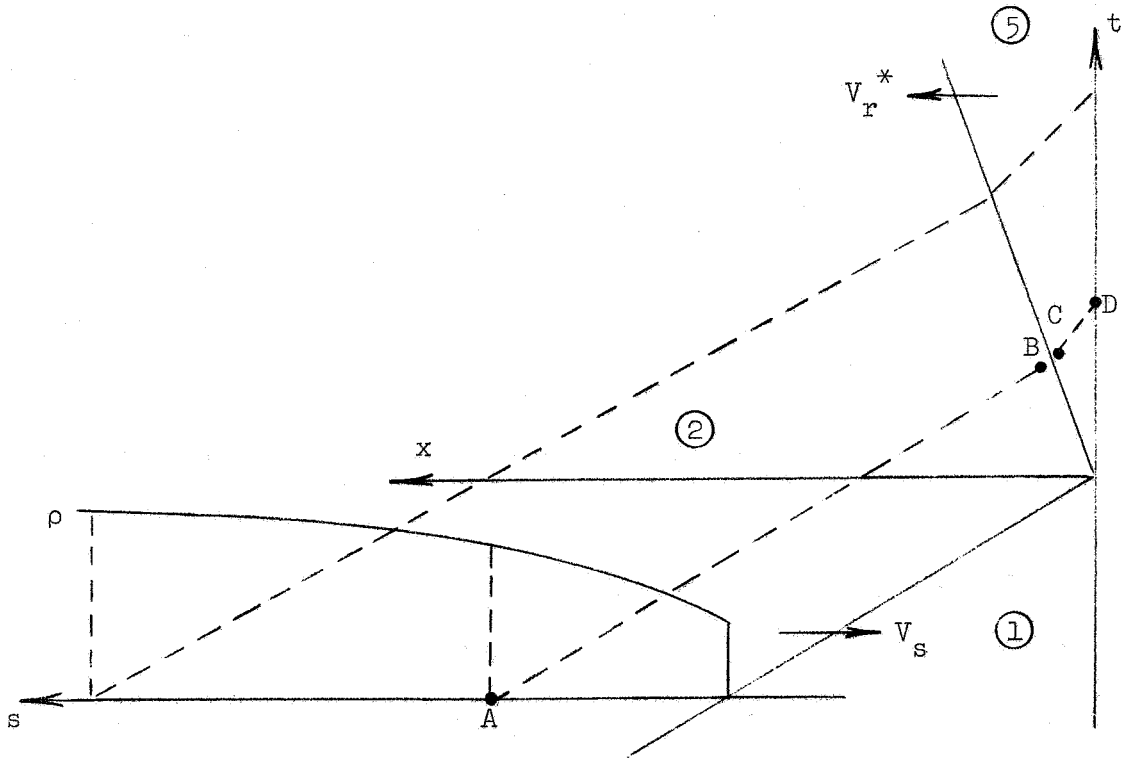

The calculational procedure for the outer solution can now be outlined. For given shock conditions and reaction rates, the incident-shock relaxation zone is first calculated. The thermodynamic conditions corresponding to any distance behind the incident shock wave are then projected on to the reflected shock wave (i.e., from point A to point B on the figure above). The conditions at B are transformed to conditions

at C using real-gas shock-jump calculations. The pressure level at C is assumed to propagate along a straight characteristic to point D on the end wall. The outer solution is composed of a number of these same calculations, each originating from a different initial position behind the incident shock wave. The accuracy of the model is demonstrated at the end of this section by comparing results with solutions obtained at Ames.

With the above summary in mind, some general comments can be made before turning to a more detailed analysis. Since the predicted end-wall pressure becomes asymptotically exact as the reflected shock finally achieves a steady equilibrium speed, the outer solution is in error only for short time when the assumed shock speed is incorrect and the relaxation length in 5 cannot be neglected. Fortunately, small changes in the speed of the reflected shock wave are not critical; this is because the pressure in region 5 depends primarily on the velocity of the gas in region 2. The neglect of a finite relaxation length in region 5 is not critical since the end-wall pressure is more sensitive to incident-shock relaxation than to relaxation in the reflected region.

3.2.1 Description of the Outer Solution

The first step of the outer solution is to calculate the properties behind the incident shock wave. For input values of shock speed, initial conditions and reaction rates, the calculations provide a set of thermodynamic properties tabulated as a function of distance behind the incident shock wave. The computations are performed using a computer code based on the one-dimensional conservation equations, the state relations for a

dissociating diatomic gas, the reaction-rate equations and an expression for the equilibrium concentration constant for the reaction in question. The techniques for solving the incident-shock flow are already well documented[14,15] and will not be discussed further.

Once the incident shock-wave properties are known, they can be projected across the x-t plane and on to the reflected shock-wave trajectory. The first important approximation is the assumption of a particular trajectory for the reflected shock. The second important approximation is the assumption that the relaxation zone behind the reflected shock is negligibly thin compared with the spatial extent of the relaxation in region 2. This assumption allows one to perform jump calculations to an equilibrium state immediately downstream of the reflected shock. These results are obtained at a large number of points along the trajectory, the interval being fixed by computer input instructions. The gas properties along the shock boundary of region 5 are thus known.

The calculation of the equilibrium gas state downstream of the reflected shock wave (point C) involves an iteration scheme. Using reflected shock-fixed coordinates, and known upstream properties (at point B), the equations to be iterated are

$$(p_5)_C = p_2 + \rho_2(u_p+V_r^*)^2(1-1/\lambda) \qquad (3.2.1)$$

and

$$(h_5)_C = h_2 + 1/2\ (u_p+V_r^*)^2(1-1/\lambda^2) \qquad (3.2.2)$$

where

$$\lambda = (\rho_{52})_C = \left(\frac{u_p+V_r^*}{V_r^*-u_5}\right)_C \quad . \qquad (3.2.3)$$

Also known is the equilibrium state relation

$$h_5 = h(p_5,\rho_5) \quad . \tag{3.2.4}$$

One form of iteration involves picking a value of λ (and hence ρ_5) and using equation (3.2.1) to find p_5. For these values of p_5 and ρ_5 equation (3.2.4) is used (or an equilibrium gas chart) to find the equilibrium value of h_5. This value of h_5 is compared with that given by equation (3.2.2). Iteration on λ continues until satisfactory agreement is achieved for h_5.

Knowing the equilibrium state of the gas along the shock boundary of region 5, the next step is to transfer this information to the end wall. Using the method of characteristics for a chemically reacting gas,[1,16] along a right-running characteristic in the x-t plane (i.e., of slope $dx/dt = u_5 - a_{5F}$) one finds

$$\frac{\delta p_5}{\delta t} + \rho_5 a_{5F} \frac{\delta u_5}{\delta t} = Y \tag{3.2.5}$$

where Y is an expression related to the rate of entropy production owing to nonequilibrium chemical processes. If the gas in local chemical equilibrium, as assumed here, $Y = 0$ and the equation reduces to the same form as that for an ideal gas. Noting that u_5 is negligible (except in the relaxation layer of 5, which has been neglected) and that the frozen speed of sound does not vary much across the flow field, one can assume that the characteristics are straight lines. As a further simplification all characteristics are taken to have the same

slope; the slope chosen corresponds to the frozen speed of sound evaluated at the equilibrium conditions of point C after the incident-shock flow becomes uniform. These are the same equilibrium conditions which are tabulated in tables of reflected shock-wave properties for real gases and referred to here as the reference equilibrium conditions (denoted with an asterisk).

In terms of the conditions at the shock wave, the end-wall pressure is given by

$$(p_5)_D = (p_5)_C + \delta p_5 \qquad (3.2.6)$$

where

$$\delta p_5 = -(\rho_5 u_5 a_{5F})_C \quad .$$

Since $|\delta p_5| \ll p_5$, to zeroth order $(p_5)_D$ is equal to $(p_5)_C$. The first-order solution for the end-wall pressure would include δp_5.

At this point in the analysis zeroth and first-order solutions for end-wall pressure have been developed. However, it is worthwhile to pause here and appeal to the physics of this problem. Since u_5 is much less than the characteristic velocity a_{5F}, the gas in the reflected region is nearly at rest. A great simplification can be made if one neglects u_5 completely and uses a jump condition across the reflected shock which brings the gas to rest rather than to an equilibrium state. In this case the density ratio is

$$\lambda^+ = \frac{u_p + V_r^*}{V_r^*} \quad .$$

The value of p_5 at both C and D is given by equation (3.2.1) using λ^+.

The advantages of calculating p_5 this way are noteworthy. Iteration on λ to find the appropriate equilibrium state is no longer necessary. A simple calculation of λ^+ at each point along the trajectory immediately establishes the end-wall pressure as a function of time. This technique was utilized in obtaining the results to be presented in the next section.

It should be noted that the simple approach for calculating p_5 always provides an answer for end-wall pressure between the zeroth and first-order solutions discussed above. For details of this proof see Appendix D.

The magnitude of the errors introduced by the simplifying assumptions can now be established. To investigate the error involved in assuming a constant-speed reflected shock wave, equation (3.2.1) is rewritten in terms of the incident-shock velocity and a corrected reflected-shock speed, i.e.,

$$p_5 \approx p_2 + \rho_2 V_s \left(\frac{\eta-1}{\eta} + \frac{V_r^* - \Delta V_r}{V_s} \right)^2 (1-1/\lambda^+) \quad .$$

For the diatomic gases studied here, $\lambda^+ \approx 8$ while η varies from about 8 to 16. Neglecting $1/\lambda^+$, setting $(\eta-1)/\eta$ equal to 1, and noting that $p_5 \gg p_2$ and $V_r^* \ll V_s$, an approximate form of the above equation is

$$p_5 \approx \rho_2 V_s^2 \left[1 + 2 \frac{V_r^*}{V_s} \left(1 - \frac{\Delta V_r}{V_r^*} \right) \right] .$$

It can be seen from equation (2.1.3) that

$$V_r^*/V_s \approx 1/\lambda \approx 1/8$$

so that

$$p_5 \approx \rho_2 V_s^2 \left[1 + .25(1-\Delta V_r/V_r^*)\right] \quad .$$

A 10% change in V_r thus results in about a 2% change in p_5. The assumption of a constant-speed reflected shock is certainly justified since the difference between the F2E5 and E2E5 reflected speeds is typically less than 10%. Furthermore, it is only for very short times that the shock speed approaches the F2E5 value.

The magnitude of the difference between the zeroth and first order pressures (and hence a rough error bound on the simple λ^+ solution) is given approximately by

$$|\delta p_5/p_5| \approx |u_5/a_{5F}| \quad .$$

Over a range of cases studied in O_2, $|u_5/a_{5F}|$ was typically less than 1% and never exceeded 2%. The simple λ^+ solution therefore introduces an error of only 1% or less in the end-wall pressure.

3.2.2 Results of the Outer Solution

Results of the outer solution are presented in Figs. 6 and 7 for two shock conditions solved at Ames Research Center. These shock conditions are the same ones used in Section 3.1 to provide comparisons

for the inner solution. The difference between the NASA solution and the outer solution is less than 1% throughout both Fig. 6 and Fig. 7, except during the brief initial period of time wherein the relaxation in region 5 is important. For these short times the inner solution is necessary.

In Fig. 6 the Ames solution was ended at 35 μsec owing to the onset of oscillations in the solution. These oscillations, not shown here, resulted from the size of the network used in the calculational scheme. Since the machine time necessary to obtain the solution amounted to nearly 10 hours, it was not feasible to reduce the network size further. The computing time was lengthy because the NASA program calculates the entire reflected flow field. The outer solution presented here applies only near the end wall but takes less than one minute of computing time per case and converges asymptotically to the exact final pressure level. The divergence between the NASA and the outer solutions for long times is caused by numerical convergence problems in the NASA program.

The purpose of this chapter was to present a new technique for obtaining end-wall pressure histories during shock reflection in a chemically relaxing gas. Now that both the inner and outer solutions have been verified, results can be presented for a wide range of shock conditions. Figs. 8 through 11 show the composite pressure histories for two initial pressures and a range of shock speeds in O_2 and N_2. The results are presented in dimensionless form with respect to the reference equilibrium pressure. Since there is no pressure gradient in the final entropy layer, all the curves shown are asymptotic to 1. Electronic excitation is considered in these results and the rates

employed are the same as those used to compute the initial pressure slopes of Figs. 2 and 3.

It should be remembered that vibrational relaxation times have been set equal to zero in these calculations so that the solutions are incorrect in this regard. The curves presented are thus a bound on the actual behavior. The result of considering this effect would be to alter the shape of the pressure histories for short time.

For very short times the thickness of the translational shock wave also becomes important. Since the incident and reflected shock waves were assumed to have zero thickness, this effect would modify the pressure histories presented for times less than about 10^{-7} seconds.

The pressure solution presented in this chapter has at least two important applications. First, the ability to relate accurately the end-wall pressure to the reaction rate in the gas, with a minimum of computing time, presents a new technique for inferring the reaction rates of shock-heated gases. A major part of this investigation has been concerned with the application of a fast-response pressure gauge, in conjunction with the outer pressure solution, to infer the reaction-rate coefficients of shock-heated N_2. This work is presented in Chapters 4 and 5.

A second important application of the pressure solution is discussed in Chapter 6. It will be shown that the time evolution of all end-wall thermodynamic variables can be calculated when the end-wall pressure history is known. These calculations also yield the steady-state thermodynamic properties which provide the upper bound on the thermodynamic variations existing in the end-wall entropy layer.

4. THE EXPERIMENT

Short-duration pressure histories have been obtained on a shock-tube end wall for a range of shock conditions in pure N_2 wherein chemical relaxation is the dominant nonequilibrium process. The pressure was recorded using a fast-response pressure gauge similar to that described recently by Baganoff.[6] The gauge has a risetime of less than .2 μsec and provides an accurate reproduction of the transient pressure on the end wall for times up to 14 μsec.

4.1 The Shock Tube

All the developmental experimentation was performed in the Stanford Aerophysics Laboratory shock tube, a 25-foot-long tube of extruded aluminum with a 2-inch-square inside cross-section. This facility, described in detail in Ref. 17, can be used in either a pressure or a combustion-driven mode. The pressure-drive mode was utilized for calibrating the pressure gauges in the ideal-gas regime; all chemical relaxation data were obtained with the combustion-driven mode.

For comparison purposes, final data were collected in two different shock tubes, the Stanford shock tube and a 3-inch-diameter combustion-driven shock tube in the Physics Branch of Ames Research Center. The latter tube is of stainless steel and 35 feet in length.

In the Stanford shock tube the incident-shock velocity was measured with barium-titanate pressure transducers located 5, 25 and 35 centimeters from the end wall. Since each crystal reacted differently to a given incident-shock pressure pulse, the individual transducer responses

were monitored to permit individual interpretation and to assure maximum accuracy. Because of shock-speed attenuation and the short transit times involved in the measurements, the shock speed is considered known only to within 2%.

The initial pressure varied from .3 to 5 torr and was measured directly with a McLeod gauge or with a Wallace and Tiernan vacuum gauge (0 to 20 torr) which was periodically calibrated with the same McLeod gauge. Owing primarily to the quality of these instruments, the initial pressure is considered known only to within 2% for initial pressures over 1 torr and approximately 3% for pressures under 1 torr.

In the NASA shock tube the shock velocity was measured between four pressure transducers, each separated by a distance of one foot. The last transducer was only one inch from the end wall. Because of shock attenuation problems and the use of counters to obtain transit times, the shock-velocity uncertainty is as large as 3% for some cases. Initial pressures were measured with a high-quality McLeod gauge so that this quantity is considered known to within 1% for all initial pressures employed.

It should be noted that a 2% error in initial pressure generates a 2% error in the reflected pressure level while a 2% error in incident shock speed causes an error of 5 to 6% in final pressure. The importance of these basic measurements to each experiment is obvious and additional time devoted to improving their accuracy is always well spent.

In both laboratories the shock tube was evacuated with a mechanical pump to a pressure level of 1 to 5 microns before filling with the test gas. The experiments were run at about 60 minute intervals in the

Stanford shock tube and the combined leak and out-gassing rate just prior to filling was usually less than 1 micron per minute. At Ames the experiments were less frequent so that the combined leak and out-gassing rate was less than 3 microns per hour. In both laboratories the runs were always completed within minutes of filling the driven chamber. The Stanford shock tube was cleaned only after several runs while the NASA shock tube was cleaned thoroughly with acetone and cheesecloth after each run.

The test gas used at Stanford was from a commercial cylinder of Liquid Carbonic Hi-Pure N_2 with a purity of 99.996%. At Ames the gas was from a cylinder of Matheson pre-purified grade N_2 with a purity of 99.997%.

4.2 The Pressure Gauge

The pressure gauge consists of an elastic capacitive element for sensing strain and the electronic circuitry necessary to convert a capacitance change to an electrical signal. The gauge face forms the end wall of the shock tube and is directly exposed to the pressure pulse created by the gas. Since the mechanics of the gauge have been extensively discussed,[2,6] these concepts will not be repeated here. The particular pressure gauge used in the present study is a slightly modified version of the gauge described in Ref. 6.

A schematic drawing of the gauge is shown in Fig. 12 for the purpose of discussing modifications to the original gauge design. Pictures of the gauge alone and of the gauge mounted in the shock tube are presented in Figs. 13 and 14 respectively. A block diagram of the electrical

circuit is shown in Fig. 15. For details of the gauge operation the reader is directed in particular to Ref. 6 which is the final report for the NASA contract which sponsored the recent developmental work on the gauge at Stanford.

The major improvements appearing in the present version of the pressure gauge, as compared with the earlier versions, can be attributed to the use of dual electrodes (see Fig. 12) and improved gauge-construction techniques. The dual-electrode design was a result of recent investigations at Stanford[6] and Caltech[5] which showed that the pressure gauge is strongly affected by the presence of charged particles in the gas adjacent to the shock-tube end wall. For tests in argon where the incident-shock Mach number is 8 or greater, the unwanted "charge" signal can contribute as much as 50% to the total output signal; this is clearly undesirable if one is interested in precise measurements. A major portion of this "noise" signal can be eliminated by using a dielectric cover on the front face of the gauge (see Fig. 12). This cover plate must be thin in order to retain the short-time response of the gauge.

The use of dual electrodes in conjunction with a differential preamplifier allows the remainder of the noise signal to be removed since the polarity of the gauge signal owing to pressure depends on the polarity of the charging voltage while the signal owing to charged particles does not. A type G Tektronix differential preamplifier was used for much of the work presented here. Note that by charging the two electrodes with voltage of opposite polarity the noise may be removed and the gauge sensitivity increased by a factor of two.

Improvements have also been made in gauge construction practices.

The discovery of the availability of Lexan material in thin films (3 and 5 mils) has eliminated the need for hand-sanding thicker sheets of Lexan to the appropriate thickness for use as the capacitance element and the dielectric cover sheet. Use of the thin films has also required additional skill in bonding the layers of the gauge because of the susceptibility of the thin films to wrinkling and developing small pin holes. The advantages of the standard film are a substantial decrease in assembly time and an improvement in gauge uniformity. Since the sensing elements are now consistent from gauge to gauge, the sensitivity no longer varies, and time-consuming gauge calibration is not necessary.

For additional details concerning the present gauge design see Appendix E.

4.3 Experimental Results

In order to reduce experimental data, the pressure-gauge sensitivity must be established. The sensitivity is measured using known pressure steps provided by low Mach-number shock waves in the ideal-gas regime. A typical response to a pressure step is shown in Fig. 16 for two different oscilloscope sweep speeds. The gauge duplicates the square pulse of the shock wave accurately for times greater than the risetime (.2 μsec) and less than the time at which strain waves from the edges of the gauge begin to reach the sensing elements (≈ 14 μsec).

In Fig. 16a the signal is obtained with one element charged and one element grounded. The single trace represents the response of the charged element minus that of the grounded element. In Fig. 16b both elements are charged but with opposite polarity so that the pressure

responses are of opposite sign. The two traces represent the individual response of each element. The equality of the signal magnitudes for the two elements is very good. In normal operation the signal from one element is always subtracted from the other (whether one or both elements are charged) so that any noise signal is removed.

Measurement of the shock speed and the initial pressure is sufficient to fix the change in pressure level caused by shock reflection in an ideal gas. This change in pressure is plotted versus the output voltage of the pressure gauge per unit of charging voltage in order to obtain the gauge calibration factor or sensitivity. The sensitivity depends only on the capacitive-element thickness so that uniformly constructed gauges have the same calibration factor. The linearity of the gauge response is confirmed in Fig. 17 which represents the response of one particular gauge over a wide range of pressure. The lower bound of pressure measurement (for a given gauge) is determined by electronic considerations such as noise level, signal amplification, gauge charging voltage and the sensitivity of oscilloscope preamplifiers. The upper bound of pressure measurement seems limited only by the tension waves which attempt to separate the sensing element from the gauge and the structural limitations of the shock tube. Reflected-shock pressure levels of up to 400 psi have been measured without causing gauge failure.

Several experimental pressure histories for shock waves in chemically relaxing N_2 are shown in Figs. 18 and 19. In each case the flat part of the trace following relaxation corresponds within experimental error to the equilibrium pressure level, p_5^*. This was verified for each experimental run by using the gauge calibration constant and tabulated

values of p_5^* corresponding to the measured shock speed and initial pressure. The upswing on the far right of the traces in Figs. 18b and 18c is to be ignored since the upswing marks the end of the useful recording time of the gauge. The magnitude of a typical noise signal for an uncharged gauge element (in these tests) is exhibited in the lower trace of Fig. 18a; the same preamplifier sensitivity was used for both traces.

The fact that each trace becomes flat at an amplitude which corresponds to the theoretical equilibrium pressure level provides evidence that non-ideal shock-tube effects are not significantly disturbing the chemical relaxation in the center of the shock-tube flow. However, some decay in pressure level has been noted after chemical equilibrium for very strong shocks at low initial pressures; see for example Figs. 19b and 19c. This effect is due either to the onset of side-wall boundary-layer effects or to a decay in density (behind the incident shock wave) associated with the combustion process. Since similar effects have been noted by other investigators[18,19] using combustion-driven shock tubes, it is felt that a density decay is possibly present. This conclusion seems even more likely since the effect of a side-wall boundary layer would probably be to increase the pressure rather than to decrease it.

The data shown in Figs. 18 and 19 were obtained with incident shock speeds varying from 4.2 to 7.5 km/sec. Over this range of shock conditions the equilibrium gas in region 2 varies from slightly dissociated to more than half dissociated. The equilibrium gas in region 5 varies from slightly dissociated to partially ionized; e.g., the case exhibited in Fig. 19c causes some ionization in region 5. Since the theory of the

pressure history for an ionizing shock wave has not been developed here, the trace in Fig. 19c was not used for data reduction. It is interesting to include this run because the thickness of the translational shock wave is noticeably larger than the risetime of the gauge at these shock conditions. Furthermore, this trace enable one to gain a feeling for the merging of the translational, vibrational, and chemical relaxation times at strong-shock conditions. The possible utility of pressure measurements for studying shock structure can be seen.

The uncertainty in each pressure measurement can be attributed to a combination of four possible errors. The total uncertainty resulting from all of these errors rarely exceeds 10% of the pressure signal. Two of these errors involve the basic measurements of incident shock speed and initial test pressure, as discussed in Section 4.1. A third error is associated with oscilloscope performance since the vertical deflection on an oscilloscope trace is known only to within about 2%. The fourth error is the deviation between the gauge response and the actual end-wall pressure. As shown by the calibration traces of Fig. 16, such error is primarily limited to the first one or two microseconds after reflection. In the final data-reduction procedure an approximate correction was applied to help eliminate this error. In brief, the experimental voltage at a given instant after reflection was simply multiplied by the factor which was required to restore the calibration signal for that same gauge back to a square wave form. The correction factor, which varies with the time after reflection, was found to differ from one gauge to another. No information was collected during the risetime of the gauge.

The effects of the experimental uncertainty were minimized by

reducing the data in dimensionless form. Each pressure history was divided by the signal amplitude obtained from the flat portion of the same trace. These experimental pressure-ratio histories were directly compared with theoretical pressure-ratio histories without considering the absolute difference in the predicted and measured equilibrium pressure levels.

5. NITROGEN REACTION RATES

Utilizing the pressure gauge and associated equipment described briefly in the previous chapter, end-wall pressure data were obtained for a range of strong shock waves in pure N_2. About half of the final experiments were performed in each laboratory (Stanford and Ames) using the same pressure gauges and experimental techniques. In this chapter the data-reduction procedure is discussed and the measured reaction rates are presented.

5.1 Data-Reduction Technique

In order to monitor the equilibrium pressure level during each run, the experiments were designed so that chemical equilibrium was attained within the useful observation time of the gauge. This means that the relaxation time behind the incident shock wave was adjusted to be about 10 μsec or less by varying the incident shock speed and the initial shock-tube pressure. The reaction rates of N_2 were so fast at these conditions that the initial relaxation period in the reflected region was always less than the risetime of the gauge, and the observed pressure histories were a result of relaxation behind the incident shock wave only. The outer solution of Chapter 3 was therefore applicable for calculating theoretical pressure histories for given reaction rates. The correct rates were inferred by adjusting the reaction rates used in the computer program until good agreement was found between theory and experiment over a range of shock conditions.

Before proceeding to some actual comparisons of predicted and

measured results, further comments are in order regarding the reaction-rate input to the computer program. The reaction in question is

$$N_2 + M \underset{k_{r,M}}{\overset{k_{d,M}}{\rightleftarrows}} 2N + M \quad . \tag{5.1.1}$$

The collision partner, denoted by M, can be either N_2 or N for a pure gas. Therefore there are four reaction rates coupled to the gas-dynamic processes, two dissociation rates and two recombination rates. It is customary, although subject to some criticism, to relate the dissociation and recombination rates throughout relaxation by the equilibrium constant evaluated at the local translational temperature,[6,13] i.e.,

$$\left.\frac{k_{d,N}}{k_{r,N}}\right)_{noneq} = \left.\frac{k_{d,N_2}}{k_{r,N_2}}\right)_{noneq} = K(T) \quad . \tag{5.1.2}$$

These relations reduce the number of independent reaction rates to two and allow the rate equation to be written as

$$\begin{aligned} \rho \frac{D\alpha}{Dt} = {} & Wk_{r,N_2} \{K[N_2]^2 - [N]^2[N_2]\} \\ & + Wk_{r,N} \{K[N_2][N] - [N]^3\} \quad . \end{aligned} \tag{5.1.3}$$

For convenience the recombination rates are specified rather than the dissociation rates. It should be emphasized, however, that it is primarily the dissociation rates which are being measured in these

experiments since the dominant nonequilibrium phenomenon is that of dissociation. The values of the recombination rates are fixed only through the artifice of requiring the equilibrium constant to apply in a nonequilibrium situation.

The recombination rates were taken to be of the form provided by classical collision theory,

$$k_{r,N} = B_N T^{-b_N} \tag{5.1.4}$$

and

$$k_{r,N_2} = B_{N_2} T^{-b_{N_2}} ,$$

so that both the reaction rates are specified with a total of four coefficients (two B's and two b's). These four coefficients were the only parameters varied in fitting the experimental data.

It is also useful to define the ratio of the recombination rates as a relative collision efficiency,[14,20]

$$R = \frac{k_{r,N}}{k_{r,N_2}} , \tag{5.1.5}$$

which is generally temperature dependent. The rate equation may now be written as

$$\rho \frac{D\alpha}{Dt} = \{k_{r,N_2}(1+R \frac{2\alpha}{1-\alpha})\}[N_2]W\{K[N_2]-[N]^2\} \tag{5.1.6}$$

where

$$2\alpha/(1-\alpha) = [N]/[N_2]$$

is the ratio of the atomic and molecular mole fractions.

Equation (5.1.6) is written for the purpose of emphasizing the relative importance of the molecular and atomic rate contributions to the total reaction rate. The total rate is seen to be determined by the molecular rate when $R\frac{2\alpha}{1-\alpha} \ll 1$ and not simply when $R \ll 1$. Conversely, whenever $R\frac{2\alpha}{1-\alpha} \gg 1$ the atomic rate is predominant. It is through an analysis of this type that one can understand how to modify the rates when fitting experimental results. It becomes obvious, however, that the molecular rate can best be inferred through studies of weak shock waves or during the initial portion of the relaxation zones behind strong shock waves; the atomic rate can best be ascertained from strong shock waves causing large values of α early in the relaxation zone.

Although nearly thirty pressure histories were initially obtained for data reduction, it was soon clear that the labor necessary to analyze the effect of the rate coefficients on all cases was prohibitive. Thirteen different cases were finally selected as a representative sample which was uniformly distributed over the full range of experimental conditions studied. The reaction-rate coefficients were inferred from these thirteen cases only.

The data interpretation began by using the rates suggested by Byron[18] to obtain predicted pressure histories for all thirteen cases. The four rate coefficients were then varied individually in the computer program until it was clear which coefficients were most sensitive or insensitive for each experimental case. Next, using those experiments where the pressure histories were sensitive to only one or two of the four parameters, a single set of rate coefficients was eventually obtained

which consistently matched the shape of the theoretical and experimental curves as closely as possible. There was a strong tendency for the theoretical profiles to have a longer time scale than the experimental traces for weak shock waves and a shorter time scale than the measured histories for strong shock waves. This set of rates was then applied to all thirteen cases, and the effect of each coefficient was analyzed further until all four coefficients were finally fixed at those values which provided the best overall compromise between experiment and theory.

5.2 Discussion of Results

Representative pressure-ratio histories are presented in Figs. 20 through 24. On each figure are shown the experimental result and the theoretical prediction using the reaction rates finally selected as providing the best compromise fit for the thirteen cases studied. Also shown on each figure is the pressure history predicted using the reaction rates reported by Byron.[18]

A perfect fit for all cases shown is not to be expected since the kinetics model employed was taken from classical collision theory and does not consider such known complications as vibration-dissociation coupling. However, owing to the reproducibility of the pressure histories, and the agreement between results from the two shock tubes, the quality of the experimental data are considered sufficient that future work with a more realistic kinetics model would be fruitful.

The rates inferred in the present study over a temperature range of 5700 to 10000°K are

$$k_{r,N_2} = 3.0 \times 10^{32}\ T^{-4.5}\ cm^6/(mole^2\text{-}sec)$$

and

$$k_{r,N} = 1.05 \times 10^{25}\ T^{-2.5} \quad .$$

The lower bound of the temperature range specified corresponds approximately to the equilibrium temperatures behind the weakest incident shock waves studied. The upper temperature bound was fixed by the earliest stages of incident shock-wave relaxation which could be monitored for end-wall times greater than the pressure-gauge risetime ($\approx .2$ μsec). The magnitudes of these rates (i.e., $|k_{r,M}|$) are felt to be correct to within a factor of two of the classical collision-theory rates which would provide the best possible description of the relaxation process behind each of the shock waves studied. The values of the temperature exponents are considered known to within ± 2. These error bounds are conservative estimates based on the quality of the fits to the experimental pressure histories, the scatter in the reproducibility of the experimental results, and a value judgment of the range of reaction rates which would provide a reasonable fit to the data. A large uncertainty is common in reaction rate studies because of the difficulties inherent in making accurate short-duration measurements.

Through use of the equilibrium constant, these rates may also be expressed in dissociation-rate form. A simplified form of the equilibrium constant, correct within 10% over the temperature range of 5700 to 10000°K, is

$$K(T) = 20\ e^{-\theta_d/T}\ moles/cm^3 \quad .$$

The dissociation rates (corresponding to the recombination rates above) are therefore

$$k_{d,N_2} = 6.0 \times 10^{33}\ T^{-4.5}\ e^{-\theta_d/T}\ \text{cm}^3/(\text{mole-sec})$$

and

$$k_{d,N} = 2.1 \times 10^{26}\ T^{-2.5}\ e^{-\theta_d/T}\ .$$

It should be noted that the temperature exponents suggested for these reaction rates are inconsistent with the upper limits imposed by classical theory, and that extrapolation of these rates provides poor agreement with room-temperature recombination-rate data. These discrepancies are felt to be an indication of the shortcomings in the rate theory rather than in the experiments.

The emphasis during this investigation has been on obtaining good quality experimental data which could be compared with data obtained in previous incident-shock studies. This approach was stimulated by the desire to prove the utility of end-wall pressure measurements for future kinetics studies. The utility of such measurements can be proven in part if one can show that the rates which describe the pressure behavior in the reflected region are the same as those rates which have been measured in the shock-heated gas behind incident shock waves. Recall that the suitability of end-wall pressure measurements for inferring vibrational-relaxation data (which agrees with that obtained behind incident shock waves) has been shown by Baganoff[3] and Johannesen.[4] The choice of N_2 as a test gas for the present study was prompted by both

the availability of existing rate data from incident-shock studies and the practical interest in understanding the behavior of the major constituent of air.

Previous data on the dissociation rate of shock-heated N_2 have been obtained by Byron,[18] Cary,[19] and Appleton et al.[21] Both Byron and Cary inferred reaction rates by using a Mach-Zehnder interferometer to monitor density histories behind incident shock waves in diluted mixtures of N_2 and Ar or N_2 and He. Appleton inferred reaction rates by using a vacuum-ultraviolet absorption technique to monitor the disappearance of molecular nitrogen behind reflected shock waves in diluted mixtures of N_2 and Ar (the incident flow was assumed to remain chemically frozen). In recombination-rate form Byron found, for temperatures between 6000 and 9000°K,

$$k_{r,N_2} = 2.6 \times 10^{16}\ T^{-.5}\ \text{cm}^6/(\text{mole}^2\text{-sec})$$

and

$$k_{r,N} = 2.4 \times 10^{21}\ T^{-1.5} \quad .$$

The uncertainty in Byron's rates was considered to be about a factor of two. For temperatures between 8000 and 15000°K, Appleton found

$$k_{r,N_2} = (2.2 \pm .6)10^{20}\ T^{-1.6}\ \text{cm}^6/(\text{mole}^2\text{-sec})$$

and

$$k_{r,N} = (9.8 \pm 2.6)10^{20}\ T^{-1.6} \quad .$$

Fig. 25 presents a comparison between the recombination rates suggested by Byron,[18] Appleton[21] and the present study. The present study provides good agreement with Byron's rate for an atomic third body while some discrepancy is noted for the rate with a molecular third body. The atomic rates of these two investigations differ by less than a factor of two throughout the temperature range mutually considered. The molecular rates predicted by Byron and the present study differ by a factor of seven at 6400°K but are within a factor of two at 9000°K. There is a sizeable difference in the value of the relative collision efficiency; Byron predicts a value of R varying from about 14 to 11 over the temperature range specified while this study predicts a value which varies from about 1.5 to 3.

Appleton's results have only recently been presented and a detailed analysis of his work has not been made. It appears, however, that his rates are substantially smaller than either those of Byron or the present study. In the narrow temperature region where the different studies overlap, Appleton's rate with N_2 as a collision partner is about 1/3 that of Byron's rate and about 1/5 that of the present study. For the same temperature range the magnitude of Appleton's rate with N as a collision partner is about 1/6 that of Byron's rate and about 1/3 that of the rate presented in this study.

Measurements very similar to Byron's have been presented by Cary.[19] However, Cary's results were criticized by Wray and Byron[22] and later modified.[23] The exact results of Cary's work are not clear since several different sets of reaction rates have been proposed to fit his data;[19,22,23] it can only be stated that his measurements provide reaction

rates with magnitudes of the same order as those presented in Fig. 25.

It should be emphasized that all of the experiments in the present investigation were performed in pure N_2 while Byron, Cary and Appleton were essentially restricted to highly diluted mixtures of N_2 and Ar or N_2 and He. Six parameters were therefore necessary to fit their data while only four are involved in a pure N_2 study. It is certainly more difficult to infer the reaction rate (and especially the temperature dependence) for N or N_2 as a collision partner when the majority of the particle collisions occur with the inert species. If one uses a diluted mixture and wishes to ascertain the rates with N or N_2 as the collision partner, the dissociation rate for collisions with the inert species would first have to be accurately known. However, the magnitude of the revised rate for Ar reported by Cary[23] differs by about a factor of two from Byron's stated value, and Appleton's rate for Ar differs by about a factor of three from that given by Byron. Although a few runs were obtained in pure N_2 by both Byron and Cary, the range of shock conditions was extremely narrow. In the present investigation a wide enough range of shock conditions has been employed to obtain conditions wherein each of the two dissociation rates is singularly important as well as conditions where both rates are simultaneously important.

The practical importance of studying the reaction rates which apply in a pure gas is obvious. Most often, it is the rates for a pure gas which are required in the calculations of actual gasdynamic flow problems. It follows that if successful experiments can be performed in pure gases, the measured rates should provide a more accurate description of the gas

behavior than that given by rates measured in diluted gases.

There is another strong argument to support studies of pure gases. Since the reaction rates which apply during relaxation are temperature dependent, one would like to observe large temperature variations within each relaxation zone in order to fix the correct temperature dependence, and the temperature variation behind a shock wave in a pure gas is greater than that with a diluted gas. Furthermore, the chemical description of a gas which applies far from equilibrium can be more realistically inferred if one can observe accurately the nonequilibrium behavior of a pure gas.

One puzzling aspect of comparing the rates measured in this investigation with those of other investigations is the disagreement in the molecular rate. One would imagine that the concept of reflected-shock testing using the outer solution would be least valid for strong shock waves. However, such shock conditions were paramount in determining the atomic rate presented here, and the atomic rates of Byron's study and the present work are in good agreement. At lower shock speeds, where the molecular rate is influential throughout each pressure history, the outer solution should be at its best, but the molecular rate of the present study differs noticeably from Byron's rate. Further experiments are definitely in order to investigate the discrepancy in the molecular rate magnitude and temperature dependence. However, the rates obtained in this study are certainly in sufficient agreement with Byron's measurements to justify future use of the pressure measurement technique.

It should be noted that while the atomic rate presented here is smaller than Byron's rate, the molecular rate presented is larger than

his value. Therefore the total rates may often be similar, and it is the total rate which determines the predicted profiles. This is the reason for the good agreement between the predicted profiles shown in Figs. 22 through 24, even though the individual rates of the two studies differ. The similarity of these predicted histories points out the difficulties of ascertaining the correct rates when several coefficients are simultaneously important. The proper rate parameters can only be inferred by studying the relaxation processes over a range of shock conditions such that the effects of the various coefficients can be essentially isolated. The discrepancies between pressure histories predicted with Byron's rates and with those of this study are much larger for the slow shock-speed cases shown in Figs. 20 and 21. The difference in the predicted results is most apparent in these cases because the molecular rate determines the profiles for weak shock waves.

The effects of changing the rate parameters from the values finally selected in the present study are also exhibited in Figs. 20 through 24. The effect of doubling B_{N_2} while holding the other three coefficients fixed is shown in Fig. 20. Fig. 21 exhibits the effect of changing b_{N_2} from 4.5 to 2.0 (the value of B_{N_2} was also adjusted in order to provide the same rate magnitude at 6400°K). Variations in the atomic-rate parameters were found to have very little effect on the profiles of these two cases. Therefore these particular experiments were especially influential in fixing the molecular-rate coefficients. The profile variations introduced by changing b_N from 2.5 to .5 and by doubling B_N are shown in Figs. 23 and 24 respectively. Variations in the molecular-rate coefficients had little effect on the pressure history of Fig.

24 except at very short times. Therefore this experiment was especially influential in fixing the atomic-rate coefficients. Figs. 22 and 23 represent cases where both rates are relatively important in the profile calculations. The variations in the predicted profiles for specified changes in the rate coefficients provide considerable insight into the accuracy of the rate coefficients finally selected and the importance of each rate in a given experiment.

It should be remembered that the final rate coefficients were not selected only on the basis of the profiles shown here, and that 13 different pressure-ratio histories were employed in the selection. It is true, however, that some experiments were more important than others in fixing the rates. For example, if one were to utilize only Figs. 22, 23 and 24, Byron's rates certainly provide a satisfactory fit to the experimental data. However, cases of the type shown in Figs. 20 and 21 require a much faster rate with N_2 as the collision partner, and a different temperature dependence than given by Byron. If Byron's molecular rate was increased in order to fit these weak shock cases, then his atomic rate would have to be reduced in order to maintain the correct total rate required to fit the moderate and strong-shock cases. The result of these rate modifications would be rates similar to those predicted here. The importance of utilizing a wide range of shock conditions is again apparent if all four coefficients are to be properly selected. For a narrow range of shock conditions, incorrect coefficients can be chosen even though a good fit to the data is obtained.

The possible effect of impurities on the experimental results should also be mentioned. Byron cited no noticeable effect owing to

impurities. Although the cleanliness and leak rates of the shock tubes employed here were comparable with those of Byron's study, his initial pressures were higher by about a factor of ten. The ratio of the number of impurities to the number of test gas particles is thus larger by about a factor of ten for the present study although this ratio is still less than 1% for the extreme cases. The reproducibility of results using two different shock tubes with different cleaning procedures and leak rates was taken as evidence in the present investigation that impurities play a minor role.

It is concluded that the measurement of the short-time pressure behavior on the center of a shock-tube end wall presents a promising technique for future chemical-kinetics studies. The accuracy of the method is sufficient that work including the effects of vibration-dissociation coupling seems feasible. The pressure-gauge technique shows particular potential because it is not restricted to a narrow range of shock conditions (as are some optical techniques, for example) and because of the time resolution which is possible. The agreement of the N_2 reaction rates measured in this study with those of Byron's study is good when one considers the difficulties of making accurate measurements and the typical scatter between rates measured in different investigations. Further work should be done, however, to investigate the temperature dependence of the rate with a molecular collision partner.

6. SOLUTION FOR THE END-WALL THERMODYNAMIC STATE

In Chapter 3 an approximate technique was developed for predicting end-wall pressure histories during shock-wave reflection in a chemically relaxing gas. It is shown here that once a pressure solution has been formulated the time evolution of other end-wall thermodynamic properties can be readily obtained; that is, for a given set of reaction rates, the complete history of the end-wall thermodynamic state can be calculated. The validity of the technique is confirmed by comparing results with those of the Ames computer program.

The importance of obtaining end-wall solutions for thermodynamic variables in addition to pressure is twofold. First, the ability to calculate the complete gas state as a function of the reaction rates provides additional possibilities for inferring the rates from experimental measurements. Second, and of special interest to those studies which assume the reflected region contains a uniform gas, the thermodynamic histories provide information on both the length of time required for the gas to relax and the particular equilibrium state finally attained. These final properties provide limiting values for the thermodynamic non-uniformities present in the entropy layer adjacent to the end wall.

6.1 Calculational Technique

The time evolution of the end-wall properties is calculated by applying the energy equation for one-dimensional adiabatic flow,

$$\rho \frac{D}{Dt} \left(h + \frac{1}{2} u^2 \right) - \frac{\partial p}{\partial t} = 0 \quad , \tag{6.1.1}$$

to the small element of gas located adjacent to the end wall. This gas element follows a known particle path $(x=0)$ in the x-t plane. For this particular trajectory the velocity is identically zero and the energy equation reduces to

$$\rho \left.\frac{\partial h}{\partial t}\right)_{x=0} = \left.\frac{\partial p}{\partial t}\right)_{x=0} \quad . \tag{6.1.2}$$

The enthalpy of a dissociating homonuclear diatomic gas can be expressed as an explicit function of the translational temperature and the mass fraction of the atomic species; that is,[8]

$$h = \frac{7+3\alpha}{2} RT + (1-\alpha) \frac{R\theta_v}{\exp(\theta_v/T)-1} + (1-\alpha)h_{el,A_2} + \alpha h_{el,A} + \alpha D \quad , \tag{6.1.3}$$

where h_{el} refers to the contribution of the electronic energy. Two more relations are also available along the end-wall particle path, the thermal equation of state,

$$p = \rho RT(1+\alpha) \quad ,$$

and the reaction rate equation (5.1.3). The pressure solution is assumed known by the techniques of Chapter 3.

The calculational procedure consists of a simple numerical integration. The initial state in the reflected region is found from calculations which assume frozen chemistry and instantaneous equilibrium of the internal energy modes with the translational temperature. Using the known solution for pressure, the values of h and α at time

$t = \delta t$ can be computed using equations (6.1.2) and (5.1.3) respectively; e.g.,

$$\alpha(\delta t) = \alpha(0) + \frac{D\alpha}{Dt}(0)\,\delta t \quad .$$

Knowledge of h, p, and α at $t = \delta t$ is sufficient to fix the values of T from equation (6.1.3) and ρ from the thermal equation of state. The new conditions are used to establish a numerical value for the reaction rate at time $t = \delta t$. The calculations continue until the final pressure (p_5^*) is reached; at that time an equilibrium state will have been attained.

The results to be presented here were obtained with a computer program so that a large number of shock conditions could be studied. The only approximations in the analysis (other than the kinetics model chosen) are the simplifying assumptions which were made in establishing the pressure solution. Since the relaxation processes on the end wall depend primarily on the reaction rates and are only weakly coupled to pressure, the solutions obtained here should be in excellent agreement with more exact theory.

For short times after reflection steep gradients are present in the thermodynamic variables since the dissociation rate is faster at the frozen temperature than at the equilibrium temperature. The steepness of these initial gradients prompted the use of a non-uniform step-size in the integration process in order to optimize computing time and to minimize errors.

An alternative approach for computing the thermodynamic histories

is possible by integrating entropy rather than enthalpy. The entropy technique was used in the initial phases of this work but was found to be more complex and to require more computing time than the procedure suggested here.

6.2 Discussion of Results

Figs. 26 and 27 provide comparisons of end-wall histories in O_2 calculated with the present model and the NASA program.[1] These are the same shock cases used for comparisons of the inner and outer pressure solutions. The agreement with the more exact calculations is remarkable, especially when one considers the difference in computing time (several hours for the NASA program as against less than a minute for the present model). It is important to note that the NASA results stop short of steady-state conditions so that values are not obtained for the final end-wall properties; the simple model obtains this information quite readily. Since both calculational techniques utilize integration procedures, some numerical error is caused by finite step-size. This error was investigated in the present study and an integration step-size was selected for each shock condition such that the error in the end-wall properties is small.

As noted previously, the NASA program does not include electronic excitation. The model used in the present study was altered for the cases shown in Figs. 26 and 27 in order to provide a fair comparison with the NASA work. Since oxygen has relatively low-lying atomic and molecular electronic-energy levels, these should have been considered at temperatures high enough to cause dissociation. The effect of this

omission on the wall histories is to change the initial and final values of all properties; the shape and time scale of the profiles are not significantly affected.

End-wall results (with electronic excitation included) are presented in Figs. 28 through 35 for shock waves in O_2 and N_2. The reaction rates used are the same as those employed in Chapter 3 to obtain composite pressure histories. The results are presented in dimensionless form with respect to the reference equilibrium conditions (given by calculations using the equilibrium reflected-shock speed). Because of the entropy layer, the final thermodynamic properties differ from the reference conditions. Values for the reference states in O_2 and N_2 are given in Figs. 36 through 43 (see also Refs. 24 and 25). The frozen reflected state (5F) and the state given by ideal-gas calculations with $\gamma = 1.4$ are also shown on these figures.

It should be remembered that these end-wall histories were computed assuming that vibrational-relaxation times and translational-shock thicknesses were zero. A realistic consideration of these effects would certainly modify the short-time behavior of the results presented.

The time scale of the profiles in Figs. 28 through 35 depends strongly on the reaction rates chosen. The effects of changing the rates can be understood as follows. If the temperature dependence remains unchanged, doubling the magnitudes of both the molecular and atomic recombination rates causes each point along an end-wall history to be reached in half the time that was required with the original rates. To make this comment plausible for a long time scale, consider the incident shock-wave region alone. Since all the properties at any one

position in the relaxation zone, except distance from the shock wave, are coupled through the rate-independent conservation equations, doubling the reaction rates at all temperatures simply shortens the relaxation profiles by exactly a factor of two.[20] Since the end-wall time scale is directly coupled to the incident-shock time scale, all end-wall variations are also shifted in time by a factor of two.

The effect of the rate magnitudes for short end-wall times is more obvious. Doubling the rates clearly doubles the rate of change of p and α as shown by the inner solution for pressure and the rate equation for α. Since the rate of change of h is linearly coupled to the rate for pressure, only half as much time is needed to reach the same values of p, α and h as before. This fixes T and ρ at their previous values as well so that all the profiles are uniformly shifted in time by a factor of two.

It may also be observed that if only the molecular rate is doubled, while the atomic rate remains at its original value, the initial part of the end-wall profiles will still be shifted in time by a factor of two. The effect on the remainder of the profiles depends on the relative size of the atomic and molecular rates as well as the relative number densities of atoms and molecules. For weak shocks causing small amounts of dissociation (so that most collisions are with molecules), the overall time scale is controlled primarily by the magnitude of the molecular rate. For strong shocks where the gas is significantly dissociated, the atomic rate usually dominates except during short times after reflection.

The effects of changes in the temperature dependence of the rates are essentially confined to the early stages of relaxation where the

nonequilibrium temperatures differ most from the equilibrium values. The temperature dependence has little effect on the overall time scale of the profiles since the relaxation time τ_{2L} is primarily determined by the rate magnitudes corresponding to incident-shock equilibrium conditions.[20]

It is also of interest to plot the final end-wall states for a range of shock conditions since these properties provide an upper bound on the thermodynamic non-uniformities within the entropy layer. Fig. 44 presents dimensionless results in O_2 and N_2 using the same reaction rates employed in Figs. 28 through 35, although the results are very nearly independent of the rates. This is because the entropy layer is primarily caused by differences in the initial energy and in the work added along each adjacent particle path in region 5 and only secondarily by the rate at which the particles adjust to their changing environment.

Another important parameter is the spatial extent of the entropy layer. If one defines a relaxation length behind the incident shock wave, L_2, then the entropy-layer thickness in region 5 is approximately given by

$$L_5 \approx L_2\left(\frac{V_r^*}{V_r^* + V_s}\right) .$$

The entropy-layer thickness and an entropy-layer formation time are shown schematically in Fig. 45. The relaxation length in the incident zone is defined here to be the distance at which the atomic mass fraction reaches 90% of its equilibrium value. Values for the entropy-layer thickness and formation time as well as the incident-shock relaxation

length are shown in Figs. 46 and 47 for chemically relaxing O_2 and N_2.

In conclusion, the procedures outlined here are not restricted to homonuclear diatomic gases. The technique should be of value in predicting end-wall histories for other chemical reactions and for other forms of relaxation phenomena whenever an end-wall pressure solution can first be established.

7. SIMPLE MODEL FOR CALCULATING THE FINAL END-WALL PROPERTIES IN A RELAXING GAS

The previous chapter presented results for the time evolution of the state of the gas adjacent to the end wall, including results for the final gas state attained. The integration technique required previous knowledge of the end-wall pressure solution. This chapter introduces a simple model which allows one to calculate the final end-wall properties in chemically or vibrationally relaxing gases without knowledge of either the relaxation rate or the pressure solution. The model is suitable for either hand or machine computations.

7.1 Calculational Technique

The overall reflection process should again be viewed in the x-t plane. Immediately after reflection the shock begins to change speed due to the combined effects of relaxation in 2 and 5. Eventually, the incident-shock flow becomes uniform and the reflected shock attains an equilibrium speed. The gas particles which pass through the unsteady reflected shock wave have entirely different particle histories and entropy levels than those which pass through the steady reflected shock wave; as a result different equilibrium states are attained than those predicted by the steady-shock calculations. The region containing this non-uniform gas is called an entropy layer. This terminology is consistent with that used to describe the region adjacent to the surface of a wedge in steady supersonic flow of a relaxing gas.

After the reflected shock reaches its equilibrium speed, the flow

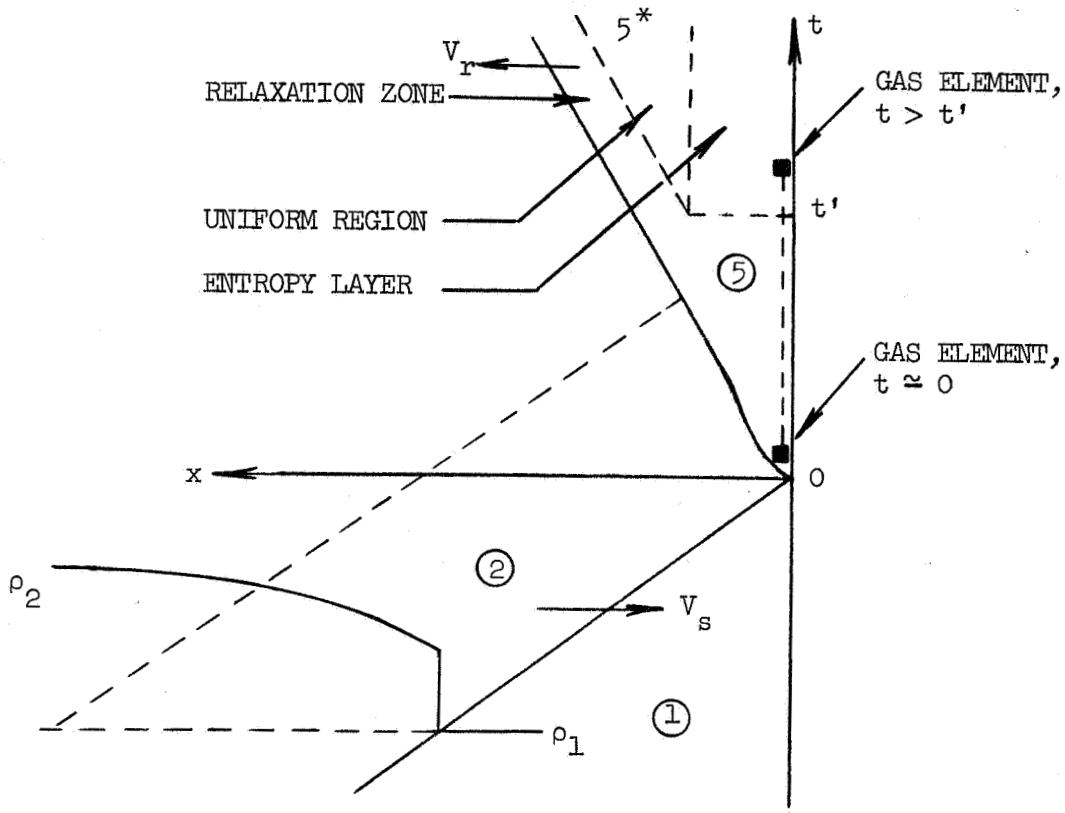

field in 5 may be crudely divided into three different regions; a constant length relaxation zone following directly behind the reflected shock, a steadily growing intermediate region with uniform equilibrium properties, and the stationary entropy layer adjacent to the end wall. As shown on the figure above, the thickness of the entropy layer is scaled by the incident-shock relaxation length.

The state of the gas in the uniform equilibrium region, denoted by 5^*, can be found from real-gas tables or by using standard calculations; the frozen state at time zero, denoted by 5F, can also be found using standard calculations. Determination of the final condition of the gas on the end wall, denoted by 5', is the subject of this chapter.

Consider the element of gas adjacent to the end wall. Applying the First Law of Thermodynamics for an adiabatic process, the change in the internal energy of this element between the initial and final states is equal to the work done on the gas element. The work is given by the area under the curve traced in the pv plane.

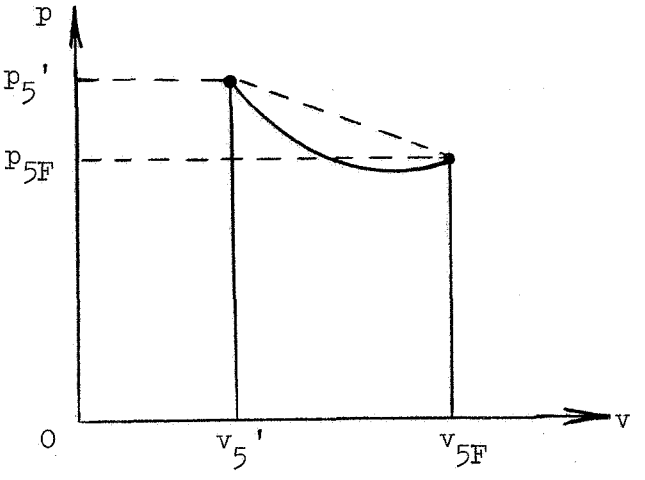

The value of p_5' is known, since it must equal p_5^*. The value of v_5' and the particular path of the curve in the pv plane are not known a priori since the compressional process is not isentropic. The work done on the gas may be written as

$$\Delta w = p_{5F}(v_{5F}-v_5') + \frac{1}{2}(p_5'-p_{5F})(v_{5F}-v_5')\epsilon \qquad (7.1.1)$$

where the only unknowns are v_5' and ϵ, a factor allowing for the curvature of the path in the pv plane. Since $(p_5'-p_{5F})$ is often

considerably less than p_{5F}, an approximate value for ϵ is usually satisfactory for calculating the "triangular area" contribution to the work. Experience with the end-wall histories of Chapter 6 indicates that an ϵ value of $1/3$ to $1/2$ provides correct results for the final gas state. A value of $1/3$ has been used throughout most of the work presented here. The particular value of ϵ chosen becomes more important as the shock strength increases. For weak shock waves causing only moderate amounts of relaxation the value of ϵ may even be set equal to 1 for convenience without introducing significant error in the final properties.

For a value of $\epsilon = 1/3$ the equilibrium internal energy is given by

$$e_5' \approx e_{5F} + p_{5F}(v_{5F}-v_5') + \frac{1}{6}(p_5'-p_{5F})(v_{5F}-v_5') \qquad (7.1.2)$$

where the only unknown is v_5'. Since the properties at $5'$ are in equilibrium, specification of any two thermodynamic variables is sufficient to determine all others, e.g., through a state relation of the type

$$e_5' = e(p_5', v_5') \quad . \qquad (7.1.3)$$

The correct final conditions can be established by iterating on the variable v_5' until agreement is obtained for e_5' between equations (7.1.2) and (7.1.3).

7.2 Discussion of Results

Dimensionless results for the final end-wall state in vibrationally relaxing CO_2, O_2 and N_2 are presented in Fig. 48. Reference equilibrium conditions for CO_2 are presented in Ref. 26. Because the pressure doesn't change across these entropy layers, the dimensionless temperature and density variations are equal in magnitude but opposite in sign (as required by the thermal equation of state for a single species gas). The results do not depend on initial pressure over typical shock-tube conditions. The curves are ended near $M_s = 10$ since chemical relaxation becomes the dominant nonequilibrium phenomenon for stronger shock waves.

Results for chemically relaxing O_2 and N_2 are presented in Figs. 49 and 50. These curves are ended at Mach 15 and 20 respectively since the gas in region 5 is then essentially fully dissociated, and the temperatures are nearly high enough to cause ionization. Since ionization effects were not included in the analysis, there is a range of shock conditions near the upper limits of these curves wherein the energy added to the entropy layer is absorbed almost entirely by an atomic gas. Because the heat-sink effect of dissociation energy is no longer acting to reduce the temperature change for a given energy addition, the work done on the gas provides large variations in temperature and density. The effect of including ionization in the analysis for slightly higher Mach numbers would be to reduce the magnitudes of the temperature and density curves and to cause new increases in the internal energy curves.

Some comments should be made concerning the range of shock speeds for which both vibrational and chemical entropy-layer results are

presented. For shock waves which cause chemical nonequilibrium, there will always be both vibrational and chemical relaxation. It is assumed here that these effects are not coupled, and that the time scale of vibrational relaxation is always much less than that of chemical relaxation. In the real case there will be a short period of time after reflection in which a vibrational entropy layer will be formed while the chemistry is still essentially frozen. For longer times a chemical entropy layer will be formed with a larger spatial extent than that of the vibrational layer. An observer interested in times of the order of the chemical-layer formation time would probably be unable to discern the vibrational layer. The assumption is thus made, over the range of shock conditions where chemical nonequilibrium occurs, that vibrational entropy-layer results are valid only for times much less than the formation time of the chemical entropy layer.

In conclusion, the magnitudes of entropy-layer non-uniformities are seen to be large enough to deserve consideration in some experiments which ordinarily assume that the gas in the reflected region is uniform. The simplicity of this calculational scheme makes it possible to consider such non-uniformities without resorting to a computer program (as in Chapter 6). Furthermore, a comparison of the results in Figs. 49 and 50 with those of Fig. 44 shows that the accuracy of this simple technique is very good.

8. SUMMARY

The problem of shock-wave reflection in a chemically relaxing diatomic gas has been investigated in detail. The results of this study extend our present understanding of the character of reflected flow fields in non-ideal gases and establish a new technique for inferring chemical reaction rates from experimental measurements in a shock tube.

It was shown that the end-wall pressure in a chemically relaxing diatomic gas is characterized by two different time scales. The separation in these time scales allows formulation of simple inner and outer solutions for the wall pressure which are in excellent agreement with more exact calculations.

A fast-response pressure gauge was used to obtain end-wall pressure histories in two different shock tubes for chemically relaxing N_2. The pressure gauge was modified from previous designs to include dual sensing elements; this eliminated difficulty with noise signals which arose whenever charged particles were present in the gas. Extensive work was done to increase the uniformity of the gauges and to reduce the length of time necessary to construct each gauge. The result of the modified design and increased uniformity is a reliable pressure-gauge response over a spectrum of shock conditions and electron densities.

The dissociation rates of shock-heated N_2 were inferred from pressure measurements by using the outer solution for end-wall pressure. The rates obtained were compared with those previously reported by Byron and Appleton on the basis of other measurement techniques. In each study the data were reduced using a rate form of the type suggested by classical

collision theory when vibration-dissociation coupling is ignored. Good agreement with Byron's work was found for the rate applying with N as a collision partner, but some disagreement was noted for the rate applying with N_2 as a collision partner. Some of the difference between the rates specified in the three studies is felt to be a result of the fact that Byron and Appleton tested in diluted mixtures of N_2 while the present study utilized pure N_2. Arguments were presented for the advantages of testing in pure N_2 when the rates of interest are those with N and N_2 as collision partners. The accuracy of the pressure measurement technique is sufficient that further studies using a more realistic model of the reaction kinetics, e.g., a model including vibration-dissociation coupling, would be fruitful.

The ability to calculate the end-wall pressure for given reaction rates was also used to calculate the time evolution of other end-wall thermodynamic properties. Calculated results were presented for pressure, temperature and density in chemically relaxing O_2 and N_2. The results were shown to agree very closely with calculations performed at Ames Research Center, although the simple model requires only a small fraction of the computing time needed by the Ames program.

One result of a reflected shock wave moving into a non-uniform gas was shown to be the formation of an end-wall entropy layer which persists after the unsteady portion of the shock-reflection process is completed. The width of this layer is scaled by the incident-shock relaxation length. The thermodynamic variations within the entropy layer were shown to be significant for some shock-tube studies which assume a uniform test gas throughout the reflected flow field. Calculated results

were presented for the thermodynamic non-uniformities and the spatial extent of the entropy layers caused by vibrational or chemical relaxation in O_2, N_2 and CO_2.

The theory developed in this investigation should be of use in predicting the character of reflected flow fields for other chemical reactions than those studied here and for other types of relaxation phenomena. The experimental techniques developed using the fast-response pressure gauge seem especially valuable since the gauge is equally useful over a wide range of shock conditions. The pressure gauge also shows promise as a means of obtaining transient information during other unsteady flow processes which occur on the microsecond time scale.

APPENDIX A

A Review of Shock-Wave Reflection in an Ideal Gas

It is useful to review shock-wave reflection in an ideal gas before considering reflection in a non-uniform gas. In ideal shock reflection a normal incident shock wave reflects from a plane non-heat conducting wall into an ideal gas (specific heats are not functions of temperature). The overall gasdynamic process can best be visualized in the x-t plane shown below.

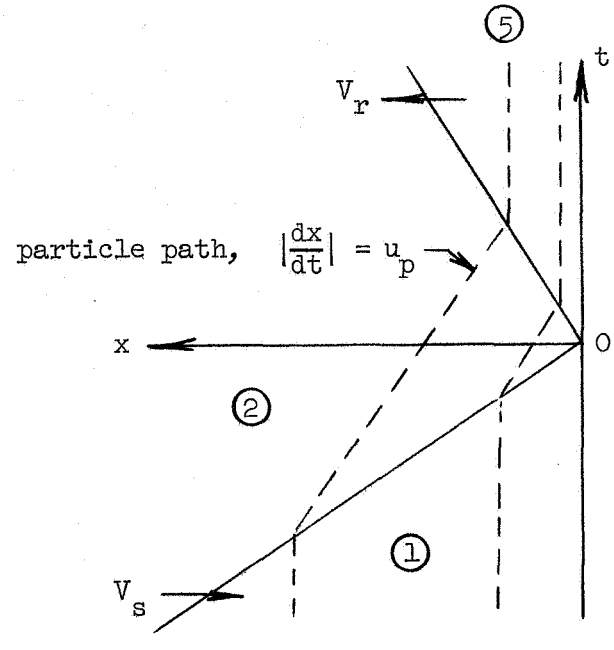

The coordinate x refers to distance from the shock-tube end wall while the coordinate t refers to the time after reflection. The incident shock wave proceeds with speed V_s toward the uniform stationary test gas in region 1 and processes the gas to a uniform state 2 given by

the following standard ideal-gas relationships:[12]

$$M_s = V_s/a_1 \tag{A.1}$$

$$\rho_{21} = \rho_2/\rho_1 = \frac{(\gamma+1)M_s^2}{(\gamma-1)M_s^2 + 2} \tag{A.2}$$

$$P_{21} = p_2/p_1 = 1 + \frac{2\gamma}{\gamma+1}(M_s^2-1) \tag{A.3}$$

and

$$T_{21} = p_{21}/\rho_{21} \quad . \tag{A.4}$$

The reflected shock wave moves away from the end wall with speed V_r but toward the gas in region 2 at a relative speed V_r+u_p, where u_p is the speed of the incident-shocked particles in laboratory coordinates. The reflected shock properties are best defined in terms of the reflected-shock Mach number,

$$M_r = \frac{V_r+u_p}{a_2} = \frac{V_r}{a_2} + \frac{V_s}{a_2}\left(\frac{\rho_{21}-1}{\rho_{21}}\right) \quad , \tag{A.5}$$

so that

$$\rho_{52} = \frac{(\gamma+1)M_r^2}{(\gamma-1)M_r^2+2} \tag{A.6}$$

$$p_{52} = 1 + \frac{2\gamma}{\gamma+1}(M_r^2-1) \tag{A.7}$$

and

$$T_{52} = p_{52}/\rho_{52} \quad . \tag{A.8}$$

Defining the Mach number of the incident-shock flow in shock-fixed coordinates,

$$M_2 = u_2/a_2 = M_s/\rho_{21}a_{21} \quad , \tag{A.9}$$

then M_r can be related to M_s using the identity

$$M_2 M_r \equiv 1 \quad . \tag{A.10}$$

This simple relation allows use of standard ideal-gas tables[12] in computing the ideal reflected-shock state.

APPENDIX B

Reaction-Rate Relations Behind Incident Shock Waves

If one uses a coordinate system attached to the incident shock wave, the pressure downstream of the shock wave is given by[12]

$$p_2 = p_1 + \rho_1 V_s^2 \, (1-1/\eta) \qquad \text{(B.1)}$$

where

$$\eta = \rho_2/\rho_1 = V_s/u_2 \quad .$$

Differential changes in pressure can be written in the form

$$dp_2 = u_2^2 \, d\rho_2 \quad . \qquad \text{(B.2)}$$

Neglecting p_1 for the strong shock waves of interest in chemical relaxation studies, equation (B.1) may be rewritten as

$$p_2 \approx u_2^2 \, \rho_2 \, (\eta-1)$$

so that dimensionless pressure variations are related to dimensionless density variations by

$$\frac{dp_2}{p_2} \approx \frac{d\rho}{\rho_2} \, (\eta-1)^{-1} \quad . \qquad \text{(B.3)}$$

Following a unit mass of gas through the relaxation zone, the First Law of Thermodynamics for an adiabatic flow yields

$$dh = v\,dp \quad .$$

Furthermore, h can be written as a function of T and α for a diatomic gas so that

$$v\,dp = \left(\frac{\partial h}{\partial T}\right)_{\alpha} dT + \left(\frac{\partial h}{\partial \alpha}\right)_{T} d\alpha \quad . \tag{B.4}$$

The subscript 2 is taken as understood and will not be used in the remainder of the equations presented. Recalling the differential form of the thermal equation of state for a diatomic gas,

$$\frac{dp}{p} = \frac{d\rho}{\rho} + \frac{dT}{T} + \frac{d\alpha}{1+\alpha} \quad , \tag{B.5}$$

one may use equations (B.3) and (B.4) in order to rewrite equation (B.5) in the form

$$\frac{d\rho}{\rho}\left\{1 - \frac{1}{\eta-1}\left[1 - \frac{R(1+\alpha)}{(\partial h/\partial T)_{\alpha}}\right]\right\} \approx \frac{d\alpha}{1+\alpha}\left[\frac{(\partial h/\partial \alpha)_{T}(1+\alpha)}{T(\partial h/\partial T)_{\alpha}} - 1\right] . \tag{B.6}$$

Neglecting electronic excitation one can write h as

$$h = (1-\alpha)(7/2\ RT + e_{v}) + \alpha(5RT + D)$$

where R is the gas constant, D is the dissociation energy, and e_{v} is the vibrational energy, all per unit mass of molecules. Since the vibrational energy is given by[8]

$$e_v = \frac{R\theta_v}{\exp(\theta_v/T) - 1} \quad ,$$

then

$$\frac{de_v}{dT} = R\left(\frac{\theta_v}{T}\right)^2 \frac{\exp\ \theta_v/T}{[\exp(\theta_v/T) - 1]^2}$$

which is very nearly equal to R for cases of interest to chemical nonequilibrium studies (i.e., $T > \theta_v$). To this approximation one finds

$$\left(\frac{\partial h}{\partial \alpha}\right)_T = -\ (7/2\ RT + e_v) + 5RT + D$$

and

$$\left(\frac{\partial h}{\partial T}\right)_\alpha \approx 9/2\ R \quad .$$

If the last two equations are substituted into (B.6), together with the assumption that $\alpha \ll 1$ (recall that immediately behind the shock wave $\alpha \equiv 0$), then changes in density are related to changes in α by

$$\frac{d\rho}{\rho}\left[1 - \frac{7}{9}\frac{1}{\eta - 1}\right] \approx d\alpha\ \frac{2}{9}\ \psi(T) \qquad \text{(B.7)}$$

where

$$\psi(T) = \theta_d/T - 3 - e_v/RT$$

and $\theta_d = D/R$ is the characteristic temperature for dissociation. Noting that

$$\frac{d\rho}{\rho} = \frac{d\eta}{\eta} \quad ,$$

and using substantial derivatives, one can rewrite equation (B.7) in the form

$$\frac{D\eta}{Dt} \approx \frac{2}{9}\,\eta\,\psi(T)\left[1 - \frac{7}{9}\,\frac{1}{\eta-1}\right]^{-1}\frac{D\alpha}{Dt} \quad . \tag{B.8}$$

APPENDIX C

Reaction-Rate Relations Behind Reflected Shock Waves

For a unit mass of gas undergoing adiabatic flow along the end-wall particle path in the x-t plane, changes in enthalpy are given by

$$dh = vdp \quad . \tag{C.1}$$

The subscript 5 is understood throughout this section. The differential enthalpy for a diatomic gas is approximately (see Appendix B)

$$dh \approx (9/2\ R)dT + (3/2\ RT + D - e_v)d\alpha \quad . \tag{C.2}$$

Using equations (C.1) and (C.2) in conjunction with the differential form of the thermal equation of state, for $\alpha \ll 1$ (recall that immediately after reflection $\alpha \equiv 0$) one obtains

$$\frac{d\rho}{\rho} \approx \frac{dp}{p}\frac{7}{9} + d\alpha\frac{2}{9}(\theta_d/T - 3 - e_v/RT) \quad . \tag{C.3}$$

Defining the notation

$$\xi = \rho_5/\rho_1 \quad ,$$

and noting that

$$\frac{d\rho}{\rho} = \frac{d\xi}{\xi} \quad ,$$

then the relation between the changes in density and changes in α along the end-wall particle path can be written as

$$\frac{D\xi}{Dt} \approx \xi\left[\frac{7}{9}\frac{1}{p}\frac{Dp}{Dt} + \frac{2}{9}\frac{D\alpha}{Dt}\psi(T)\right] \qquad (C.4)$$

where

$$\psi(T) = \theta_d/T - 3 - e_v/RT$$

and θ_d and e_v are defined in Appendix B.

APPENDIX D

Comparison of End-Wall Pressure Calculations

The simplified x-t diagram shown in Chapter 3 is repeated below.

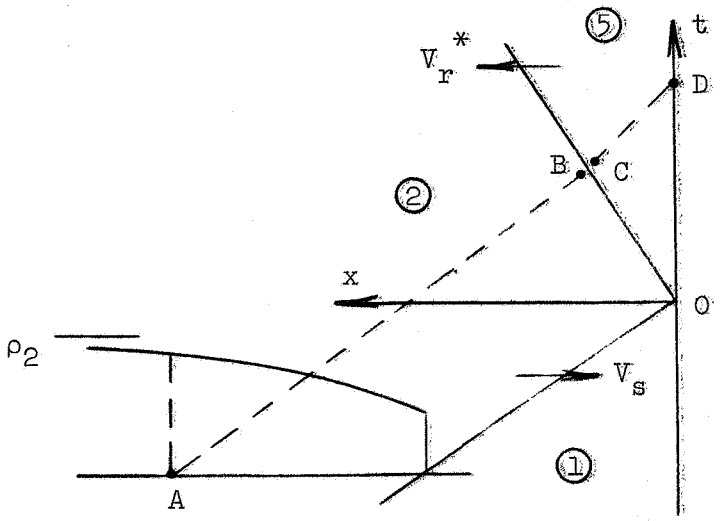

For given thermodynamic conditions at point A, the object is to calculate the end-wall pressure at point D. Neglecting the thickness of the relaxation zone behind the reflected shock, and assuming a constant equilibrium speed for the reflected shock wave, the shock-jump conditions are first assumed to be those which bring the gas to an immediate state of chemical equilibrium at point C. In this case the pressure at C is given by

$$(p_5)_C = p_2 + \rho_2(u_p + V_r^*)^2(1-1/\lambda)$$

where u_p is the laboratory speed of the gas at point B, V_r^* is the equilibrium value for the reflected shock speed, and

$$\lambda = (\rho_5/\rho_2)_C = \left(\frac{u_p+V_r^*}{V_r^*-u_5}\right)_C .$$

All velocities are referred to laboratory coordinates and taken to be positive, except u_5 which may be either positive or negative since the gas in region 5 may move away from or toward the end wall.

To zeroth order the pressure on the end wall at D is simply $(p_5)_C$. To first order the pressure is

$$(p_5)_D = (p_5)_C + \delta p_5 ,$$

where

$$\delta p_5 = (-\rho_5 u_5 a_{5F})_C$$

is a small correction due to the curvature of the characteristic along which the pressure wave propagates. If u_5 is negative the pressure at the end wall is greater than that at the shock wave.

A simpler method of obtaining the end-wall pressure is to assume the shock-jump condition is that which brings the gas immediately to rest. In this case the end-wall pressure at D is the same as that at C; i.e.,

$$p_5^+ = p_2 + \rho_2(u_p+V_r^*)^2(1-1/\lambda^+) ,$$

where

$$\lambda^{+} = \frac{u_p + V_r^{*}}{V_r^{*}} \quad .$$

The difference between p_5^{+} and $(p_5)_c$ is

$$\Delta p_5 = \rho_2 (u_p + V_r^{*})^2 (1/\lambda - 1/\lambda^{+})$$

which reduces to

$$\Delta p_5 = \rho_5 (-u_5)(V_r^{*} - u_5) \quad .$$

Since

$$\frac{\Delta p_5}{\delta p_5} = \frac{V_r^{*} - u_5}{a_{5F}} \approx 1/3 \quad ,$$

the simple jump condition of bringing the gas to rest <u>always</u> provides a solution between the zeroth and first-order solutions for the end-wall pressure.

APPENDIX E

Modifications to the Pressure Gauge

Much of the progress in the development of the gauge described in Ref. 6 was accomplished through the use of trial-and-error methods. Progress was hindered by the fact that the construction of each gauge was nearly an art and several days were required to assemble each new model. The design selected after a one-year developmental program at Stanford (sponsored by a NASA contract) was a dual-element gauge of Lexan material. This gauge eliminated the problems previously encountered whenever charged particles were present in the gas. The length of time necessary to construct a single gauge was still excessive, however, and the performance from gauge to gauge was not uniform. The major problem was the necessity of hand-sanding thicker sheets of Lexan material to the appropriate final thickness for use as the capacitance element or the dielectric cover sheet. This procedure was time consuming and resulted in large variations in the final thickness of the capacitance element.

The effort described here involves the work done since the end of the one-year contract period. The goal has been to improve gauge uniformity and to reduce the time required to build each gauge. This was important for the experiments of interest in this investigation since the extreme conditions (e.g., $M_s = 20$ into 1 torr of N_2) caused severe burning of the gauge surface and frequent guage failure. The mechanism for gauge failure was usually the burning of a hole in the dielectric cover sheet, thus exposing the ground of the gauge to charged

particles in the gas. The use of thicker cover sheets prolonged the life of each gauge but also resulted in a deterioration of the response for short times.

In an attempt to reduce construction time, several new materials were tested for possible use as the dielectric sensing element. The hope was to find a dielectric material which provided a good response to a pressure pulse, could be satisfactorily bonded, and was available in standard film thicknesses of 2 to 5 mils. Preferably, the speed of sound in the material should also be slow in order to obtain a maximum amount of test time with the gauge. Several materials were tested (e.g., Mylar, Teflon FEP, Tedlar and Teflon) but none was completely satisfactory, even with various combinations of epoxy and film material. Tests with different film thicknesses were also unsatisfactory. Gauges were then built of Lucite although this material was not available in standard film thicknesses. The Lucite gauge provided a good response but suffered from a fast sound speed and hence a short test time.

At this point it was decided to try a new source of Lexan material, since a difference in color and hardness was noted between two consecutive orders from a local distributor. Upon further investigation it was found that the General Electric Company manufactured thin films of Lexan. These films proved to be the most satisfactory capacitance elements of all the materials tested. Previous undesirable features in the performance hand-sanded Lexan gauges were much improved in the new gauges. Use of these thin Lexan films has required additional skill in bonding the layers of the gauge, however, because of the susceptibility of the thin films to wrinkling and to developing small pin holes during the bonding

process. Pin holes in the capacitance element near the high-voltage electrodes cannot be tolerated since such cavities provide a path for the voltage to discharge through the capacitor to ground.

The use of the thin-film Lexan has resulted in a large reduction in assembly time for each pressure gauge. Furthermore, gauges with the same nominal thickness for the capacitance element now respond very nearly the same. The uniformity of the response has removed the time-consuming necessity of individually calibrating each gauge.

In the hope of further reducing the gauge construction time, other ideas have been tried in a preliminary fashion. At present the high-voltage electrodes and ground are composed of conducting epoxy. Two gauges have been constructed using thin metal foil (1/8 mil) as the conducting material. There is some difficulty in bonding this material to the Lexan, but the gauges which were eventually built performed as well as the gauges with conducting epoxy (although a few cycles of wave reflection were noticeable in the initial part of the response to a pressure step). The metal foil allows the gauge construction time to be further reduced since the entire sensing element and cover plate can be bonded as a pre-made sandwich. Further work is needed with this promising concept.

REFERENCES

1. L. L. Presley and R. K. Hanson, "Exact Solutions of Reflected Shock-Wave Flow Fields with Non-Equilibrium Chemical Reactions," to be presented at the AIAA Fluids and Plasmadynamics Conference, Los Angeles, Calif., June (1968).

2. D. Baganoff, "Pressure-Gauge with One-Tenth Microsecond Risetime for Shock-Reflection Studies," Rev. Sci. Instr. 35, 288 (1964).

3. D. Baganoff, "Experiments on the Wall-Pressure History in Shock-Reflection Processes," J. Fluid Mech. 23, 209 (1965).

4. N. H. Johannesen, G. A. Bird and H. K. Zienkiewicz, "Theoretical and Experimental Investigations of the Reflection of Normal Shock Waves with Vibrational Relaxation," J. Fluid Mech. 30, 51 (1967).

5. J. A. Smith, "An Experimental Investigation of the Structure of Reflecting, Ionizing Shocks in Xenon," Ph.D. Thesis, Calif. Inst. of Tech., Pasedena, Calif., (1967).

6. D. Baganoff, "Pressure-Gauge Instrumentation for Studies in Ionized Gases," SUDAAR No. 315, Stanford University, Stanford, Calif., (1967).

7. D. A. Spence, "Unsteady Shock Propagation in a Relaxing Gas," Proc. Roy. Soc. A264, 221 (1961).

8. W. G. Vincenti and C. H. Kruger, Jr., Introduction to Physical Gas Dynamics (Wiley, New York, 1965).

9. S. S. Penner, Chemistry Problems in Jet Propulsion (Pergamon Press, New York, 1957).

10. N. Davidson, "The Rate of Dissociation of the Halogens," Fundamental Data Obtained From Shock-Tube Experiments, edited by A. Ferri (Pergamon Press, New York, 1961).

11. R. H. Fowler and E. A. Guggenheim, Statistical Thermodynamics (Cambridge University Press, Cambridge, England, 1952).

12. H. W. Leipmann and A. Roshko, Elements of Gasdynamics (Wiley, New York, 1962).

13. K. L. Wray, "Chemical Kinetics of High Temperature Air," AVCO-RR 104, Avco-Everett Research Lab, Everett, Mass., (1961).

14. R. K. Hanson, "Chemical Relaxation Behind Strong Shock Waves in Diatomic Gases," M. S. Thesis, Ariz. State Univ., Tempe, Ariz., (1965).

15. J. T. Howe and Y. S. Sheaffer, "Chemical Relaxation Behind Strong Normal Shock Waves in Carbon Dioxide Including Interdependent Dissociation and Ionization Processes," NASA TN D-2131 (1964).

16. A. Ferri and L. G. Napolitano, "Fluid Dynamics of Nonsteady Flow," Fundamental Data Obtained From Shock-Tube Experiments, edited by A. Ferri (Pergamon Press, New York, 1961).

17. H. Wong, "Interferometric Study of Thermal Equilibrium of a Shock Heated Plasma," Ph.D. Thesis, Stanford University, Stanford Calif., (1964).

18. S. R. Byron, "Shock-Tube Measurement of the Rate of Dissociation of Nitrogen," J. Chem. Phys. 44, 1378 (1965).

19. B. Cary, "Shock-Tube Study of the Thermal Dissociation of Nitrogen," Phys. Fluids 8, 26 (1965).

20. R. K. Hanson and R. Watson, "Effects of Dissociation Rate Magnitudes

and Relative Collision Efficiencies on Relaxation Profiles in Diatomic Gases," AIAA J. 4, 749 (1966).

21. J. P. Appleton, M. Steinberg and D. J. Liquornik, "Shock-Tube Study of Nitrogen Dissociation Using Vacuum-Ultraviolet Light Absorption," J. Chem. Phys. 48, 599 (1968).

22. K. L. Wray and S. Byron, "Comments on "Shock-Tube Study of the Thermal Dissociation of Nitrogen"," Phys. Fluids 9, 1046 (1966).

23. B. Cary, "Reply to Comments by K. Wray and S. Byron," Phys. Fluids 9, 1047 (1966).

24. C. H. Lewis and E. G. Burgess, III, "Charts of Normal Shock Wave Properties in Imperfect Nitrogen," AEDC-TDR-64-104 (1964).

25. L. Bernstein, "Tabulated Solutions of the Equilibrium Gas Properties Behind the Incident and Reflected Normal Shock-Wave in a Shock Tube. I-Nitrogen; II-Oxygen," ARC22, 778, April (1961).

26. C. D. Simcox and V. L. Peterson, "Charts for Equilibrium and Frozen Flows Across Plane Shock Waves in Carbon Dioxide," NASA SP-3018 (1965).

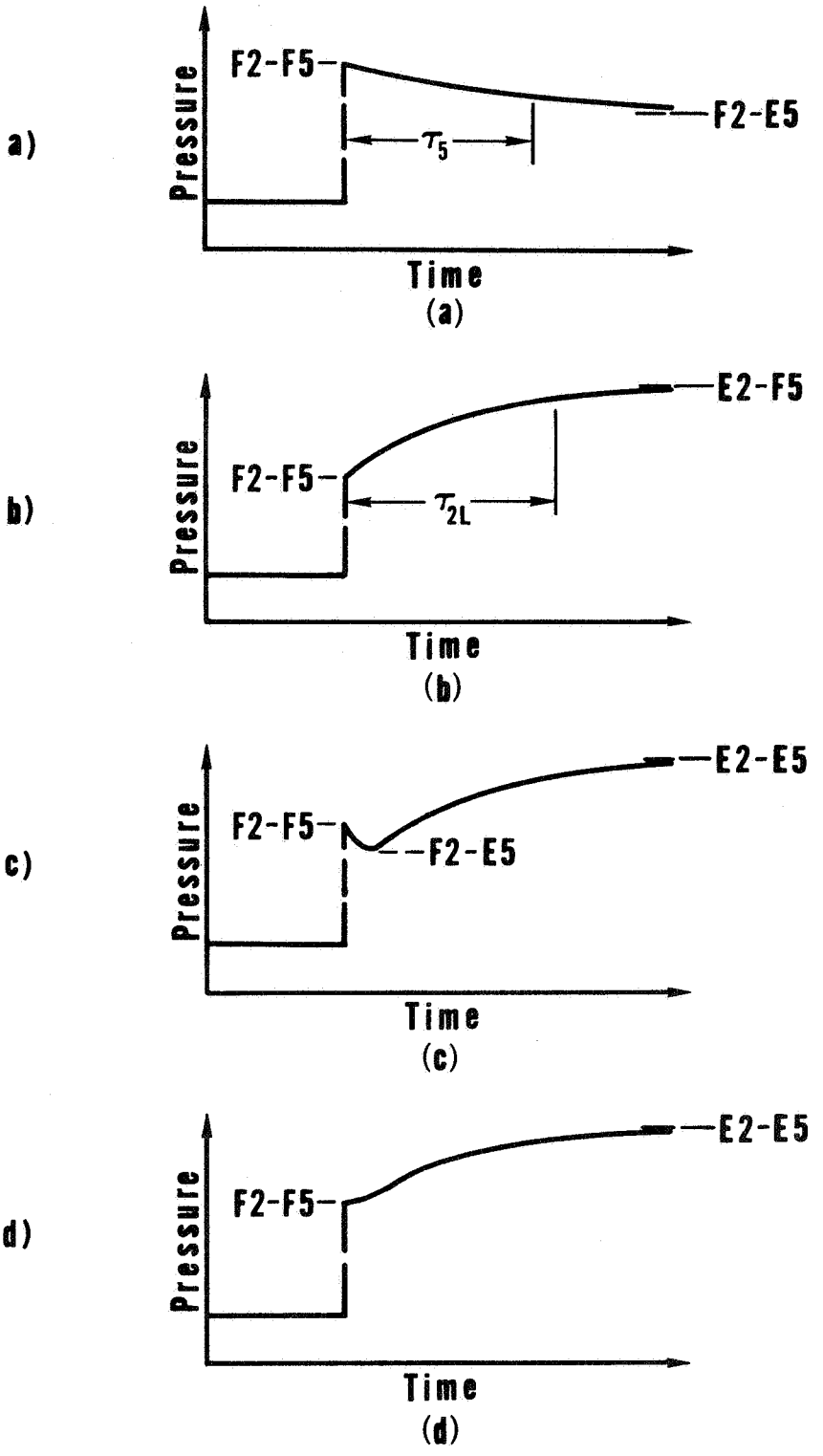

Fig. 1. End-wall pressure history during shock-wave reflection in a relaxing gas: a) relaxation in region 5 alone; b) relaxation in region 2 alone; c) combined process when $\tau_5 \ll \tau_{2L}$; and d) combined process when $\tau_5 \lesssim \tau_{2L}$.

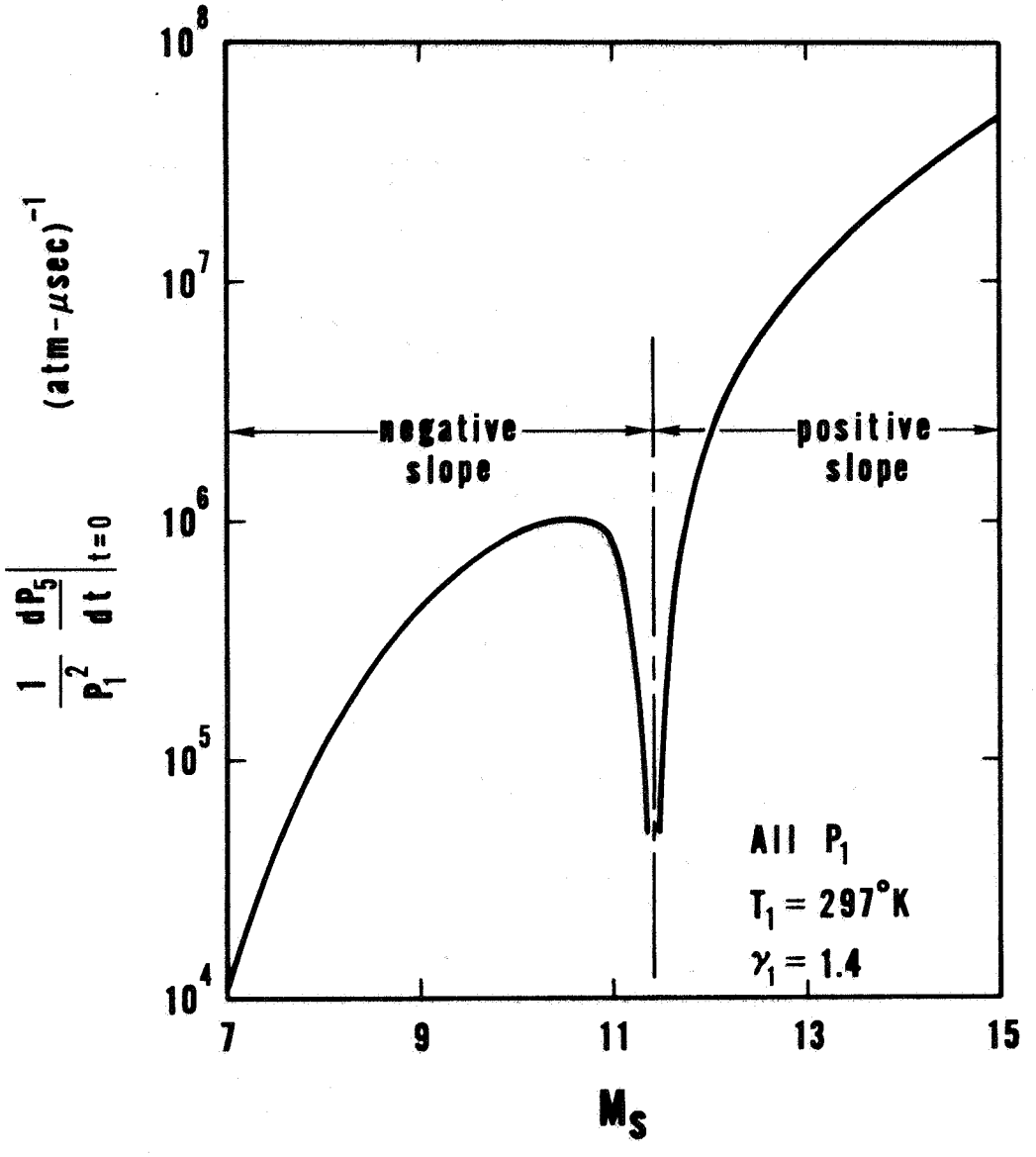

Fig. 2. Initial rate of change of end-wall pressure in chemically relaxing O_2.

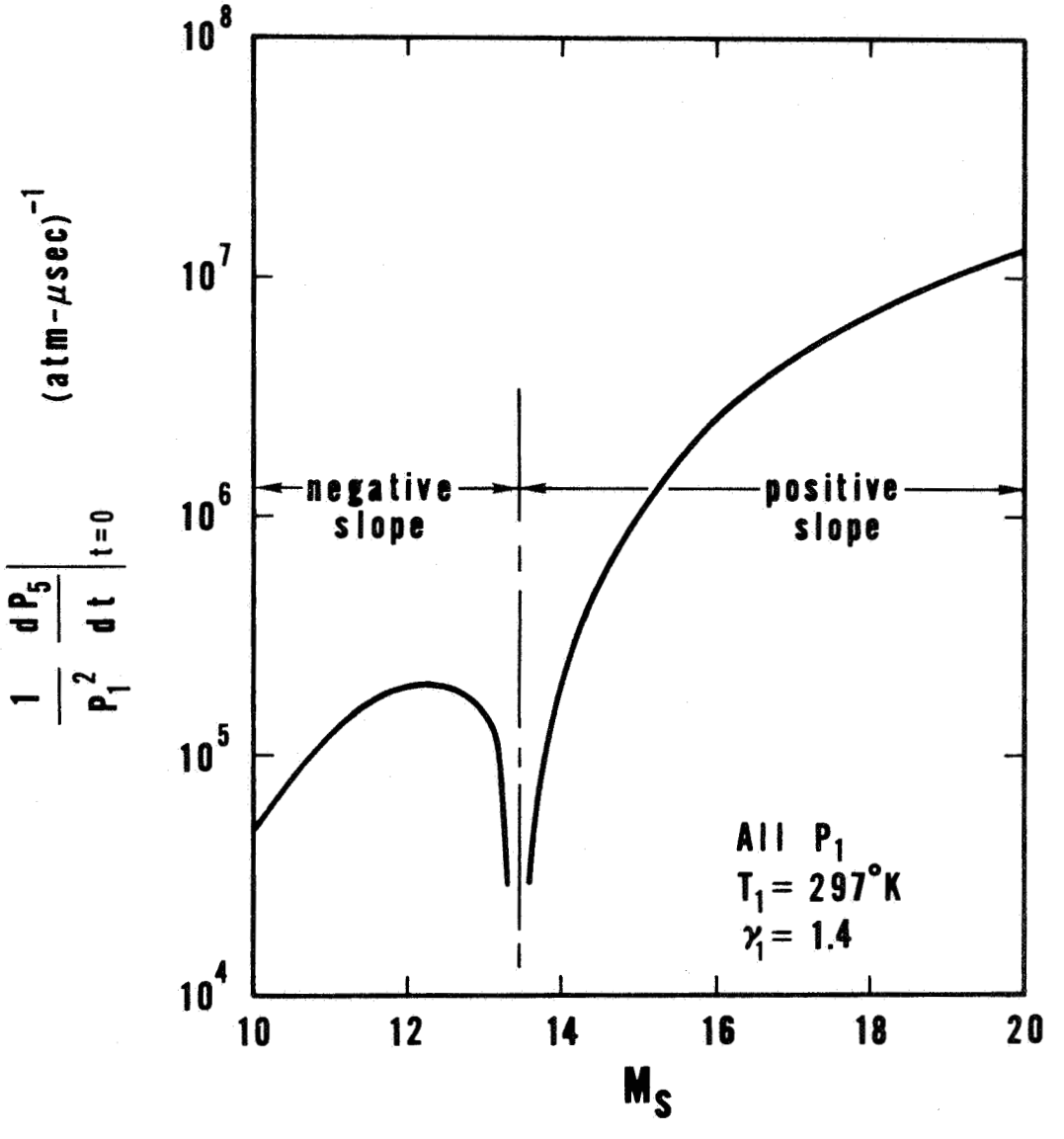

Fig. 3. Initial rate of change of end-wall pressure in chemically relaxing N_2.

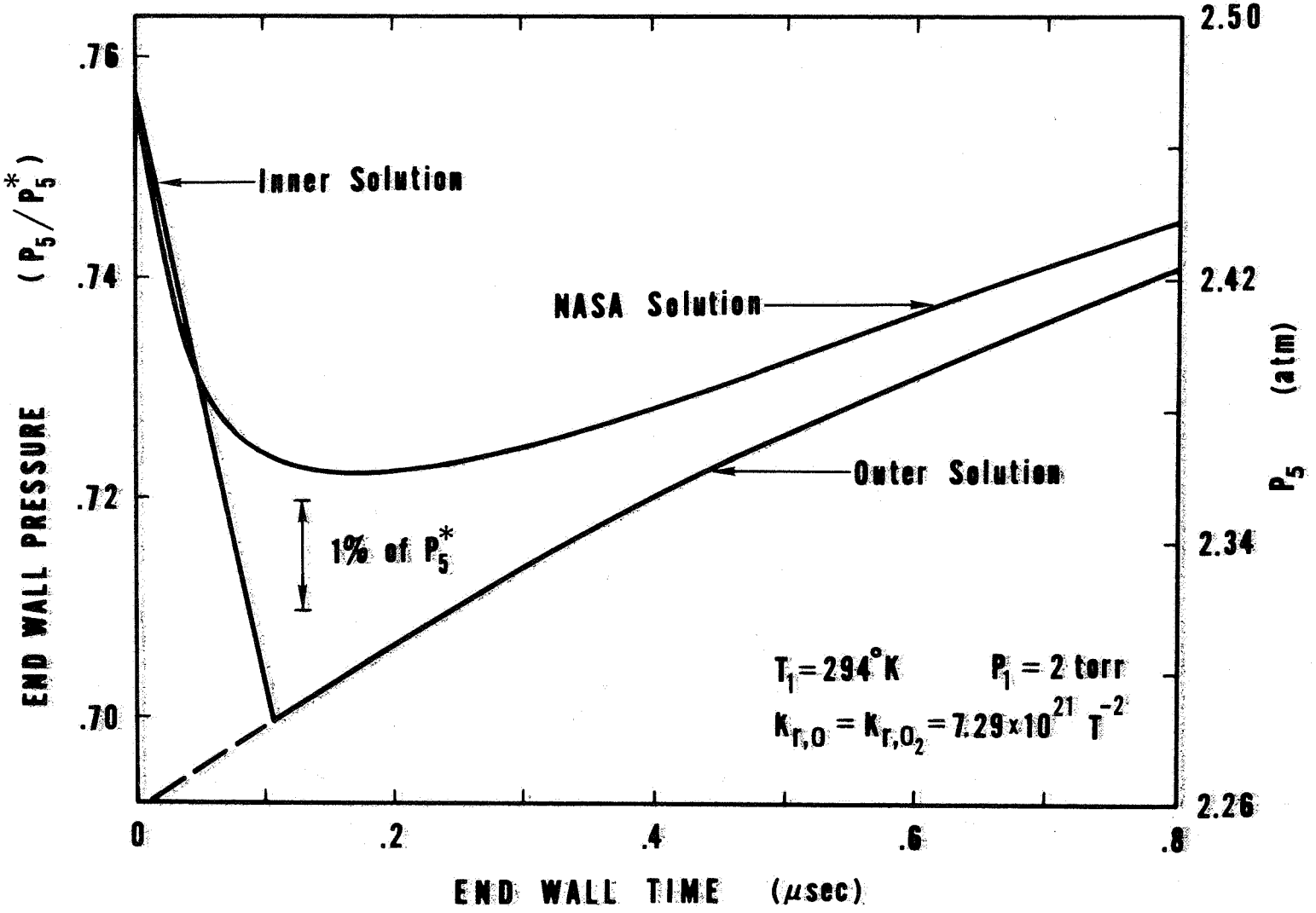

Fig. 4. Comparison of short-time end-wall pressure histories in chemically relaxing O_2, V_s = 3.05 km/sec.

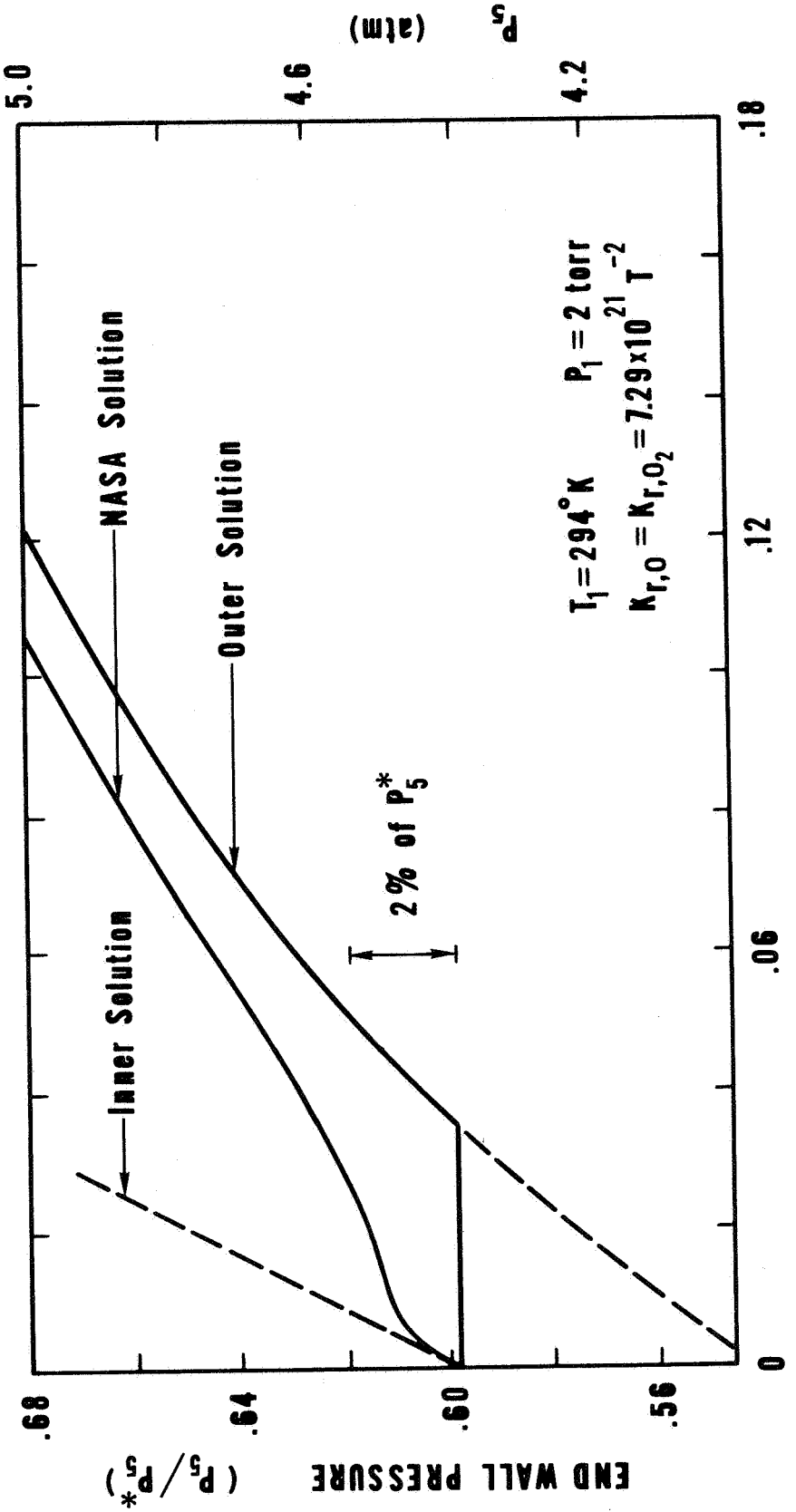

Fig. 5. Comparison of short-time end-wall pressure histories in chemically relaxing O_2, $V_s = 3.96$ km/sec.

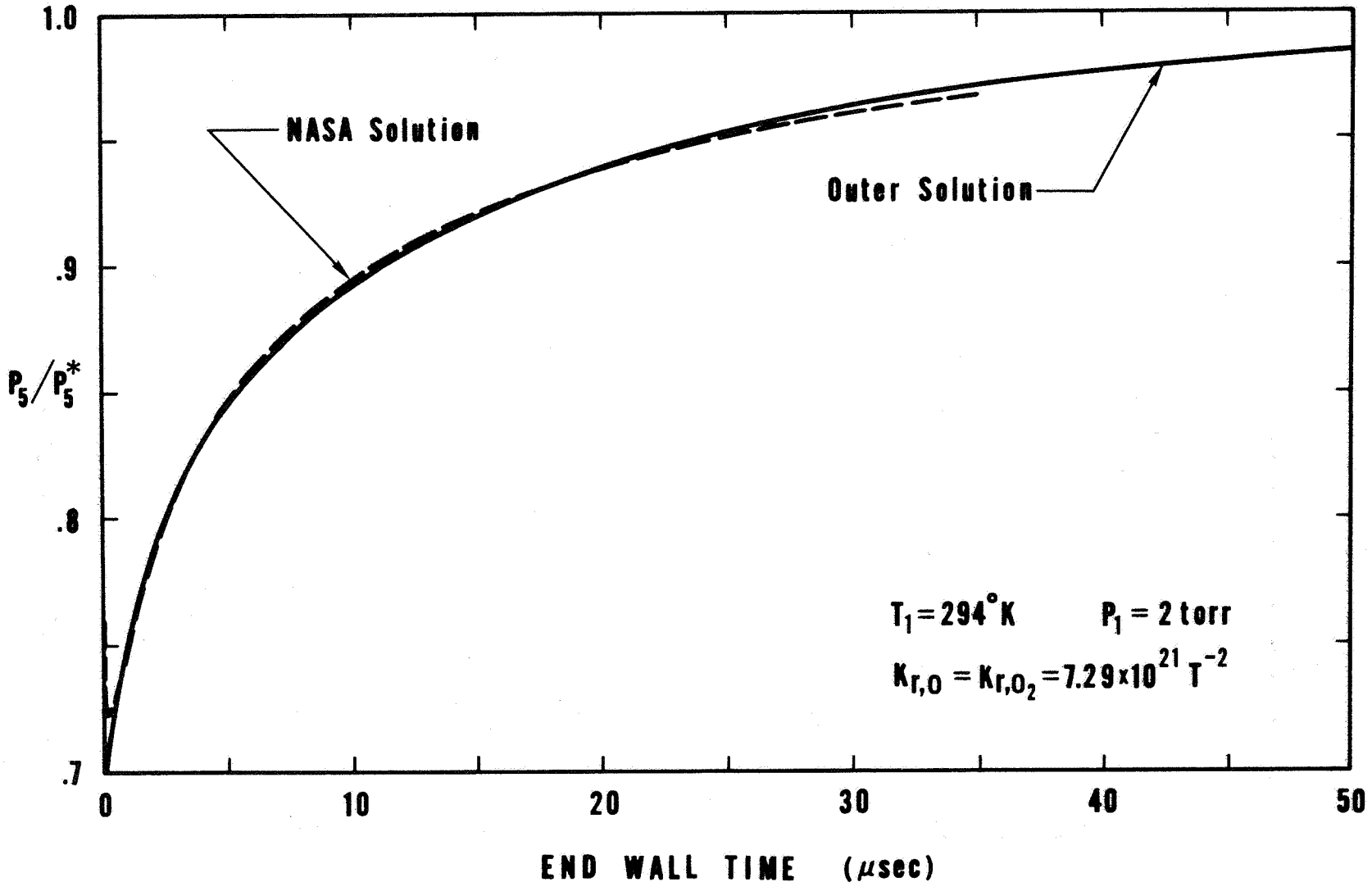

Fig. 6. Comparison of long-time end-wall pressure histories in chemically relaxing O_2, V_s = 3.05 km/sec.

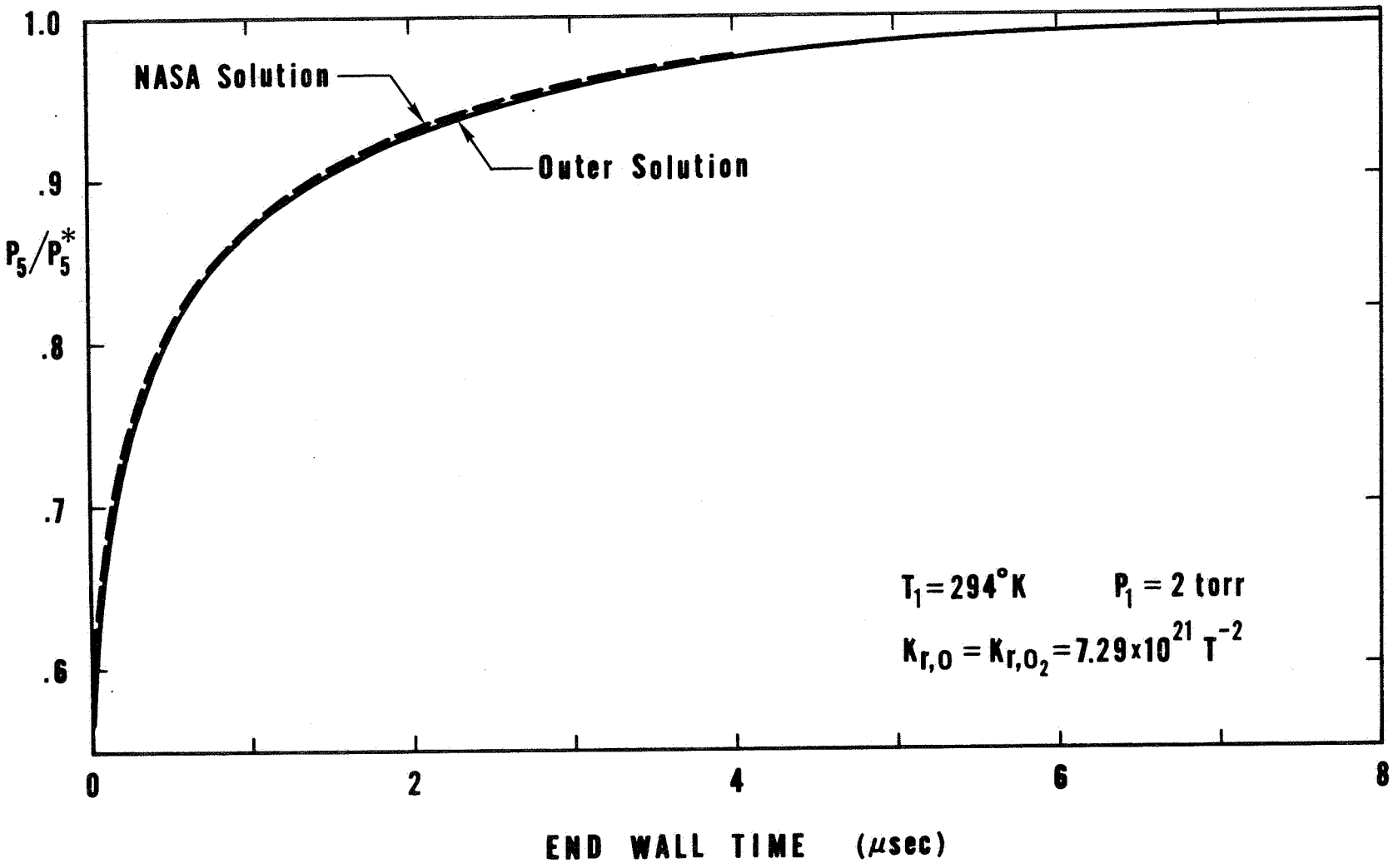

Fig. 7. Comparison of long-time end-wall pressure histories in chemically relaxing O_2, $V_s = 3.96$ km/sec.

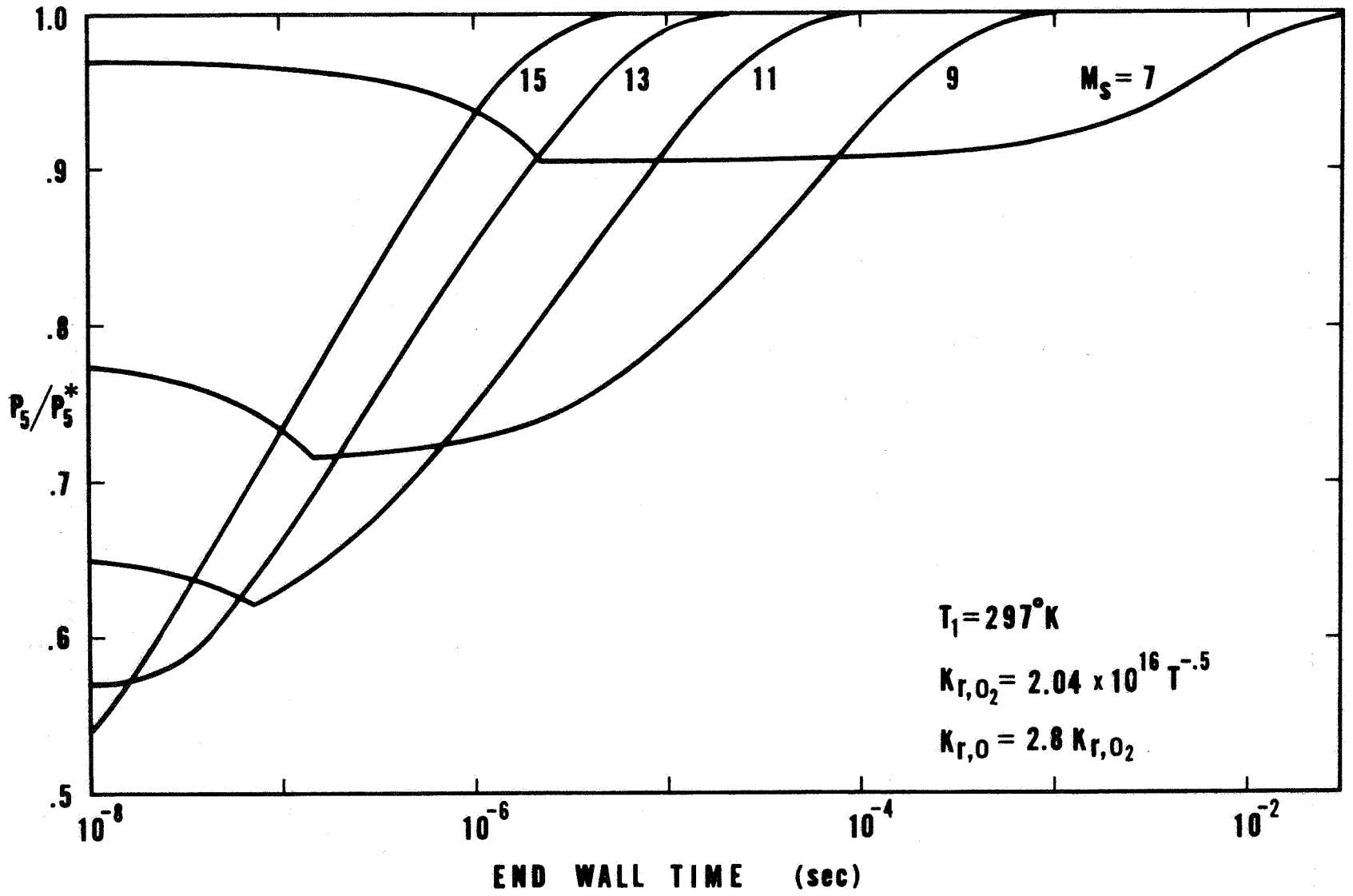

Fig. 8. Composite end-wall pressure histories in chemically relaxing O_2, P_1 = 1 torr.

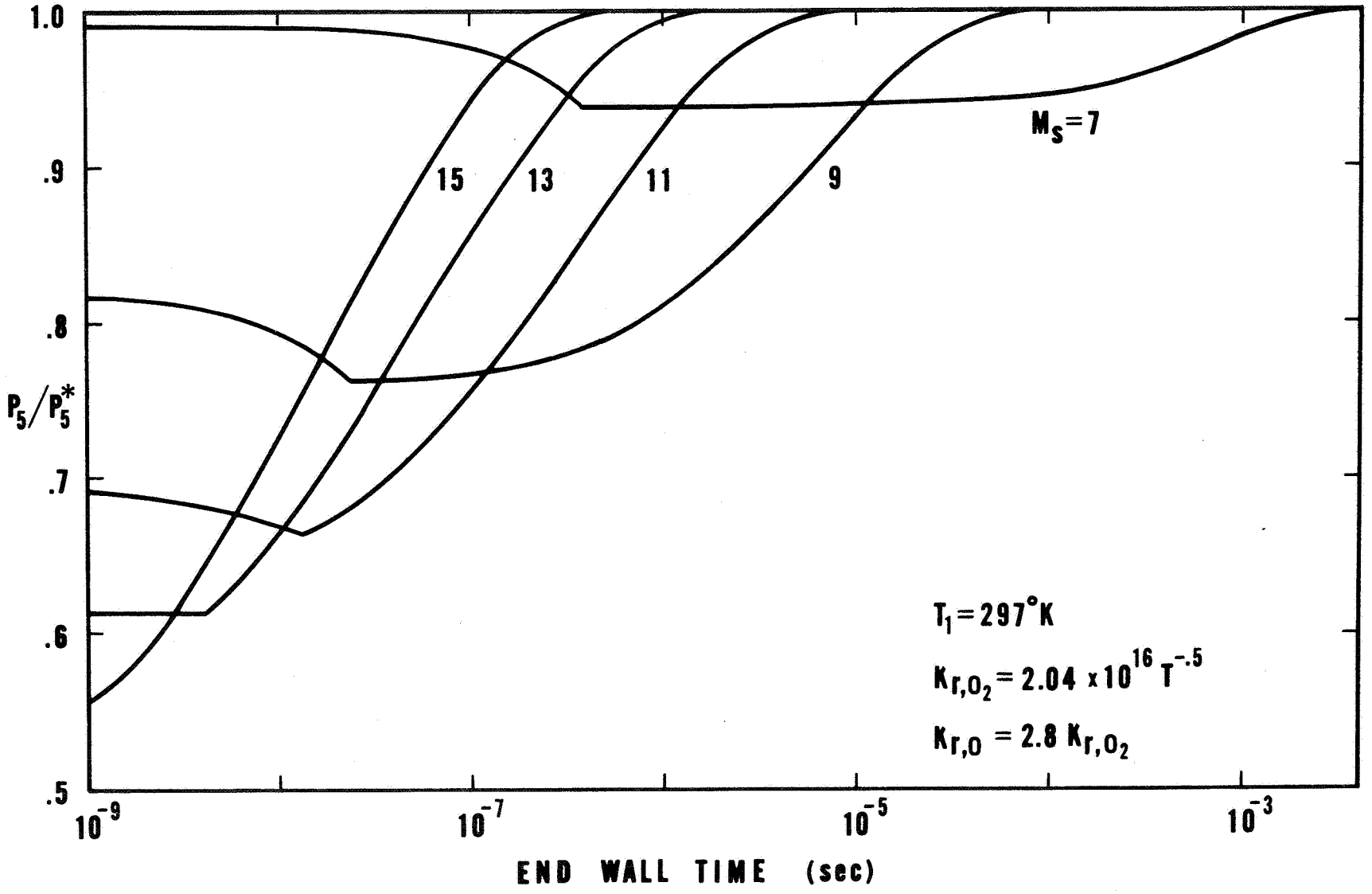

Fig. 9. Composite end-wall pressure histories in chemically relaxing O_2, P_1 = 5 torr.

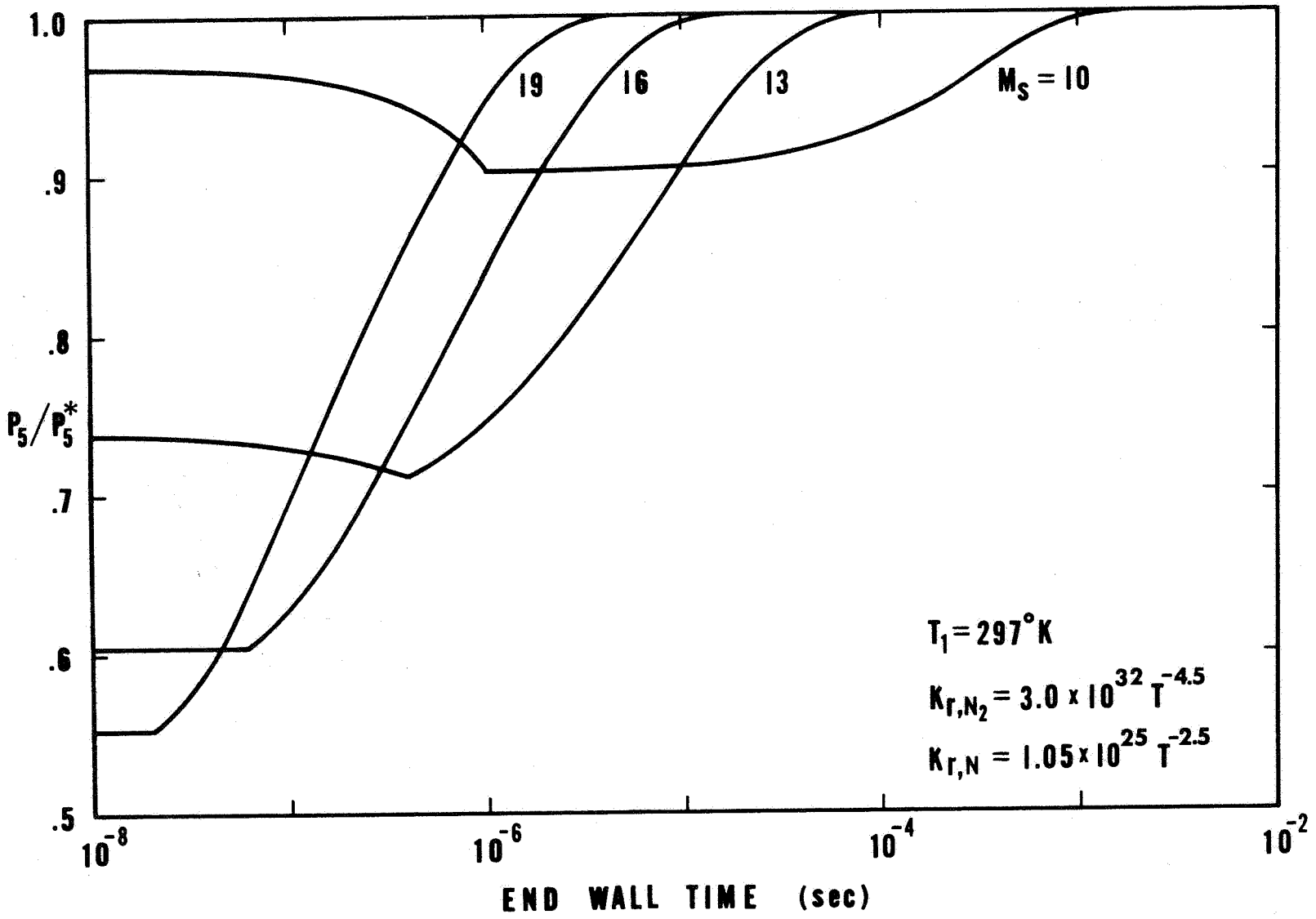

Fig. 10. Composite end-wall pressure histories in chemically relaxing N_2, P_1 = 1 torr.

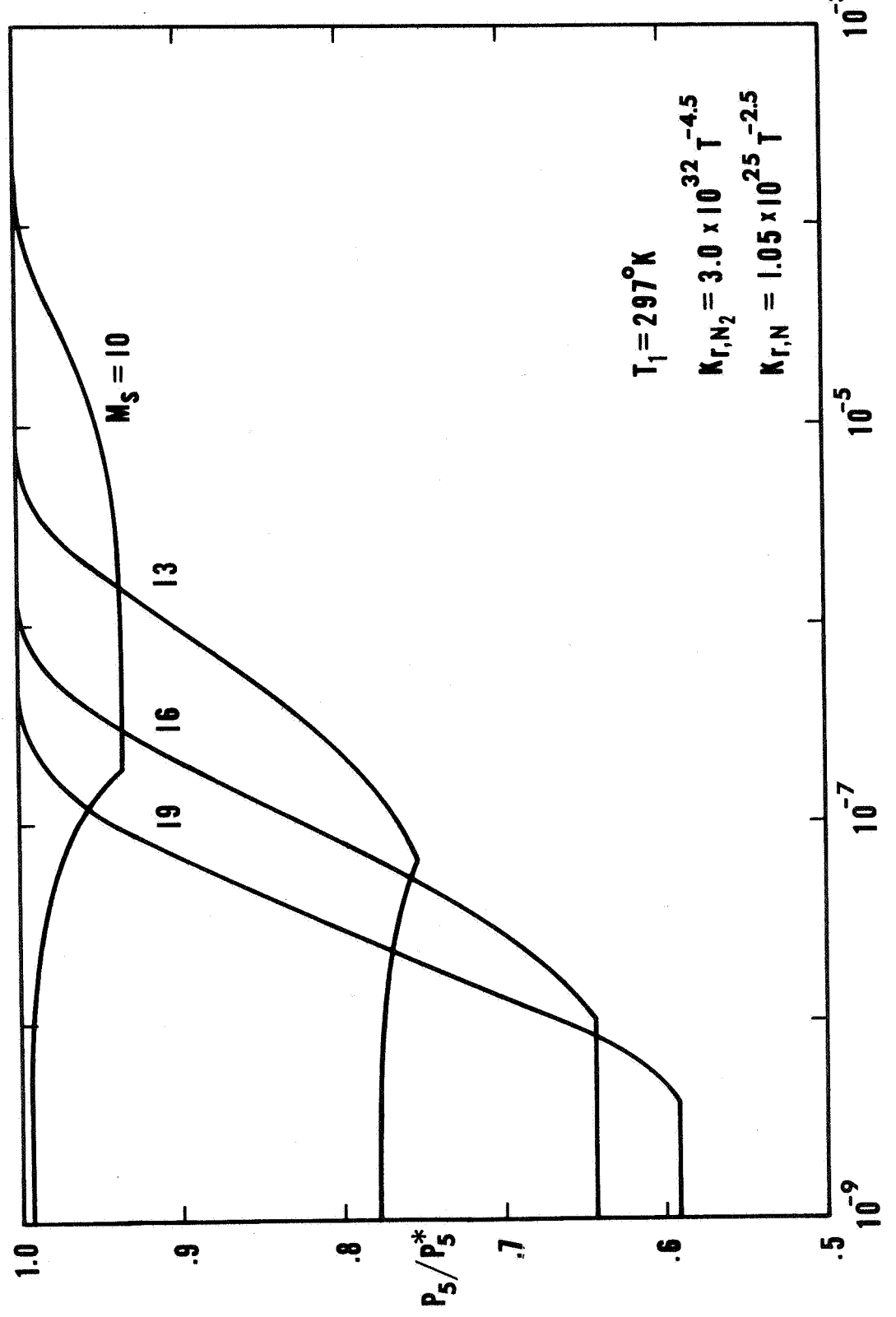

Fig. 11. Composite end-wall pressure histories in chemically relaxing N_2, $P_1 = 5$ torr.

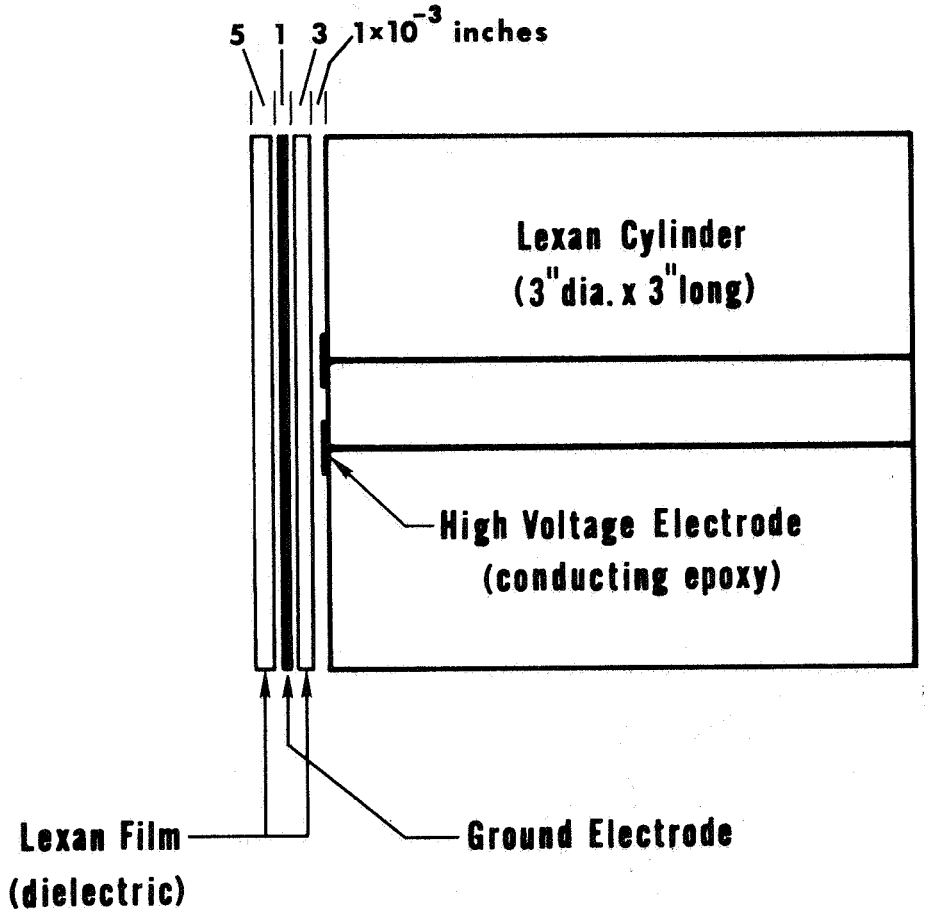

Fig. 12. Schematic drawing of the dual-element pressure gauge.

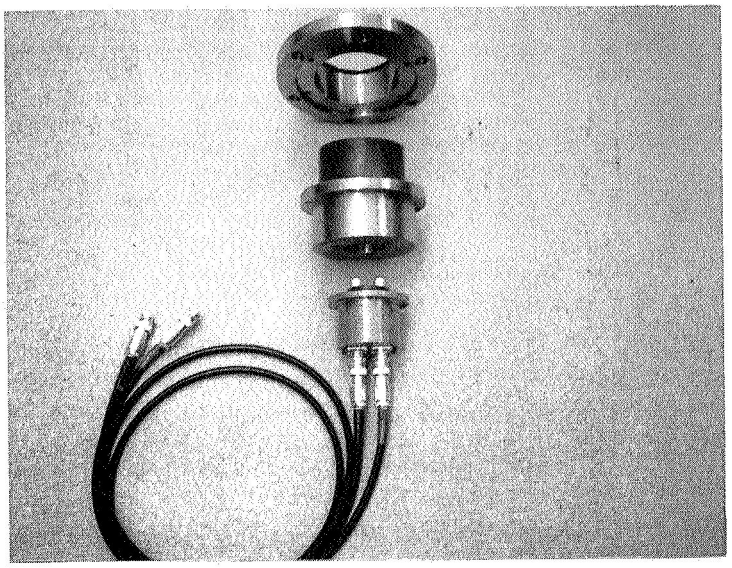

a) Partially disassembled gauge

b) Gauge together with charging unit

Fig. 13. Dual-element pressure gauge and pressure-gauge electronics.

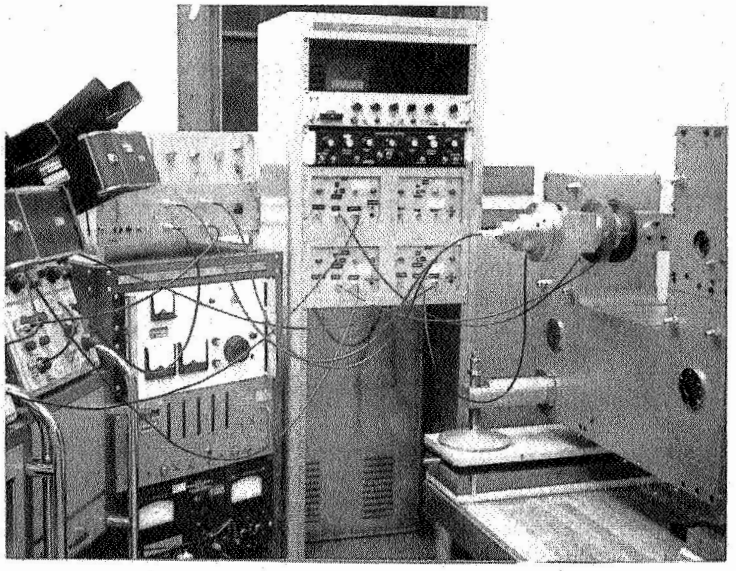

a) Typical test setup

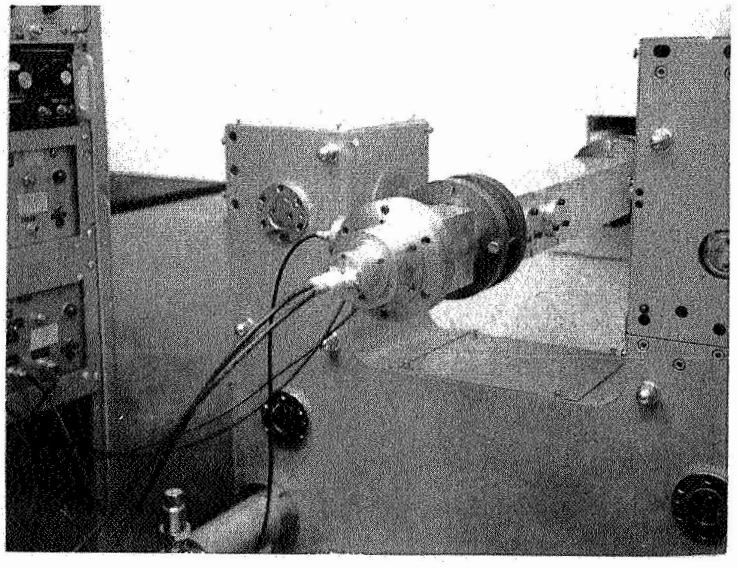

b) Pressure gauge installation

Fig. 14. Photographs of the dual-element pressure gauge and associated equipment.

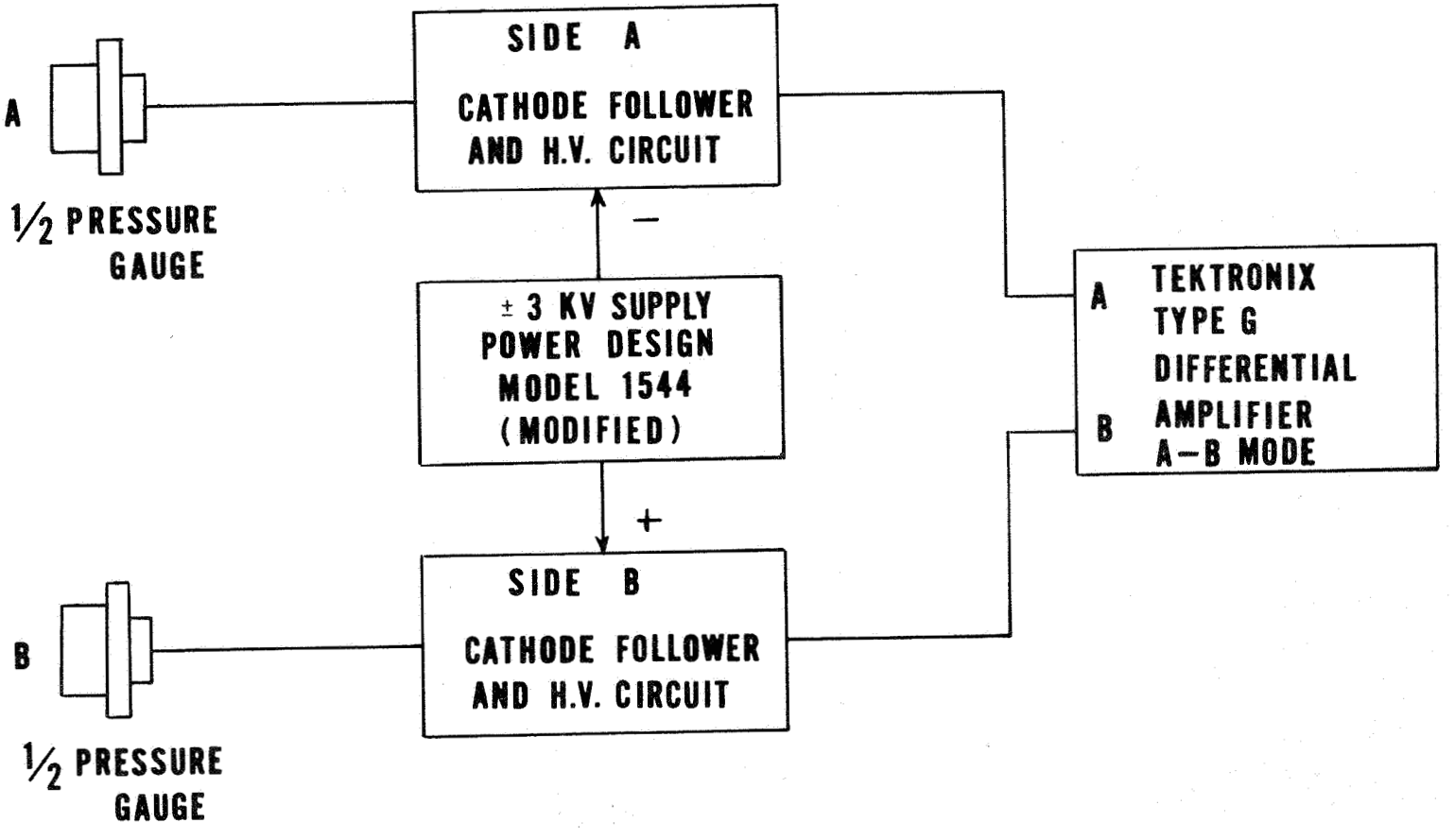

Fig. 15. Block diagram of the electrical circuit for the dual-element pressure gauge.

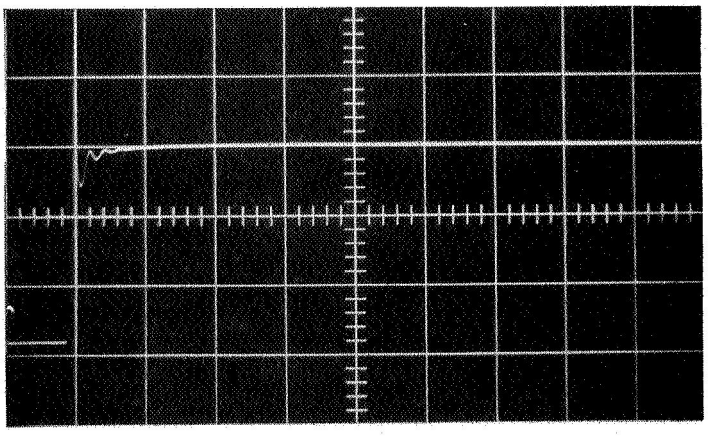

a) Response of a charged element minus the response of a grounded element;

Sweep speed = 1 μsec/div.

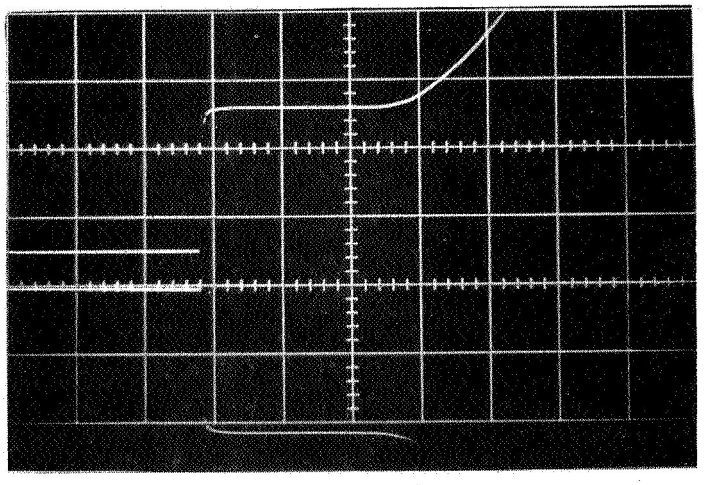

b) Upper Trace: response from a single element charged to positive voltage;

Lower Trace: response from a single element charged to negative voltage;

Sweep Speed = 5 μsec/div.

Fig. 16. Pressure-gauge response to a pressure step: a) single element charged; b) both elements charged.

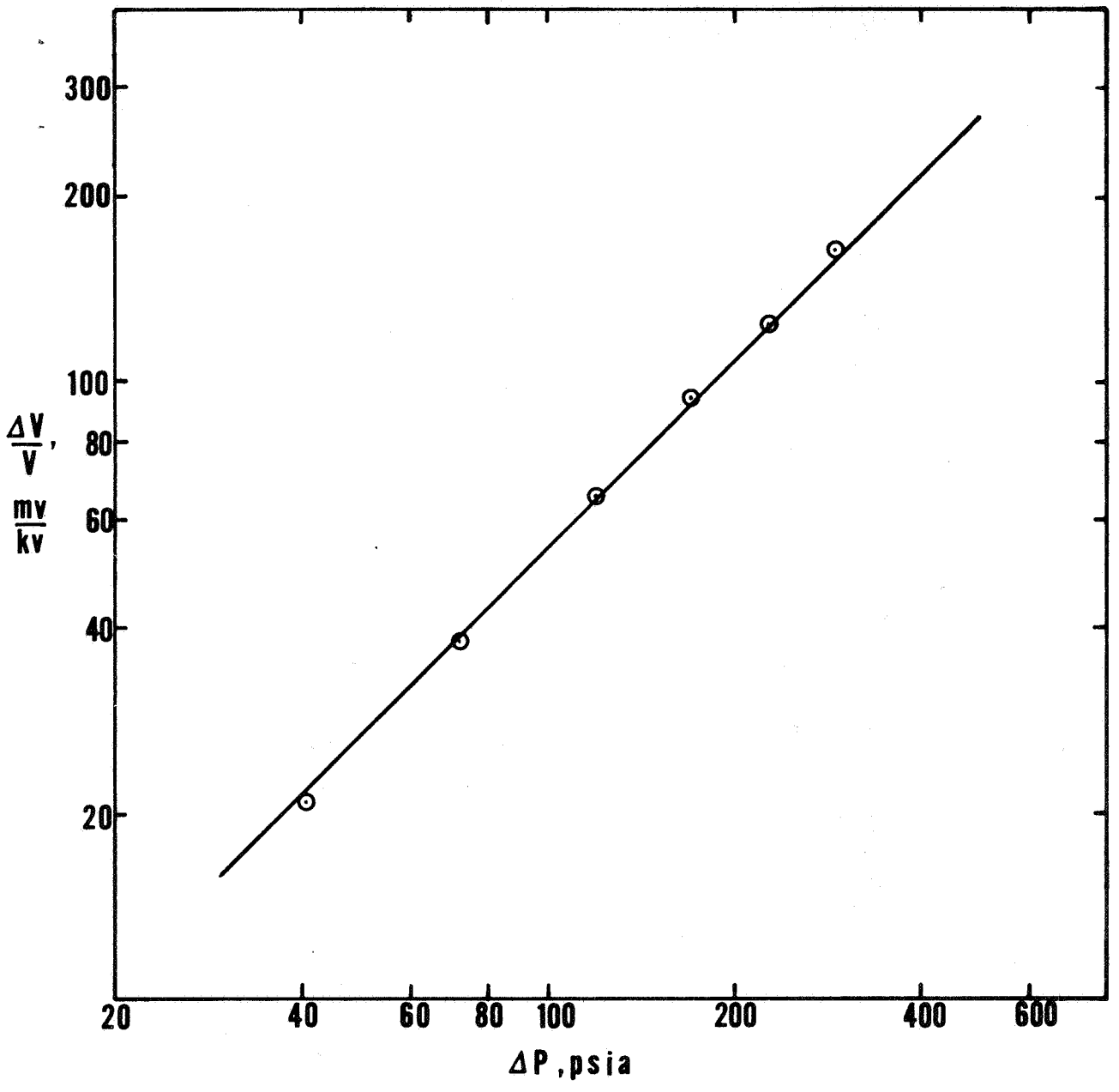

Fig. 17. Pressure-gauge calibration curve. Gauge sensitivity = 0.53 mv/psi-kv.

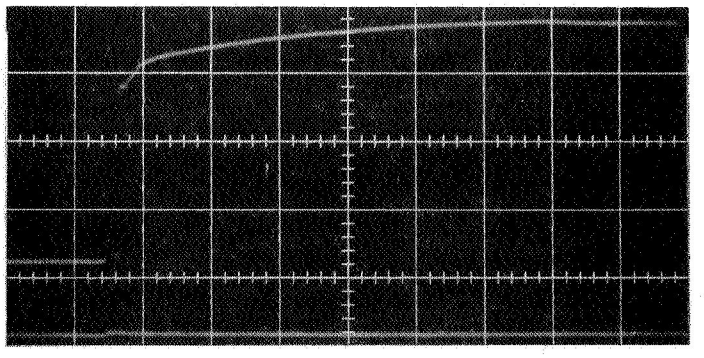

a) V_s = 4.26 km/sec; P_1 = 5 torr;
Sweep Speed = 1 μsec/div.

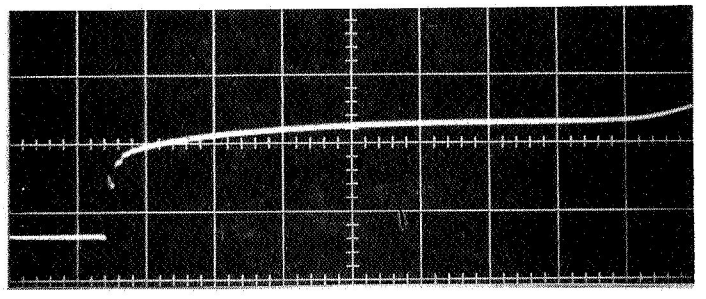

b) V_s = 4.7 km/sec; P_1 = 1 torr;
Sweep Speed = 2 μsec/div.

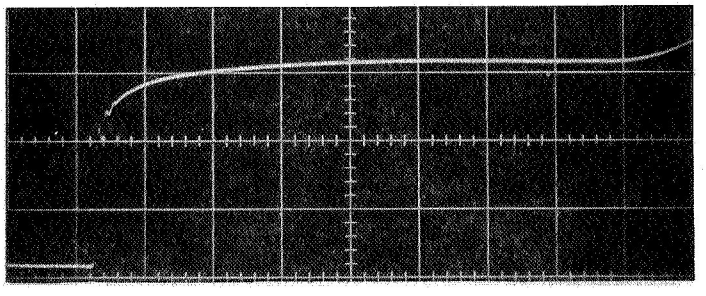

c) V_s = 5.3 km/sec; P_1 = 2 torr;
Sweep Speed = 2 μsec/div.

Fig. 18. Experimental end-wall pressure histories in chemically relaxing N_2, T_1 = 297°K.

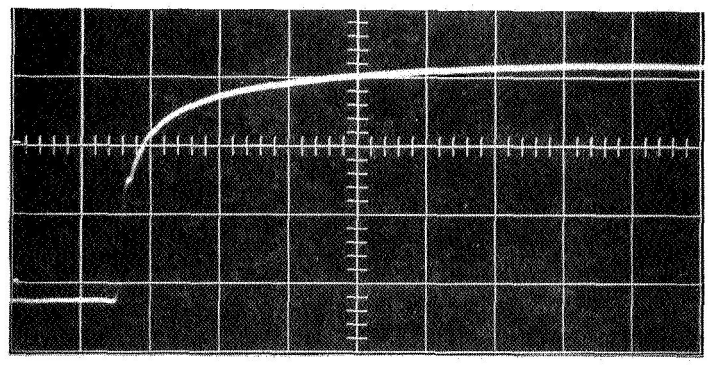

a) V_s = 6.0 km/sec; P_1 = .86 torr;
Sweep Speed = 1 μsec/div.

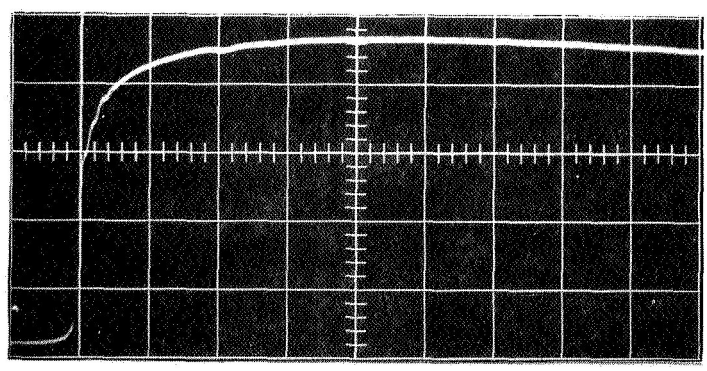

b) V_s = 7.1 km/sec; P_1 = .53 torr;
Sweep Speed = 1 μsec/div.

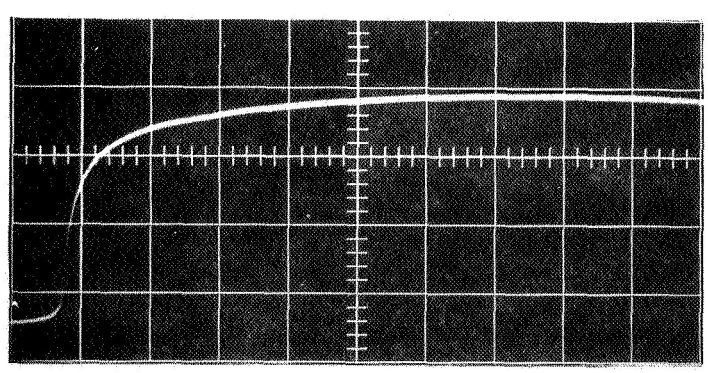

c) $V_s \approx$ 7.5 km/sec; P_1 = .31 torr;
Sweep Speed = 1 μsec/div.

Fig. 19. Experimental end-wall pressure histories in chemically relaxing N_2, T_1 = 297°K.

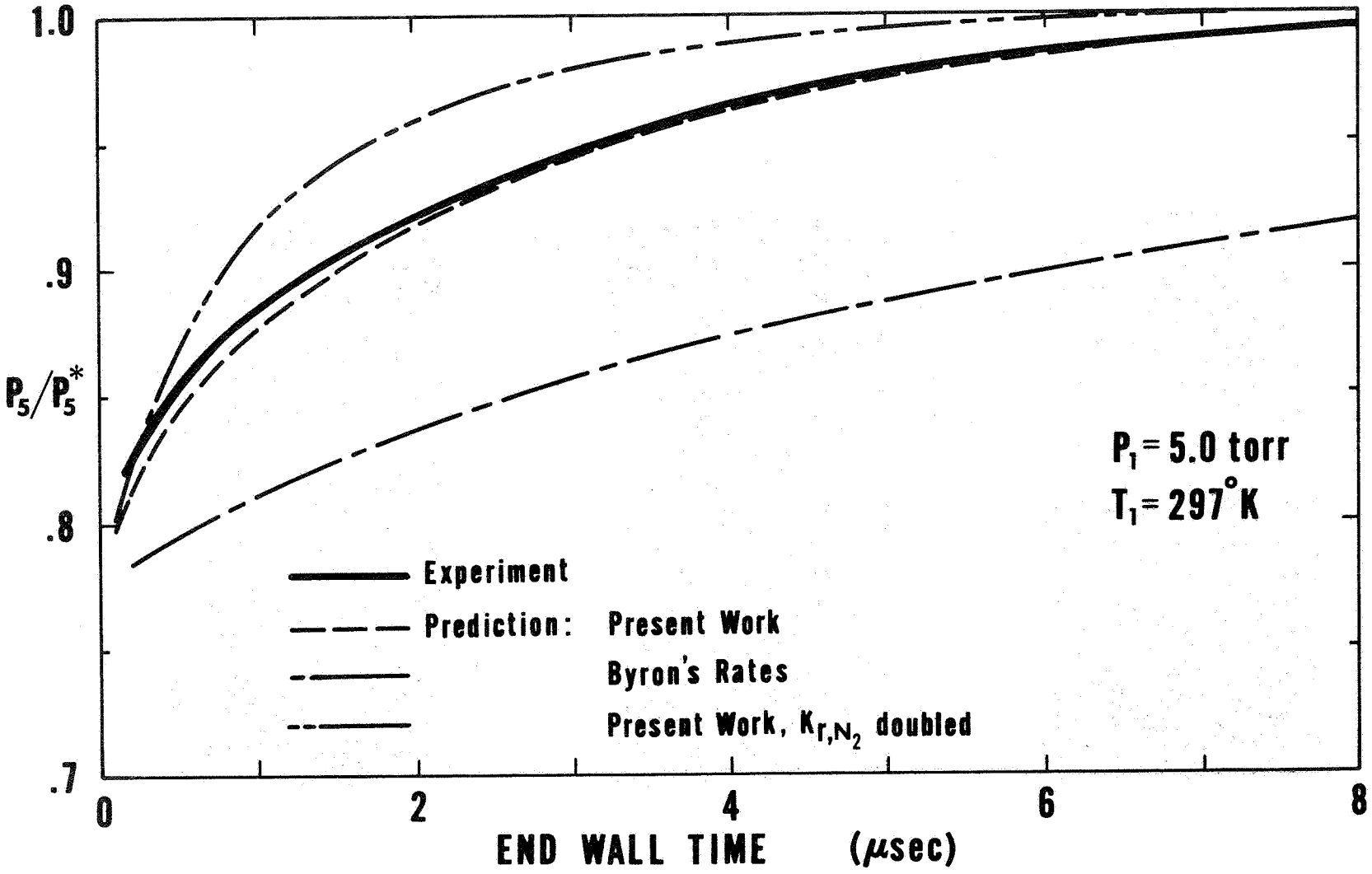

Fig. 20. End-wall pressure history for chemically relaxing N_2, V_s = 4.26 km/sec.

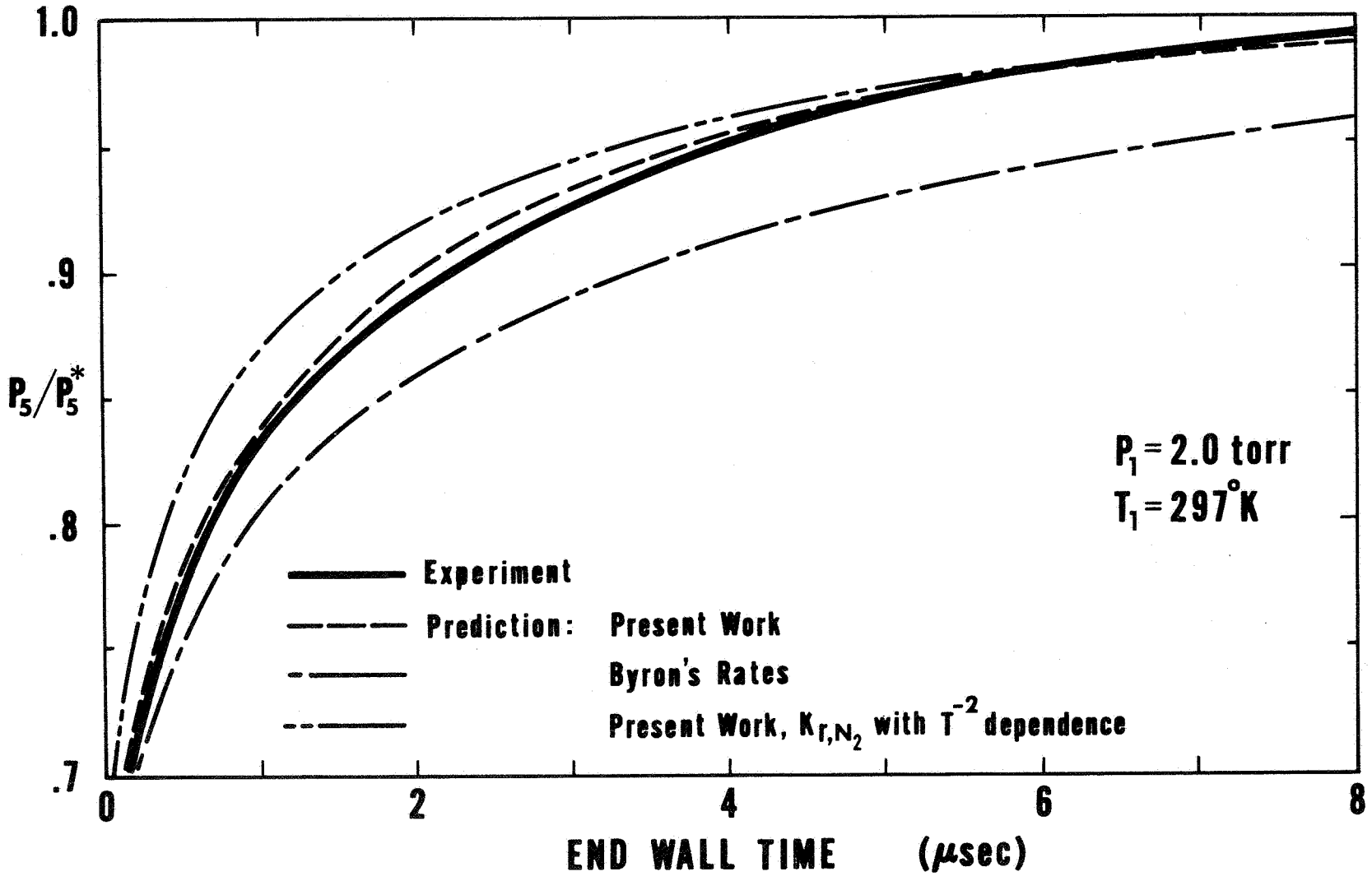

Fig. 21. End-wall pressure history for chemically relaxing N_2, V_s = 4.9 km/sec.

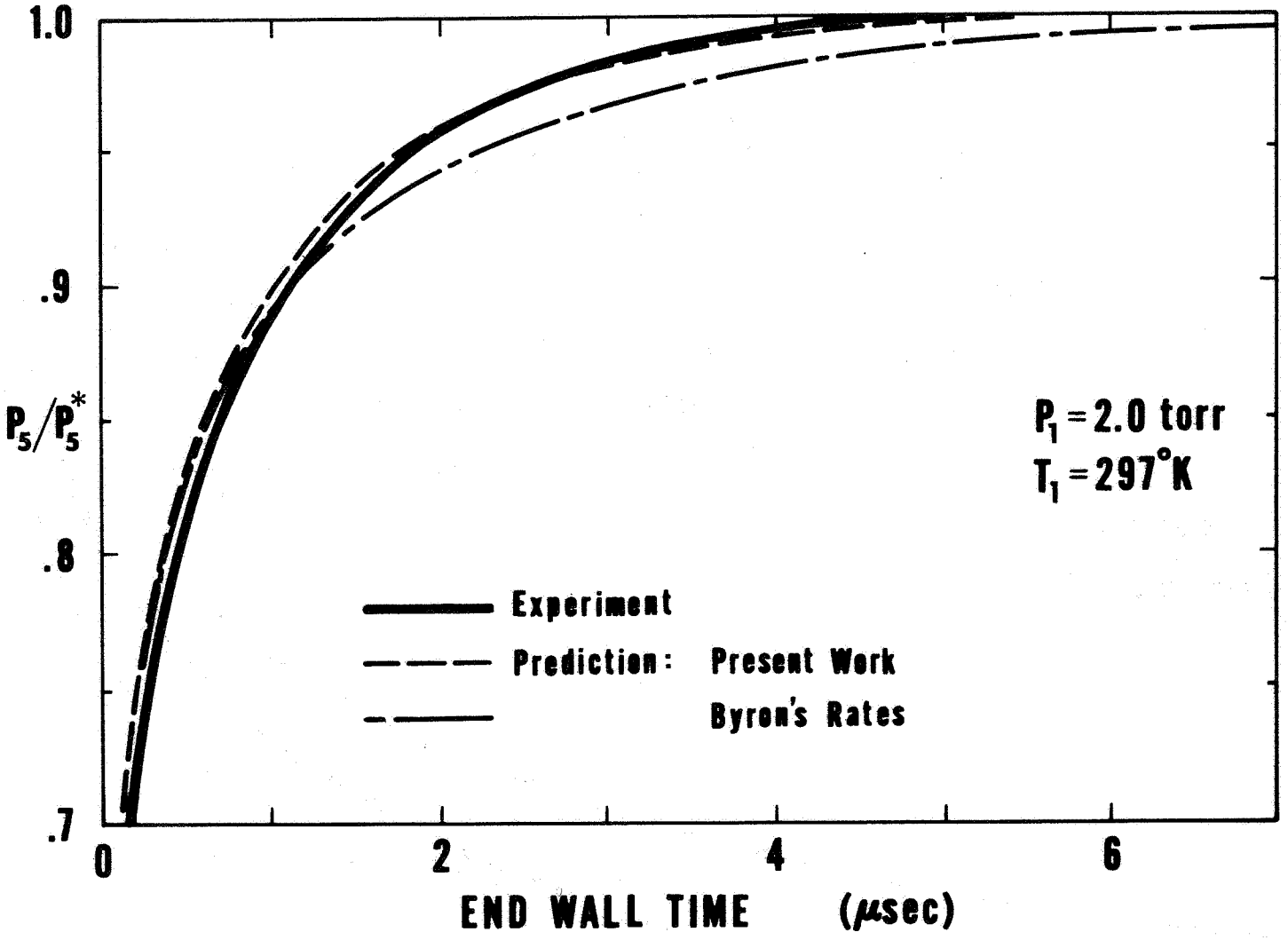

Fig. 22. End-wall pressure history for chemically relaxing N_2, V_s = 5.38 km/sec.

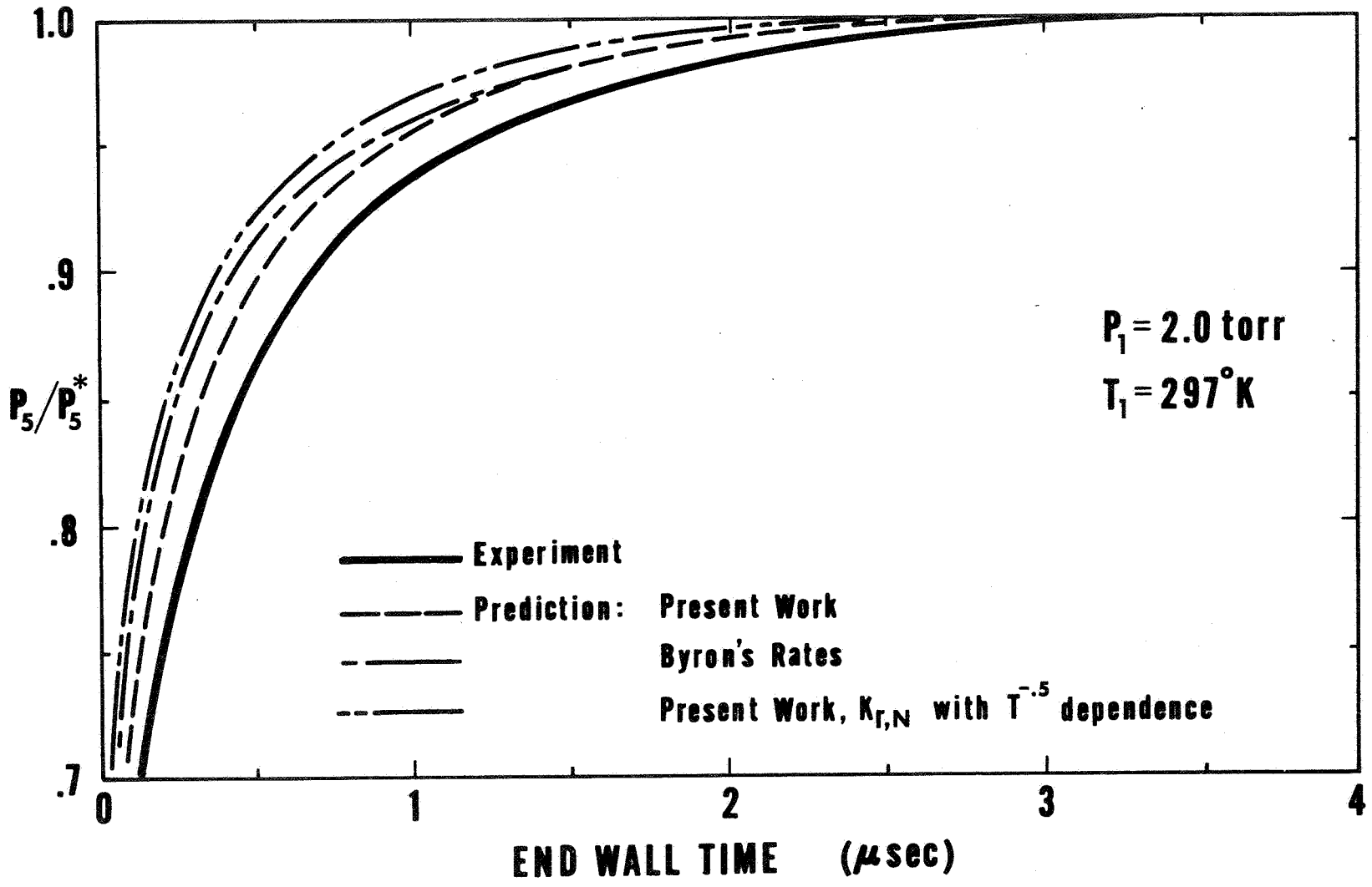

Fig. 23. End-wall pressure history for chemically relaxing N_2, V_s = 5.94 km/sec.

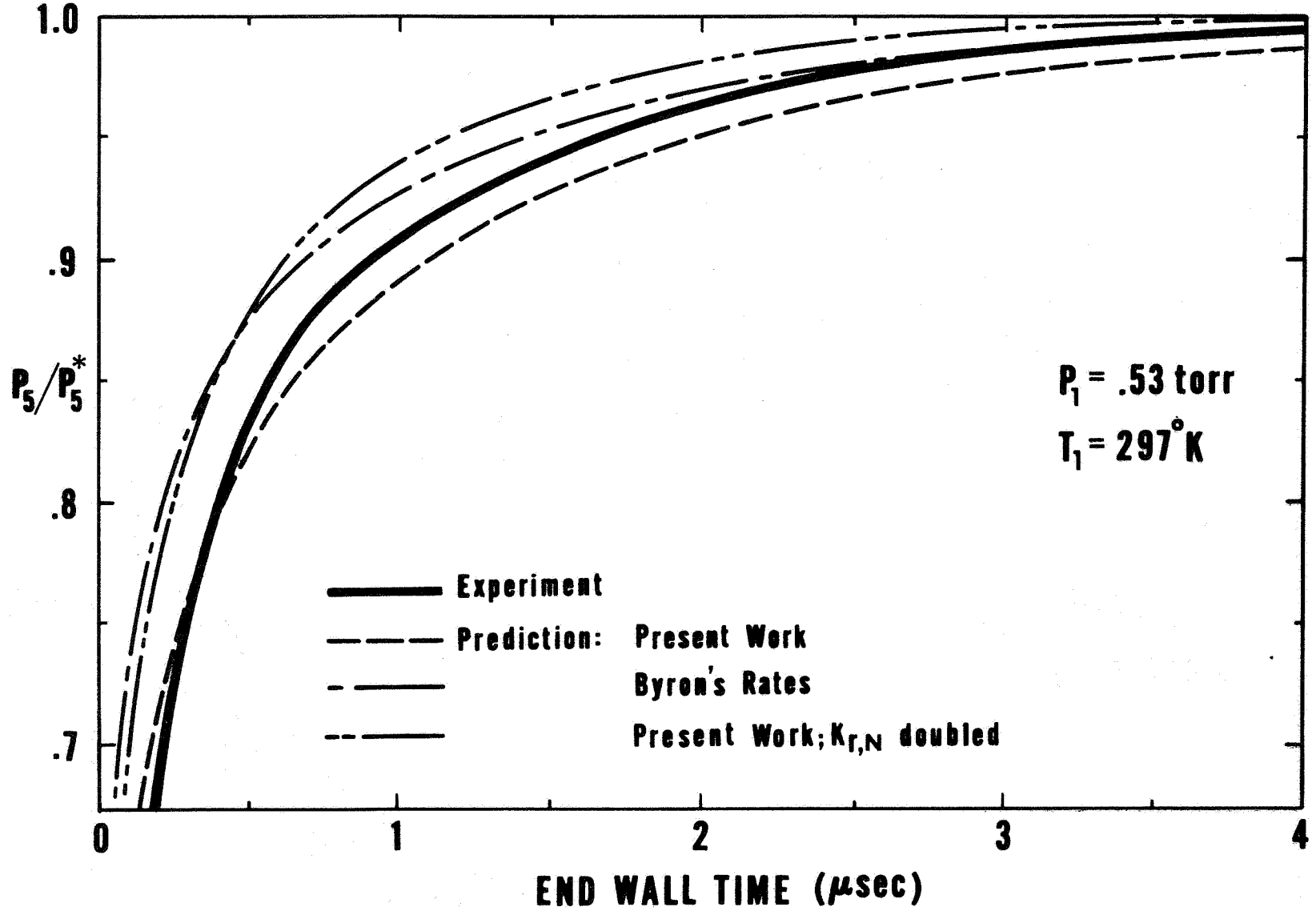

Fig. 24. End-wall pressure history for chemically relaxing N_2, V_s = 7.1 km/sec.

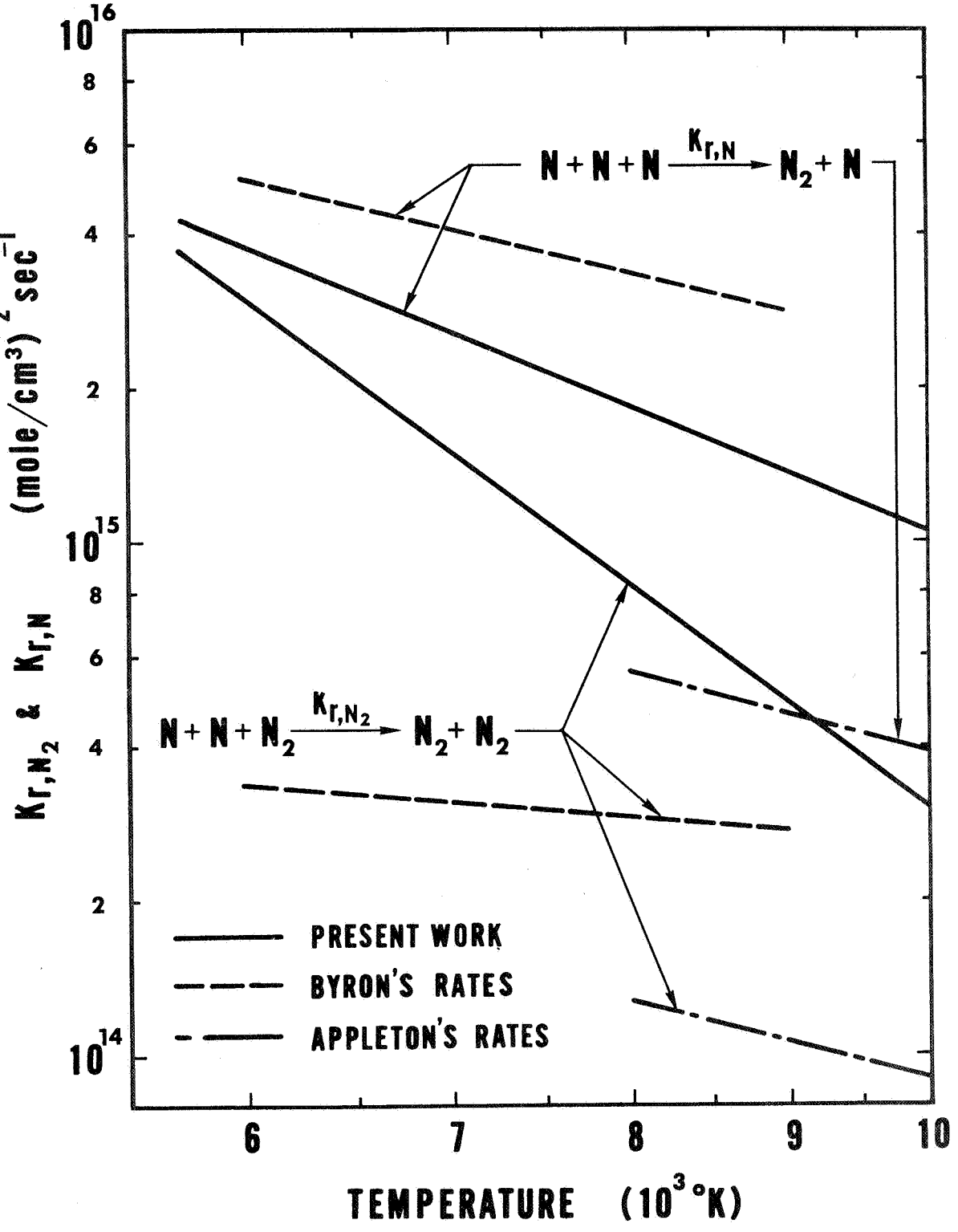

Fig. 25. Recombination rates for shock-heated N_2.

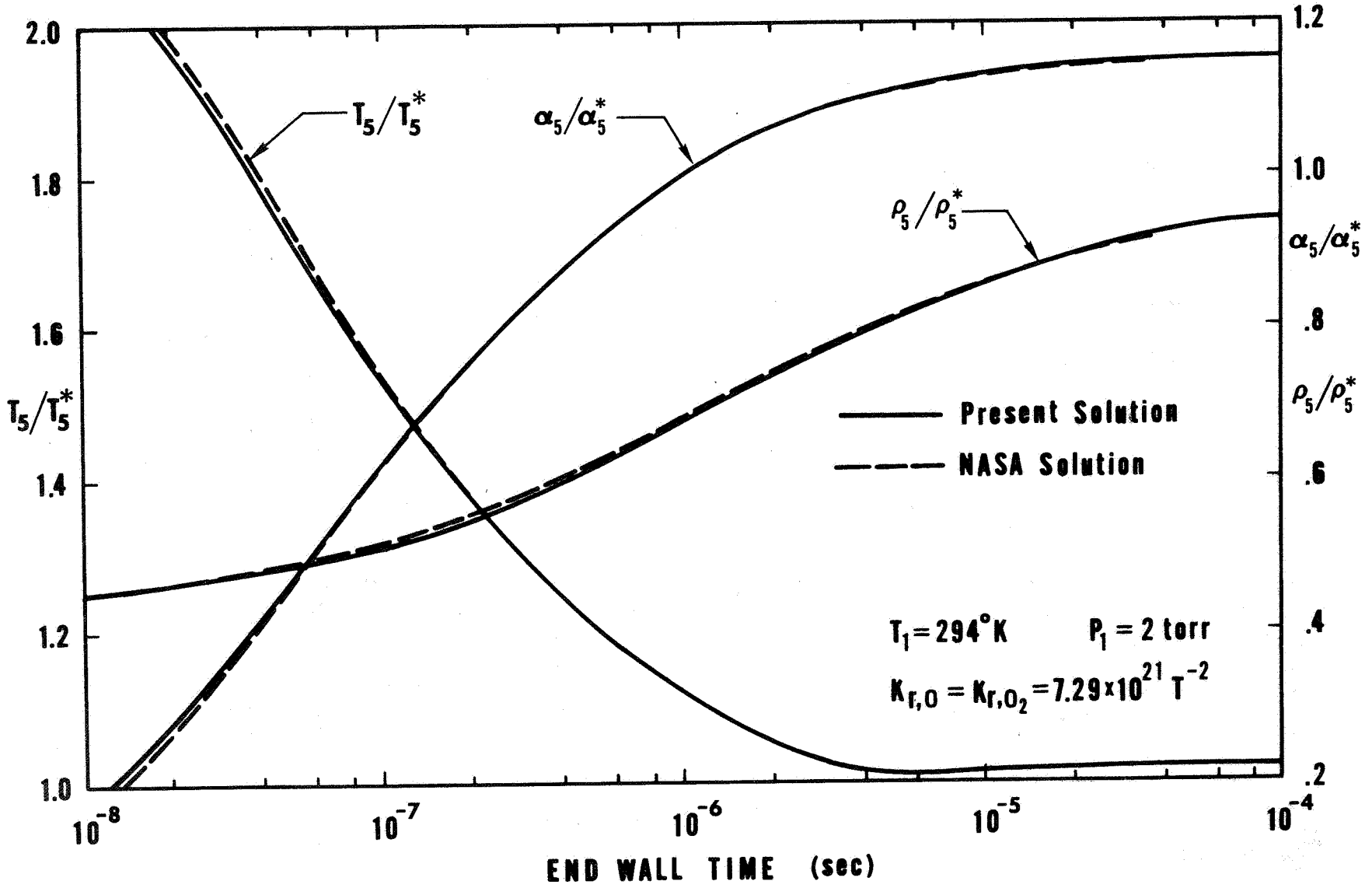

Fig. 26. Comparison of solutions for end-wall thermodynamic properties in chemically relaxing O_2, V_s = 3.05 km/sec.

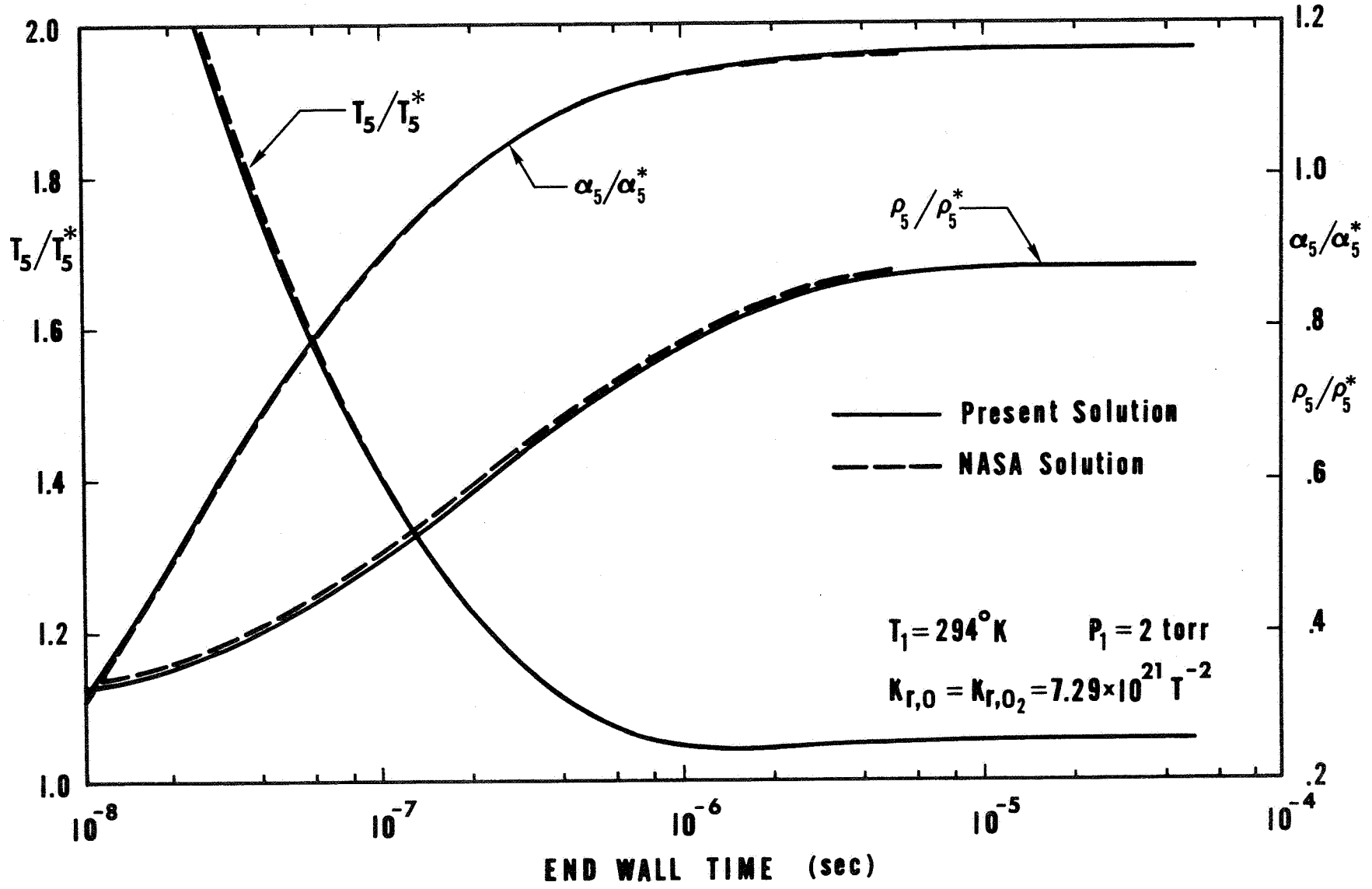

Fig. 27. Comparison of solutions for end-wall thermodynamic properties in chemically relaxing O_2, $V_s = 3.96$ km/sec.

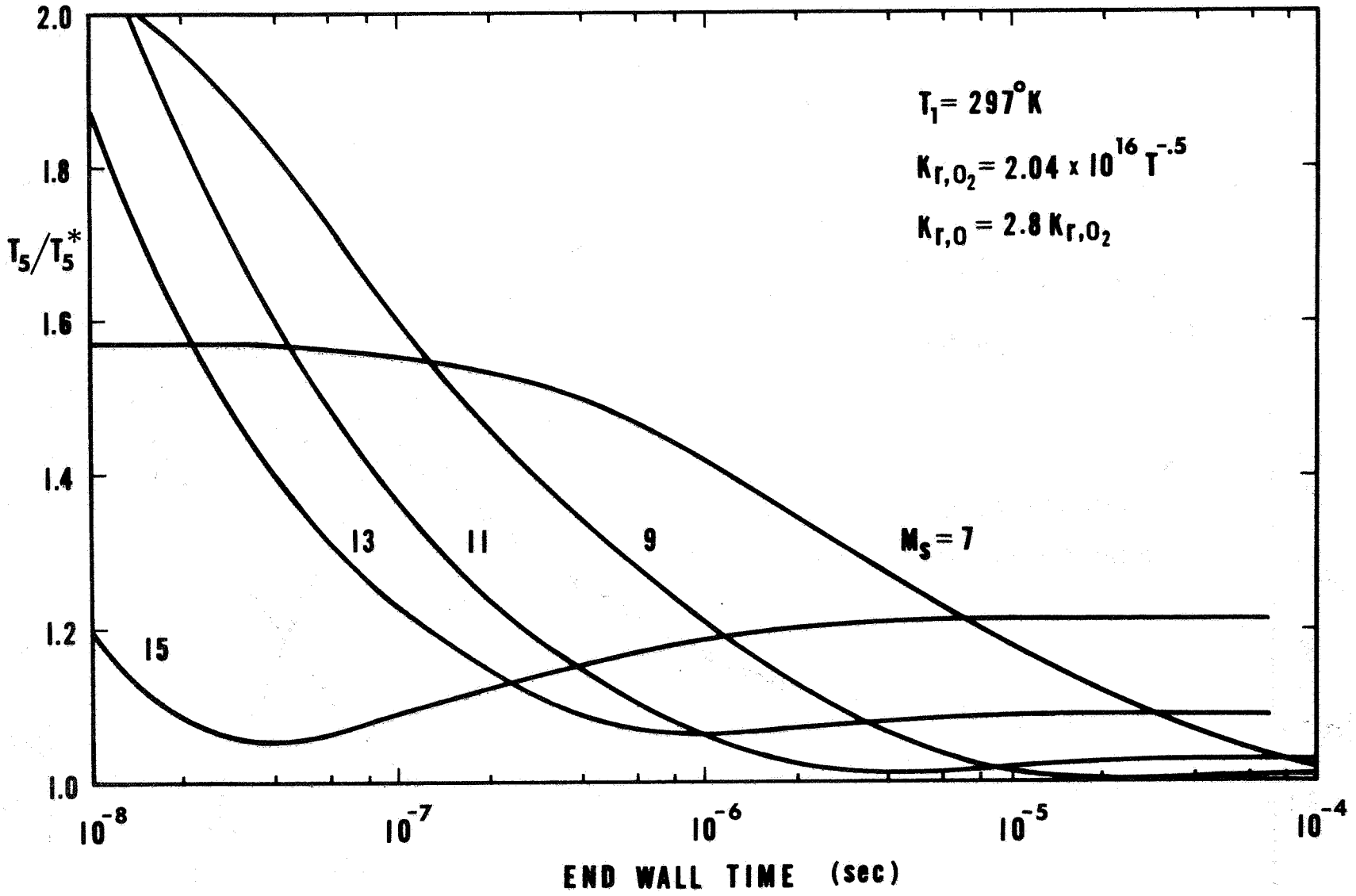

Fig. 28. End-wall temperature histories in chemically relaxing O_2, P_1 = 1 torr.

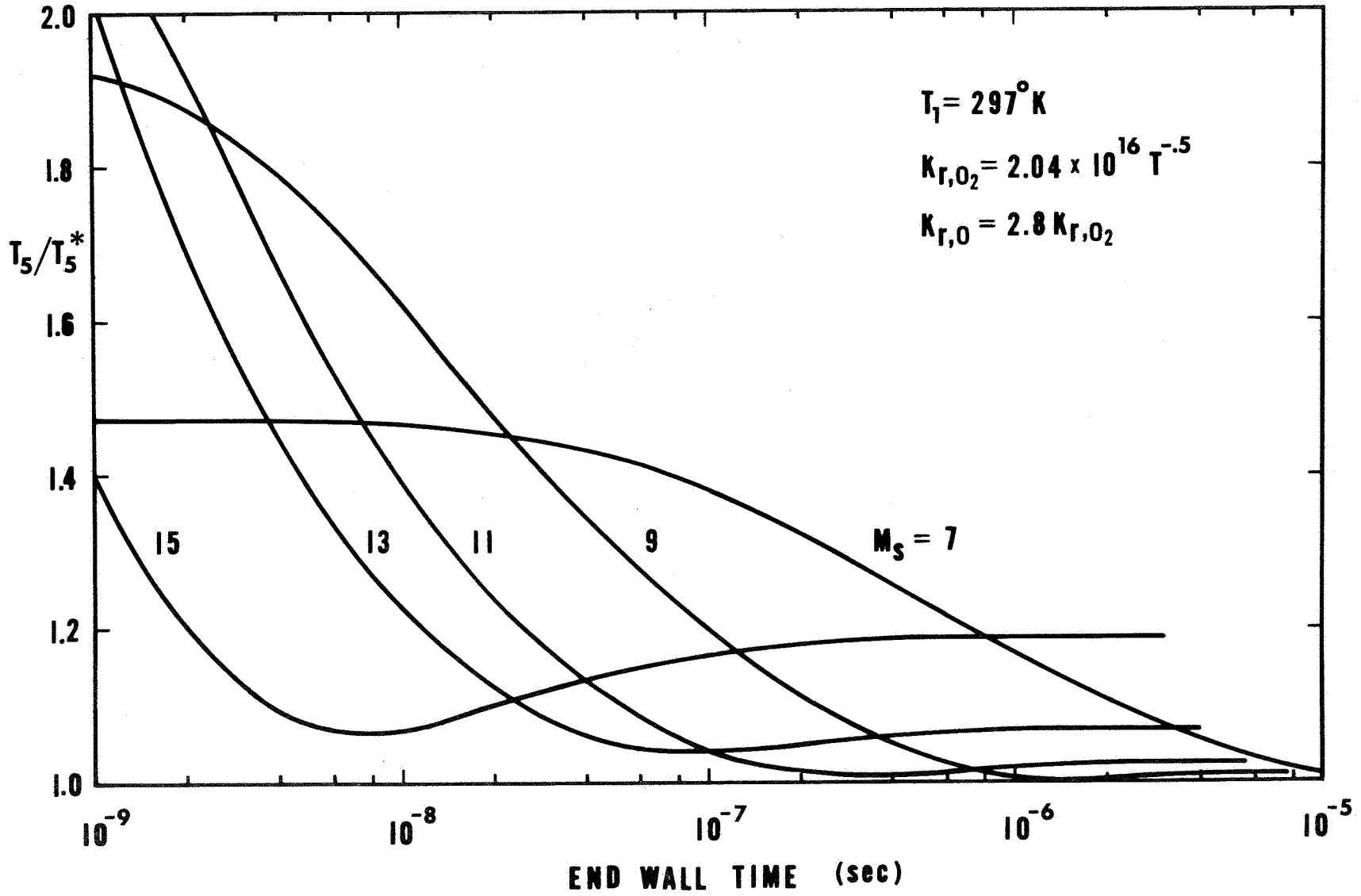

Fig. 29. End-wall temperature histories in chemically relaxing O_2, P_1 = 5 torr.

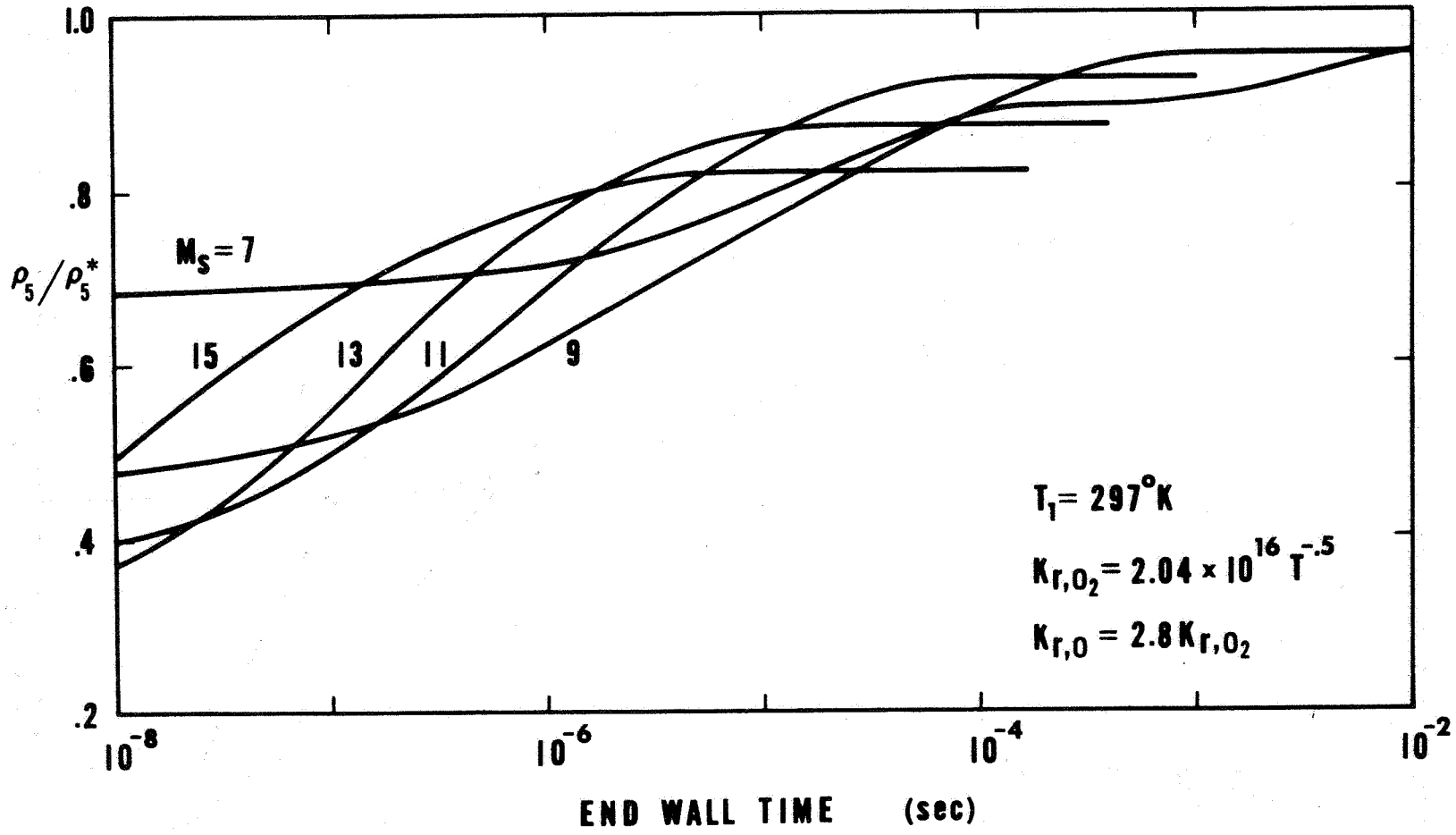

Fig. 30. End-wall density histories in chemically relaxing O_2, P_1 = 1 torr.

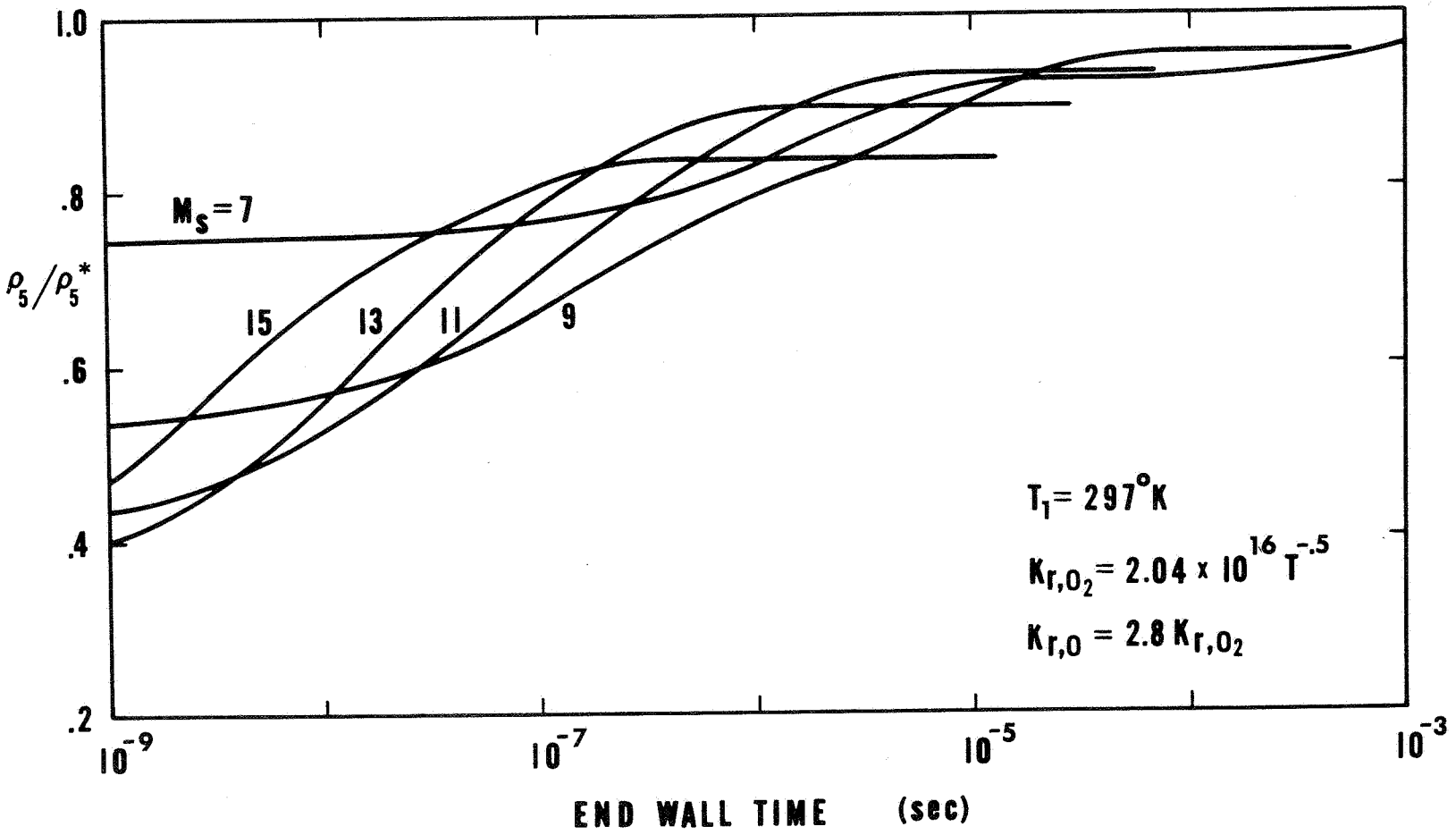

Fig. 31. End-wall density histories in chemically relaxing O_2, P_1 = 5 torr.

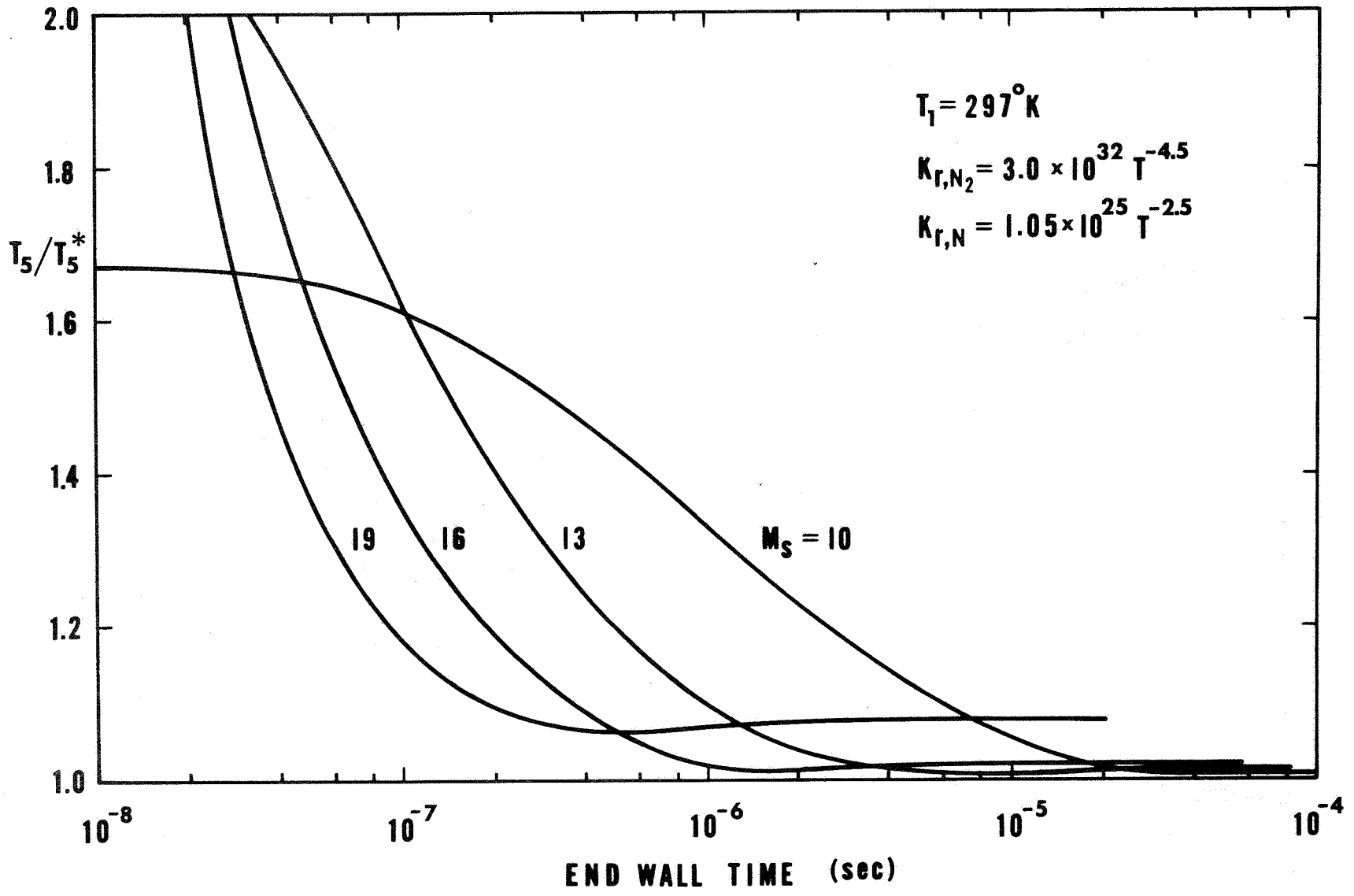

Fig. 32. End-wall temperature histories in chemically relaxing N_2, P_1 = 1 torr.

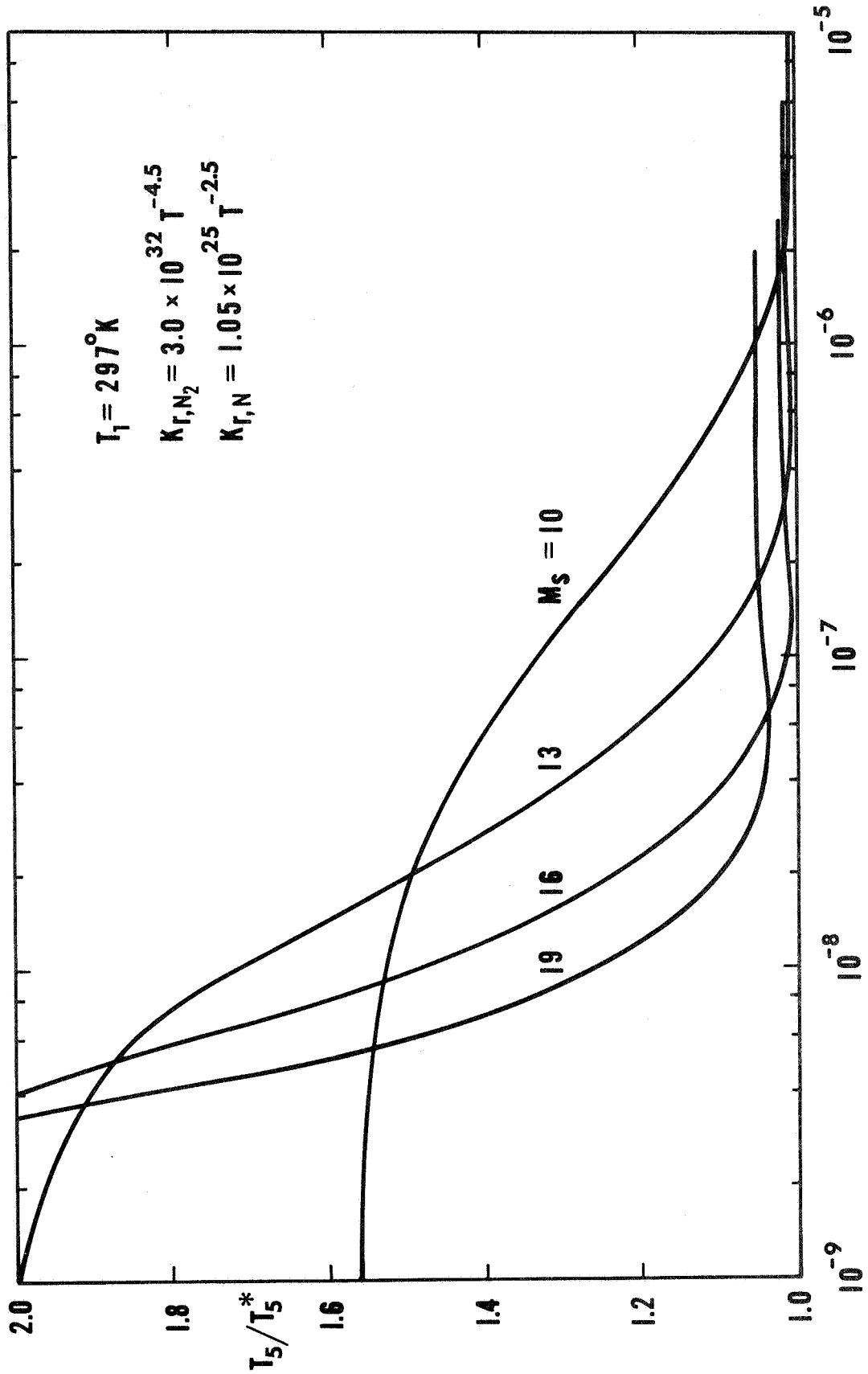

Fig. 33. End-wall temperature histories in chemically relaxing N_2, P_1 = 5 torr.

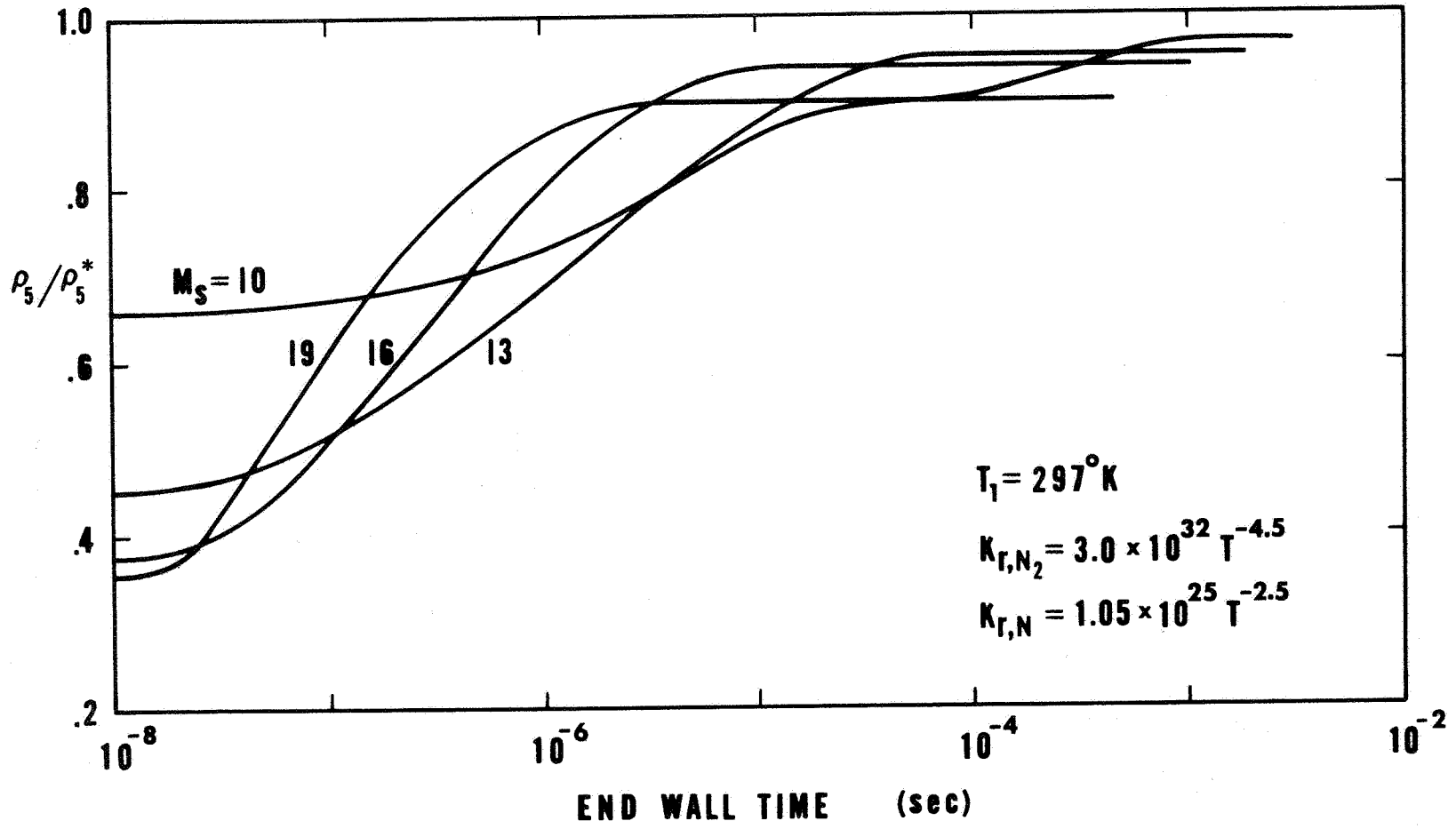

Fig. 34. End-wall density histories in chemically relaxing N_2, P_1 = 1 torr.

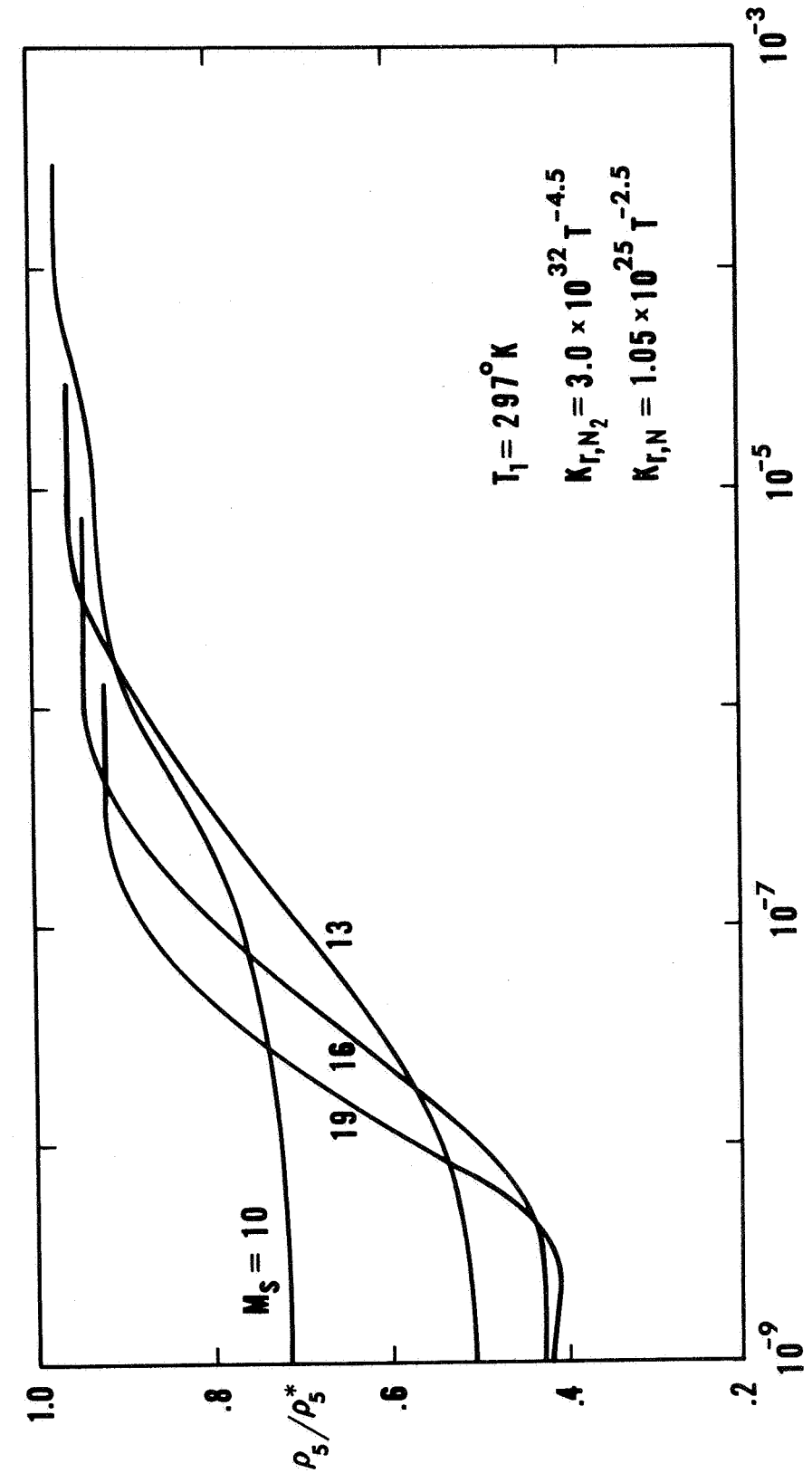

Fig. 35. End-wall density histories in chemically relaxing N_2, P_1 = 5 torr.

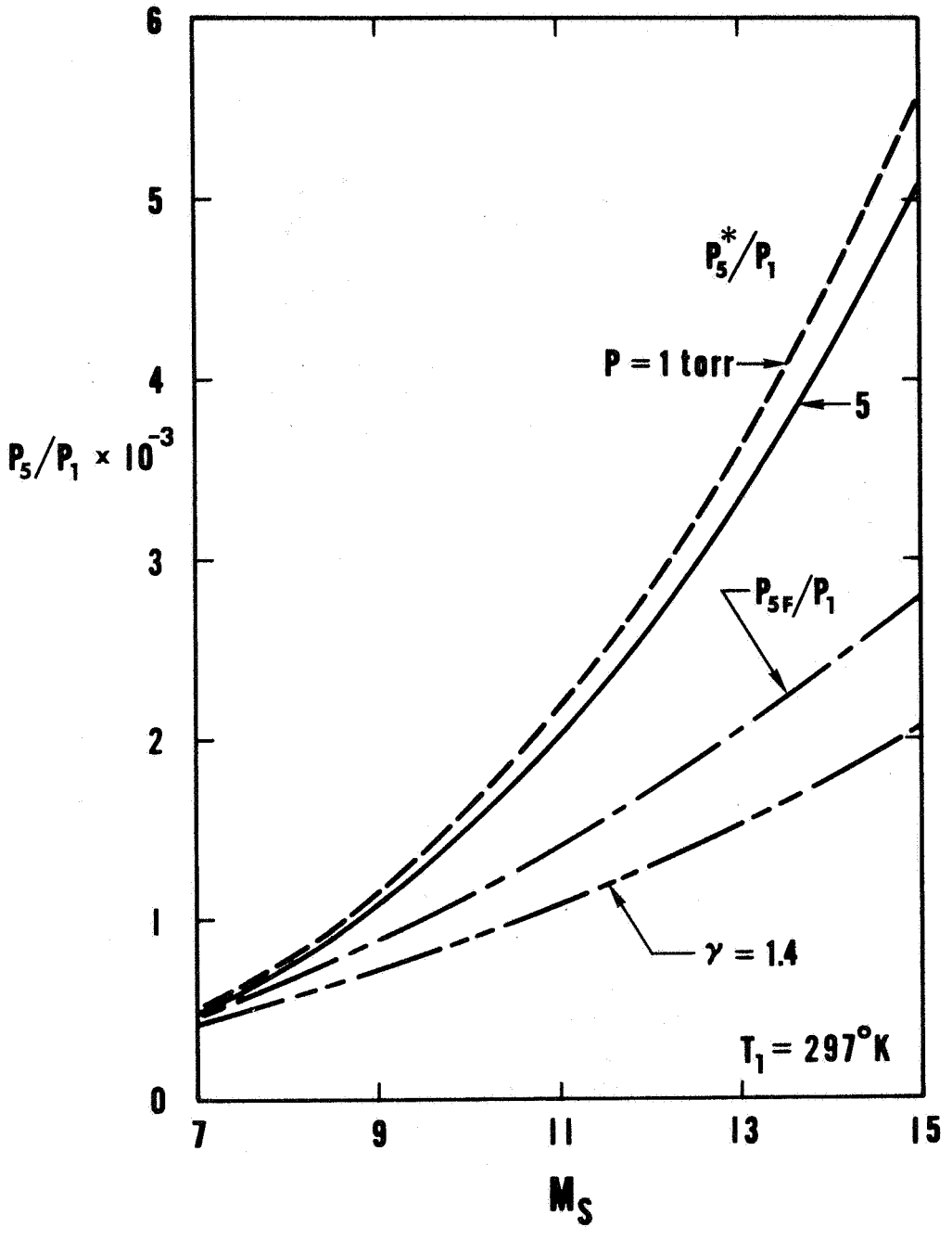

Fig. 36. Reference pressure levels behind reflected shock waves in O_2.

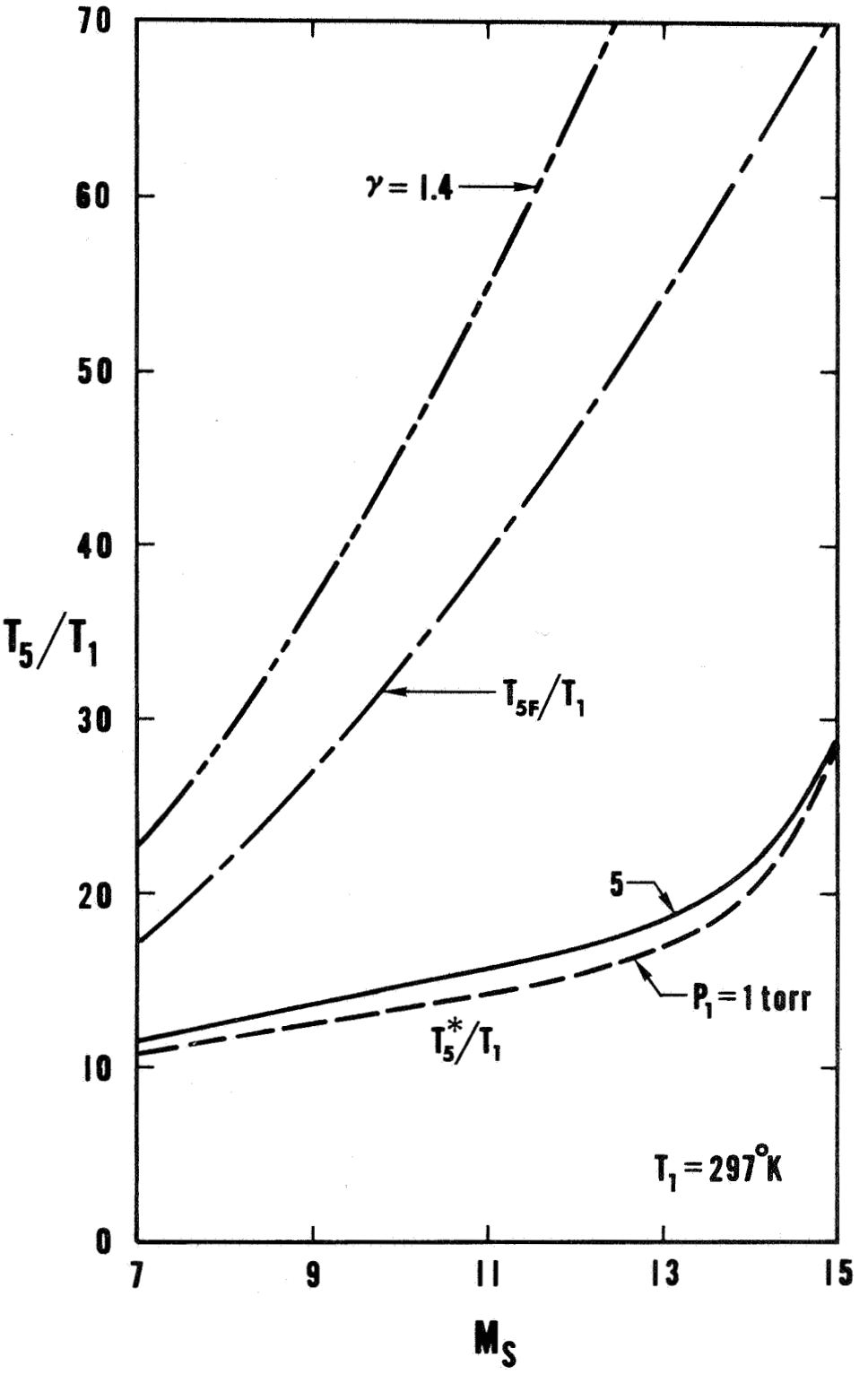

Fig. 37. Reference temperature levels behind reflected shock waves in O_2.

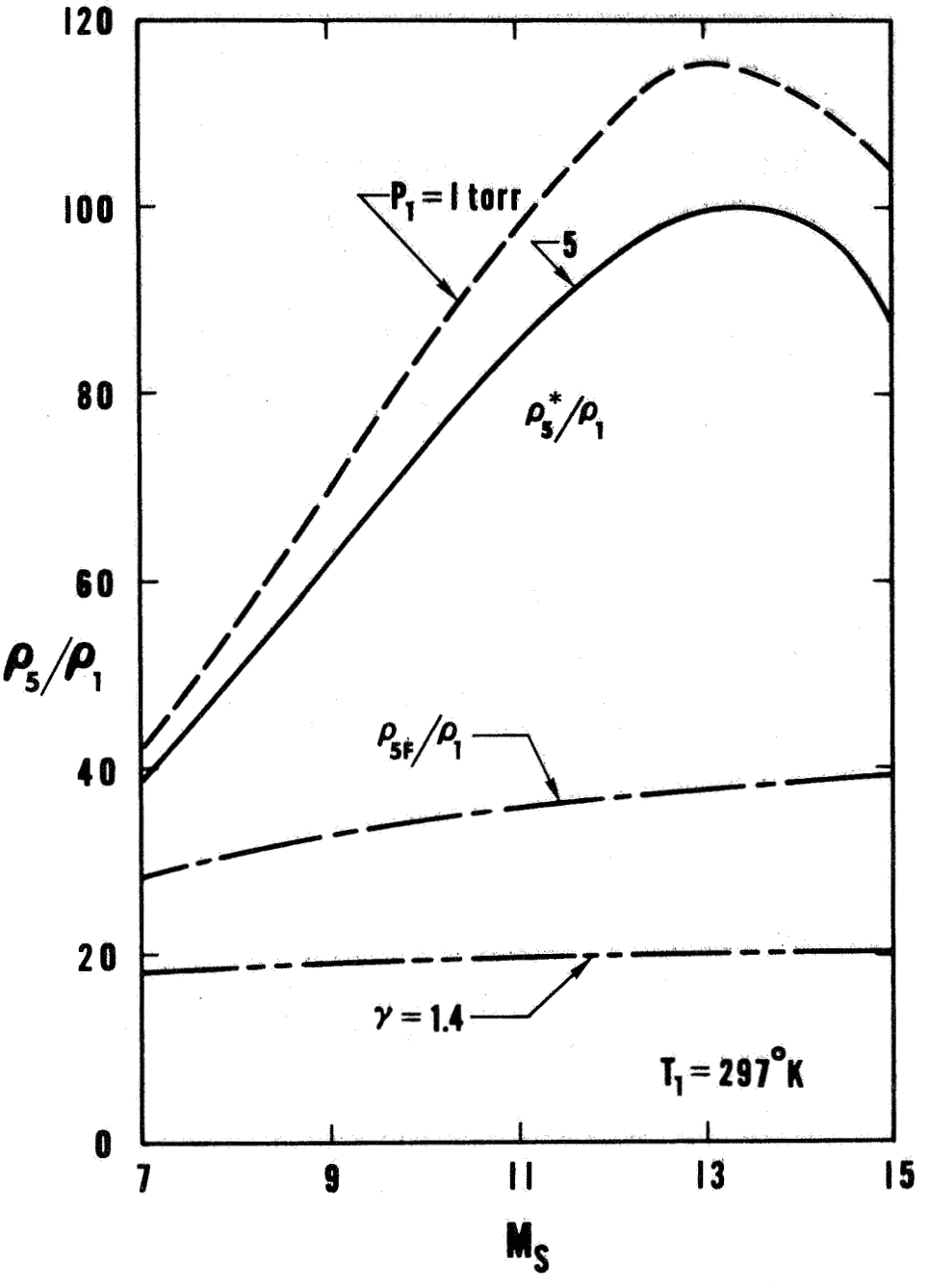

Fig. 38. Reference density levels behind reflected shock waves in O_2.

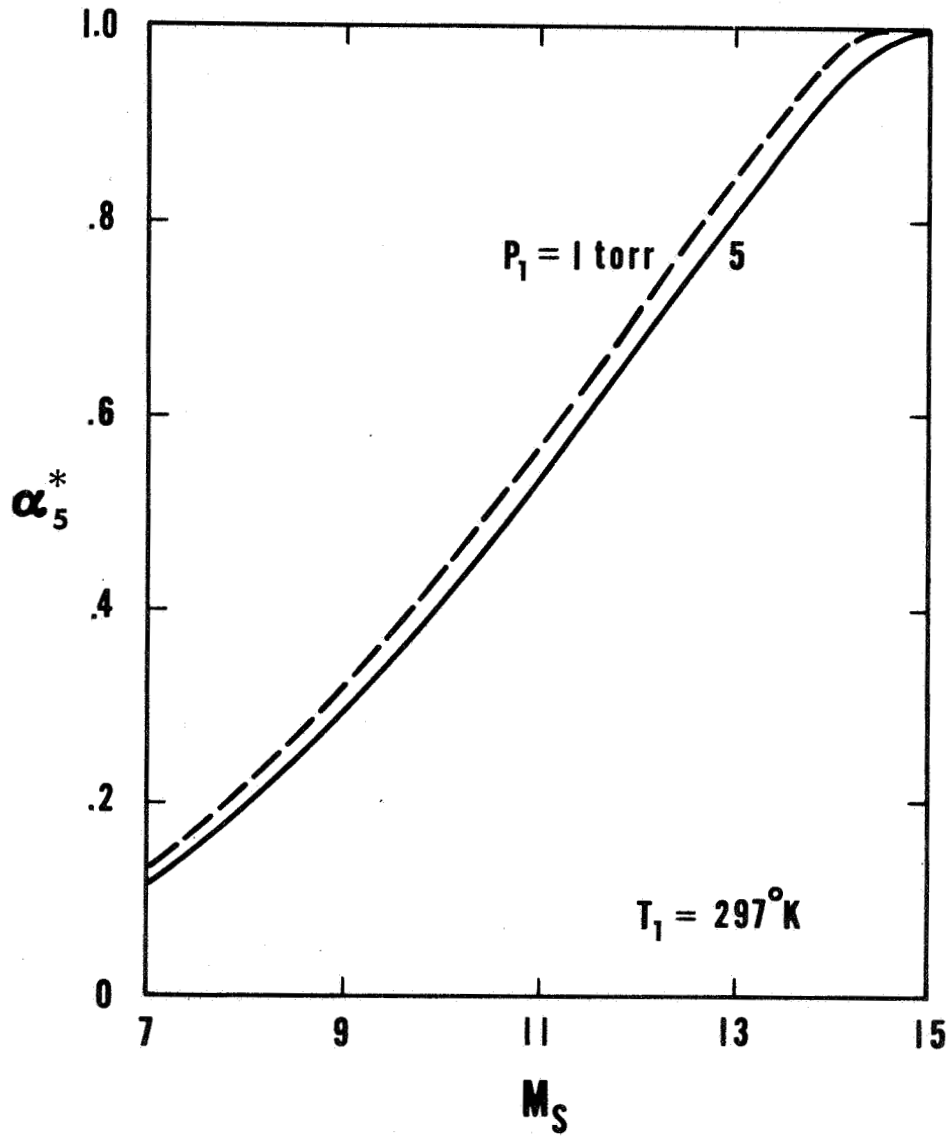

Fig. 39. Reference mass fraction of O atoms behind reflected shock waves in O_2.

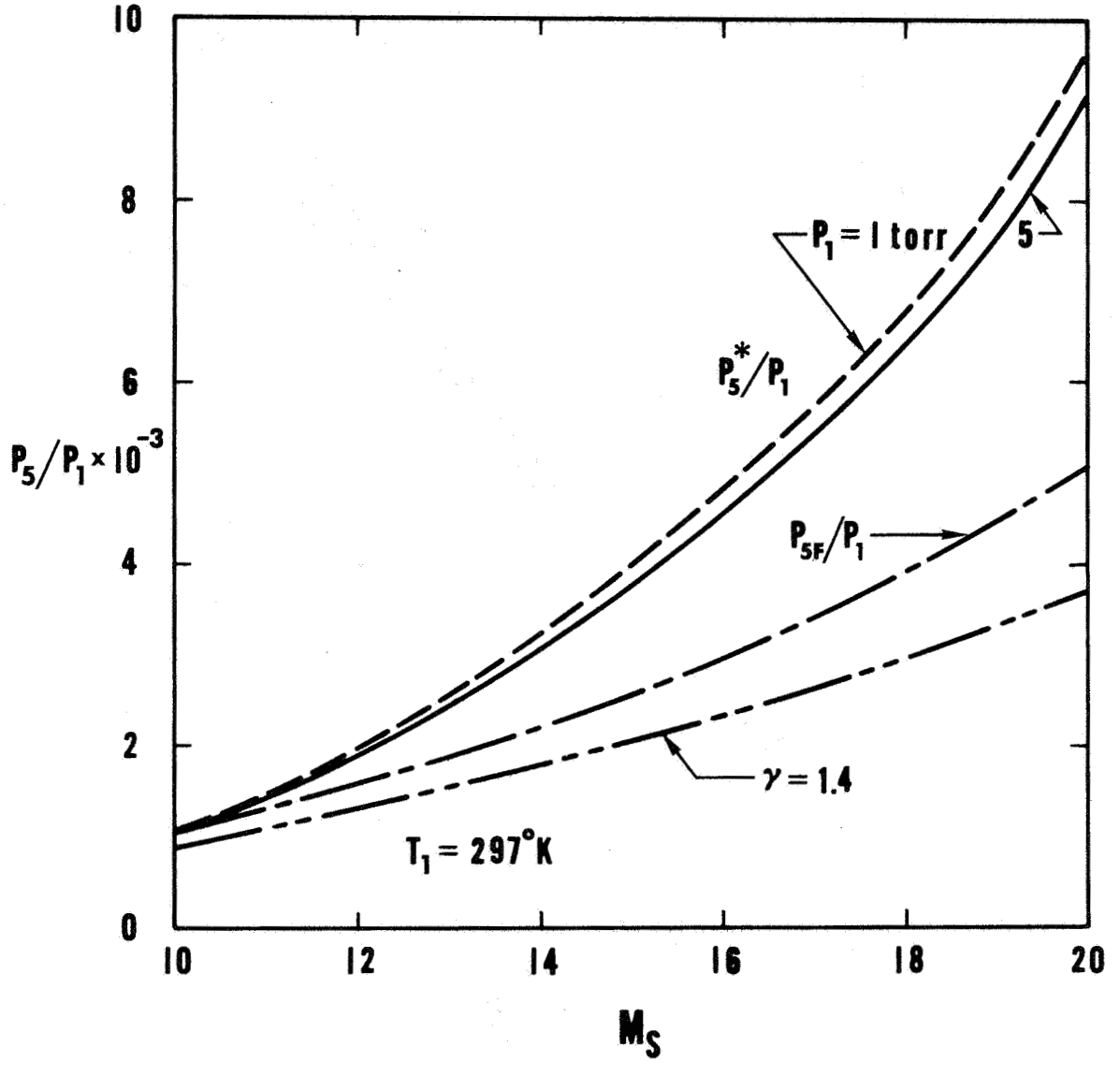

Fig. 40. Reference pressure levels behind reflected shock waves in N_2.

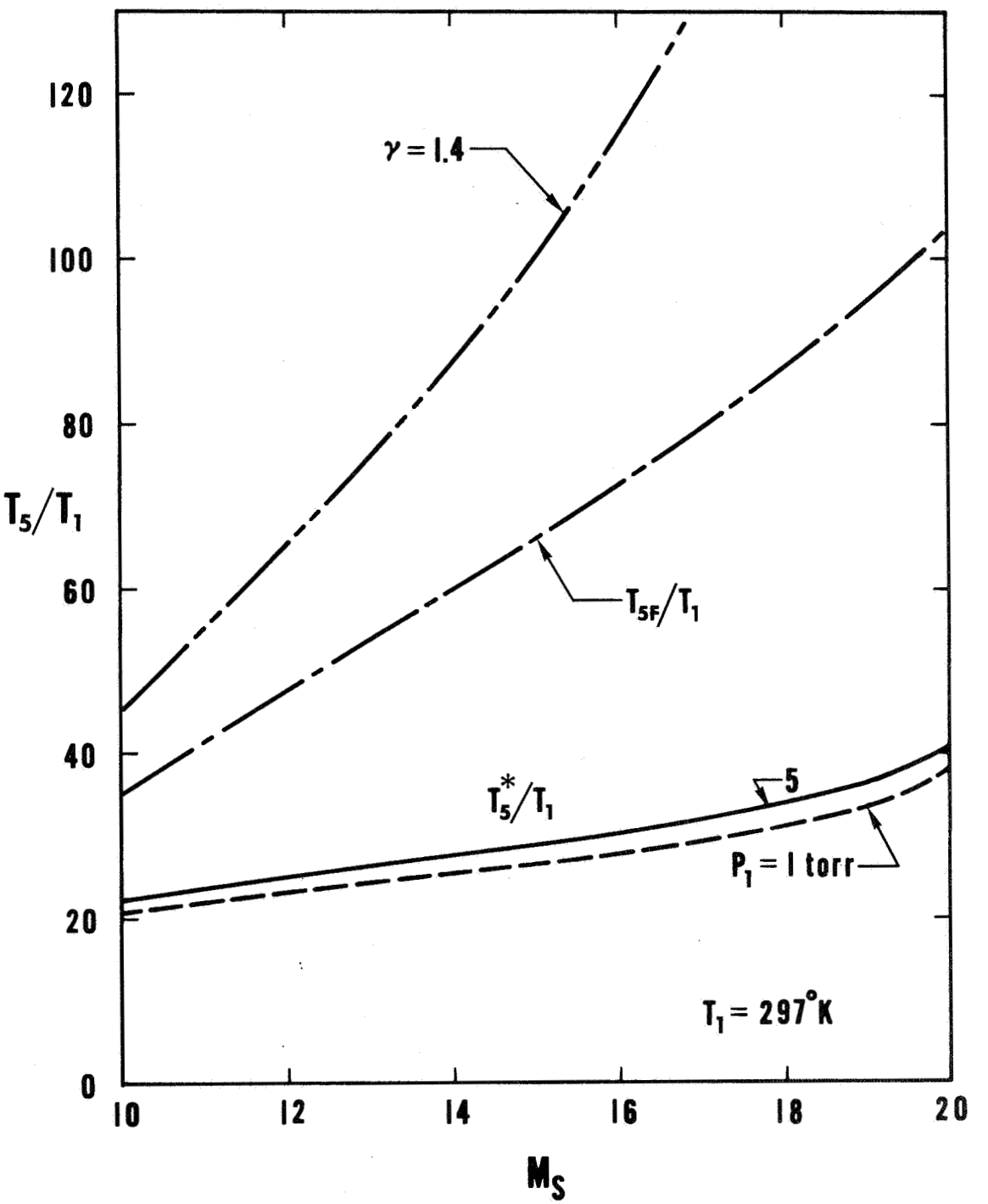

Fig. 41. Reference temperature levels behind reflected shock waves in N_2.

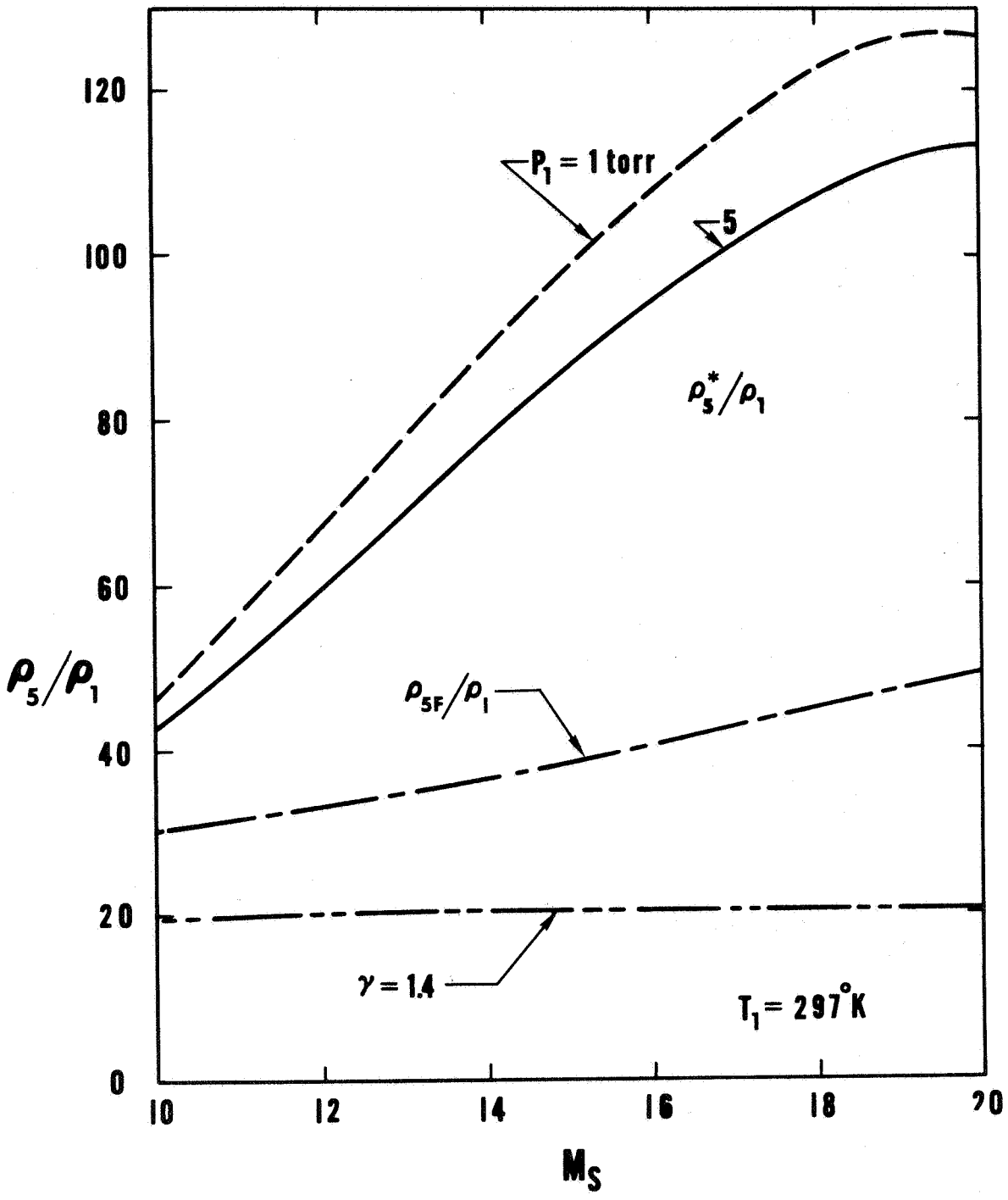

Fig. 42. Reference density levels behind reflected shock waves in N_2.

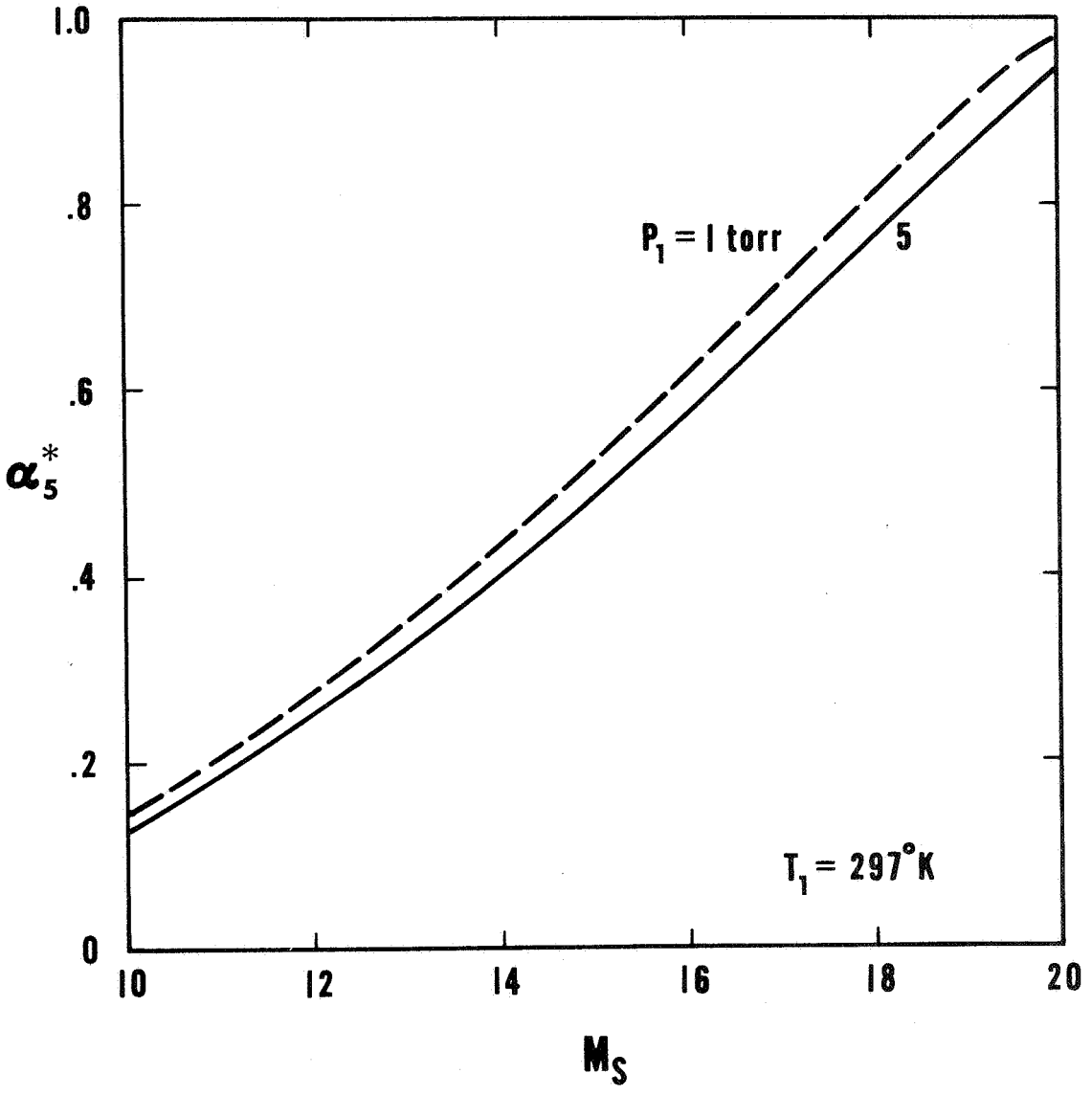

Fig. 43. Reference mass fraction of N atoms behind reflected shock waves in N_2.

a)

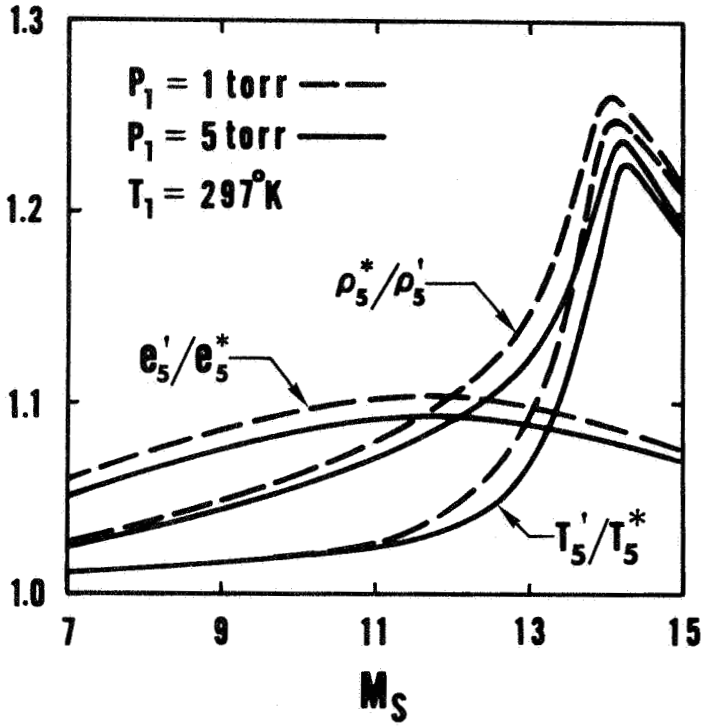

b)

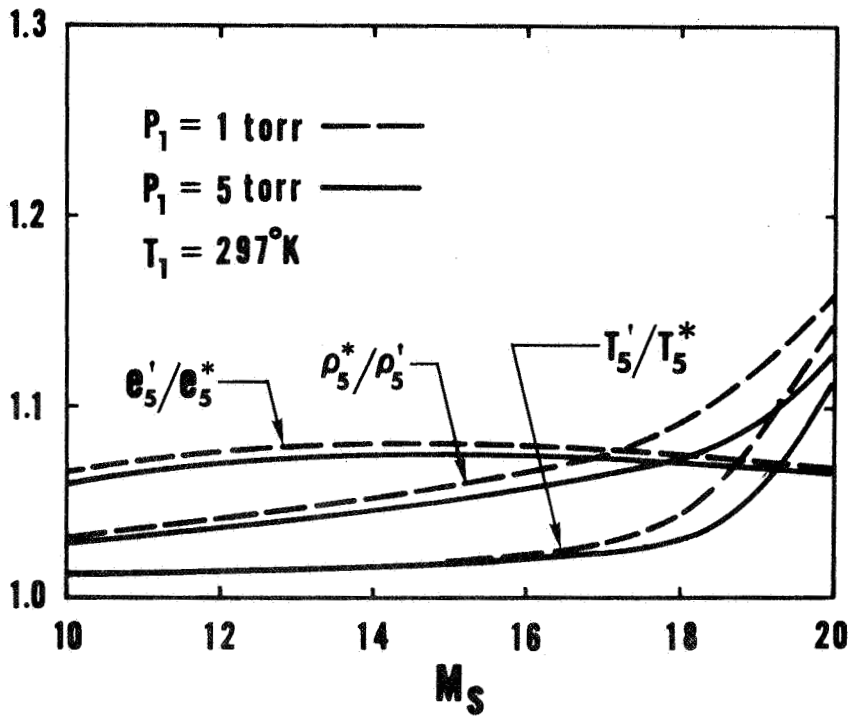

Fig. 44. Final end-wall states in chemically relaxing O_2 and N_2: a) O_2; b) N_2.

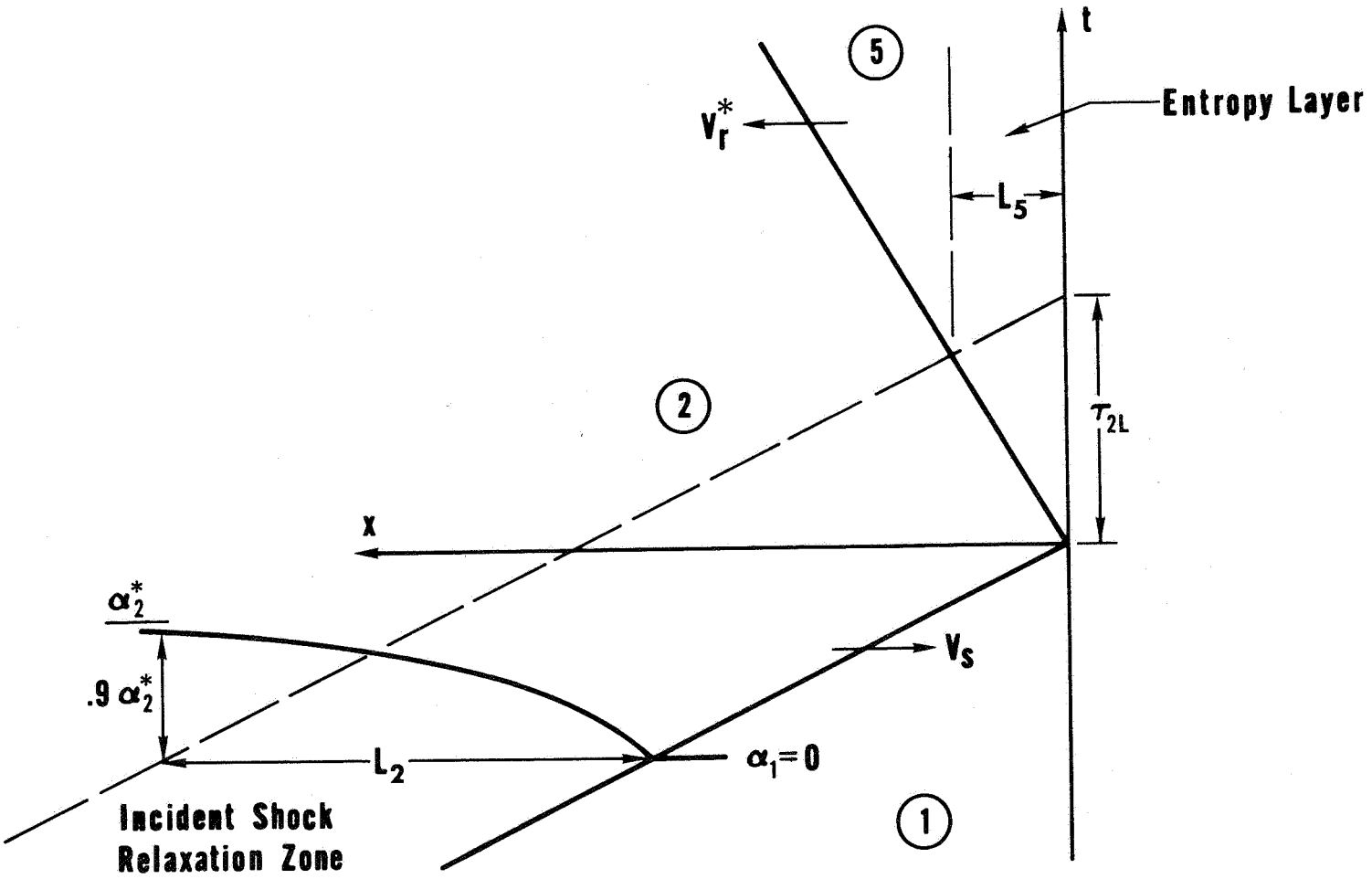

Fig. 45. Schematic definitions of the entropy-layer thickness (L_5) and formation time (τ_{2L}), and the incident-shock relaxation length (L_2), in a chemically relaxing gas.

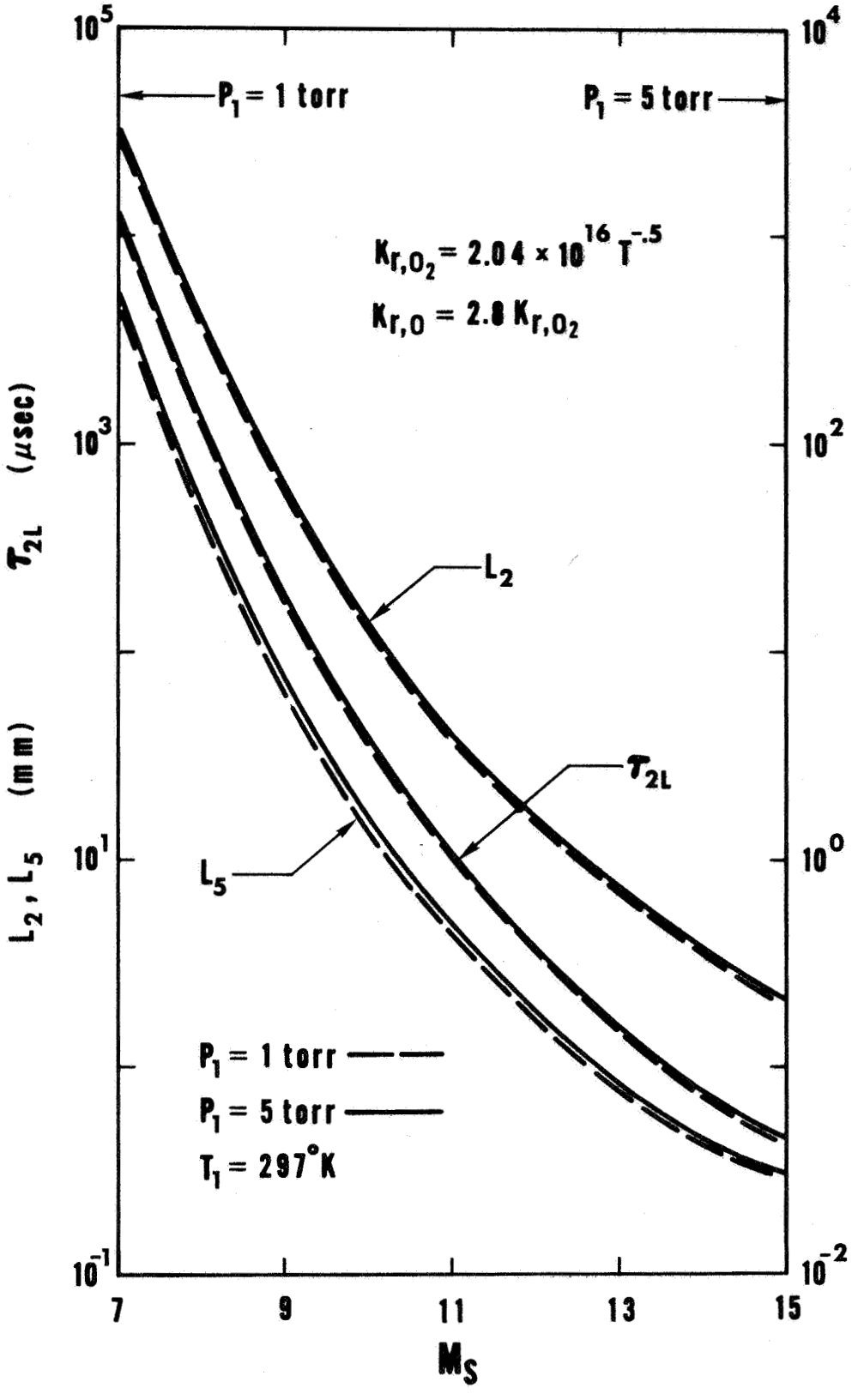

Fig. 46. Entropy-layer thickness (L_5), entropy-layer formation time (τ_{2L}), and incident-shock relaxation length (L_2) in chemically relaxing O_2.

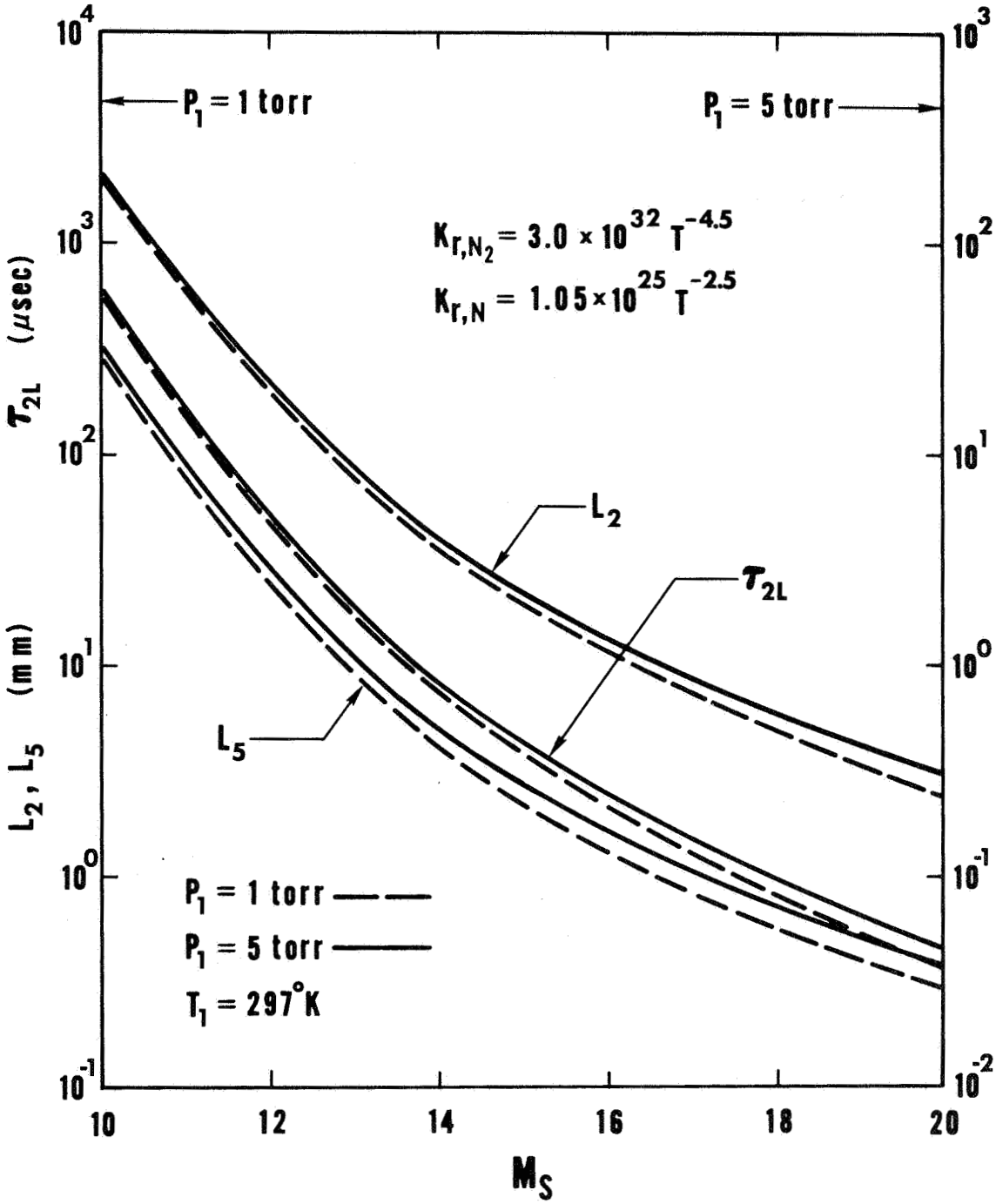

Fig. 47. Entropy-layer thickness (L_5), entropy-layer formation time (τ_{2L}), and incident-shock relaxation length (L_2) in chemically relaxing N_2.

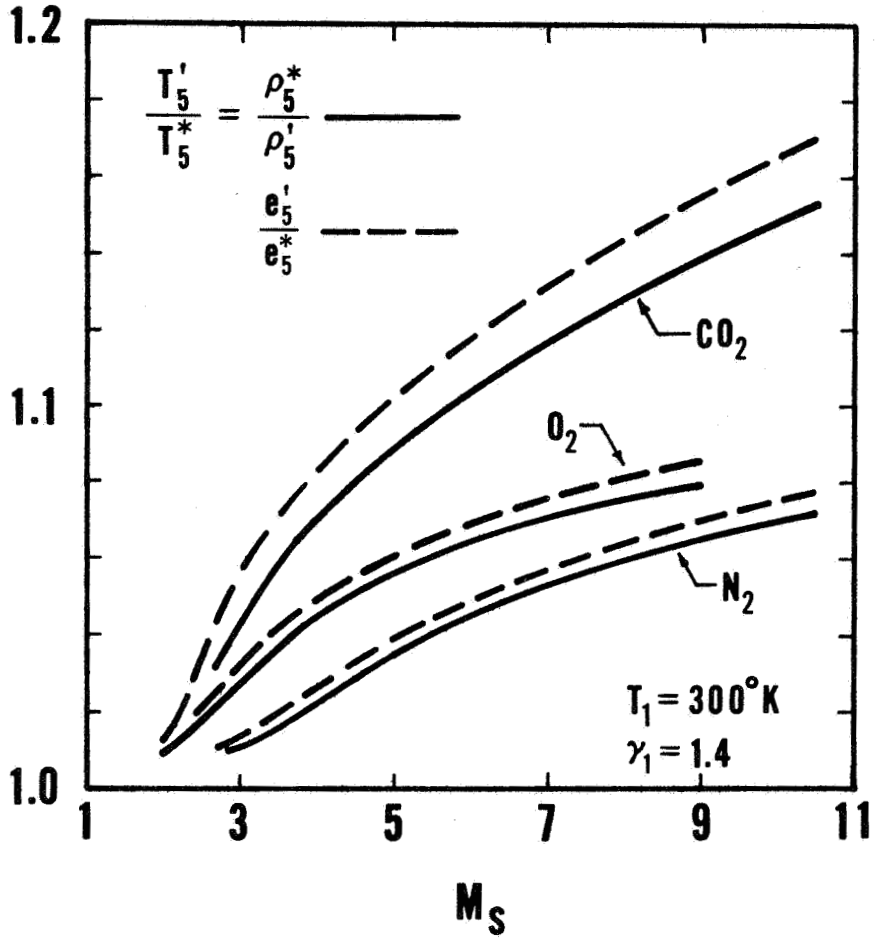

Fig. 48. Simple model predictions for final end-wall states in vibrationally relaxing CO_2, O_2 and N_2.

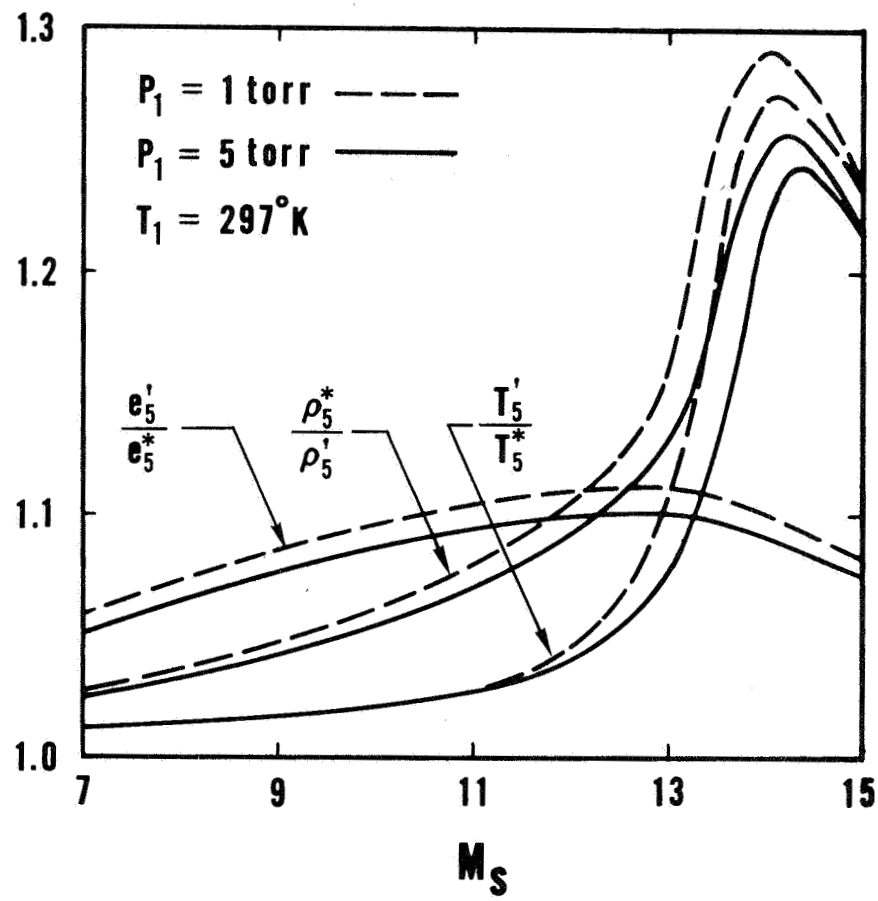

Fig. 49. Simple model predictions for final end-wall states in chemically relaxing O_2.

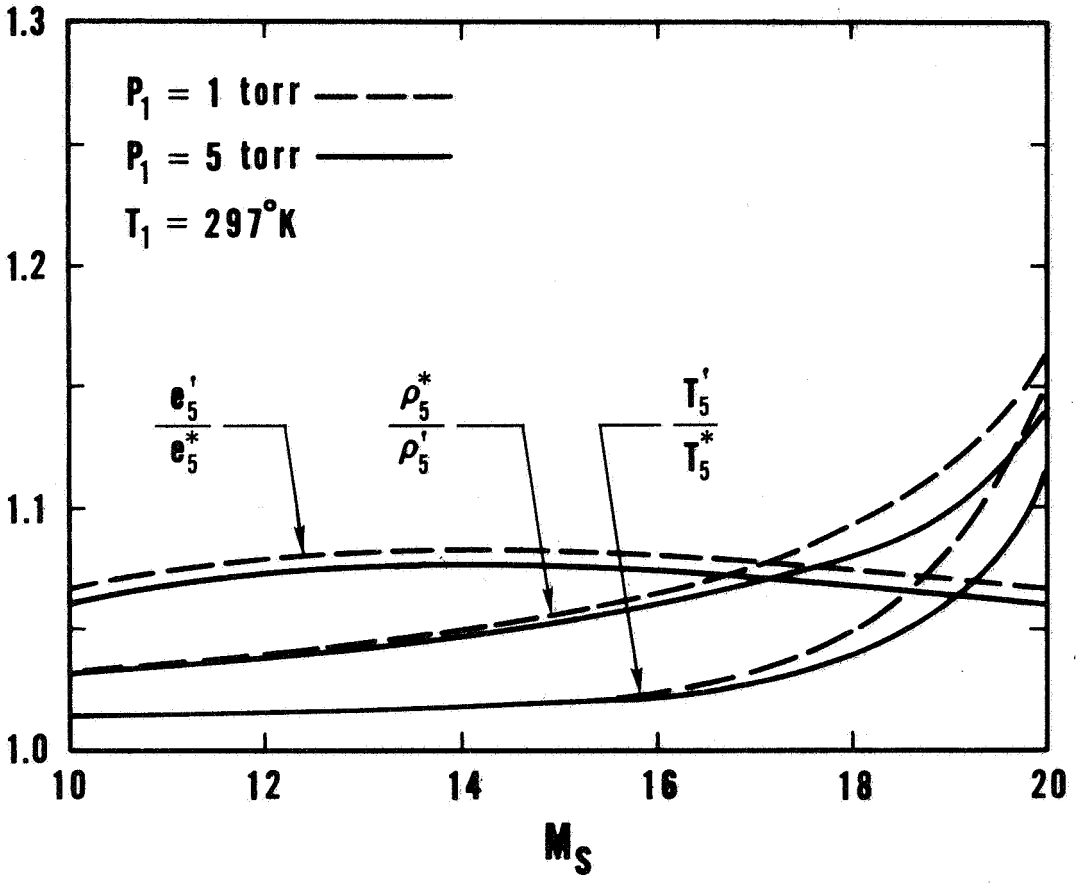

Fig. 50. Simple model predictions for final end-wall states in chemically relaxing N_2.